OCS Study
BOEM 2016-076

Arctic Air Quality Modeling Study – Final Photochemical Modeling Report

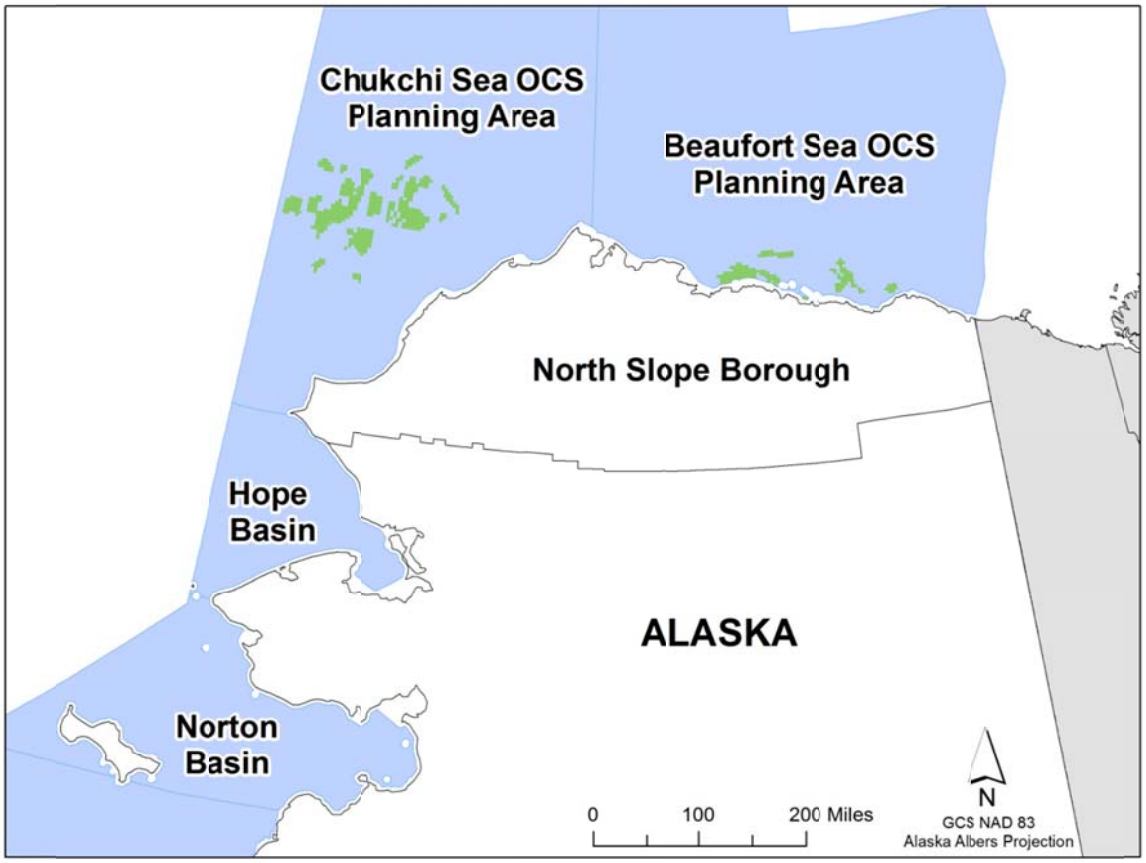

U.S. Department of the Interior
Bureau of Ocean Energy Management
Alaska OCS Region

Eastern Research Group, Inc.
8950 Cal Center Drive, Suite 325
Sacramento, CA 95826

Ramboll Environ
773 San Marin Dr.
Suite 2115
Novato, CA 94998

Arctic Air Quality Impact Assessment Modeling Study – Final Photochemical Modeling Report

Prepared by:
Ramboll Environ
773 San Marin Dr., Suite 2115
Novato, CA 94945

and

Eastern Research Group, Inc.
8950 Cal Center Drive, Suite 230
Sacramento, CA 95826

Prepared for:

U.S. Department of Interior
Bureau of Ocean Energy Management
Alaska OCS Region
3801 Centerpoint Drive, Suite 500
Anchorage, AK 99503-5823

7 July 2017

U.S. Department of the Interior
Bureau of Ocean Energy Management
Alaska OCS Region

Eastern Research Group, Inc.
8950 Cal Center Drive, Suite 325
Sacramento, CA 95826

Ramboll Environ
773 San Marin Dr.
Suite 2115
Novato, CA 94998

Disclaimer

This report has been reviewed by the Bureau of Ocean Energy Management and approved for publication. Approval does not signify that the contents necessarily reflect the views and policies of the Bureau, nor does mention of trade names or commercial products constitute endorsement or recommendation for use.

This report discusses a conservative "full build-out scenario" that describes air emissions sources associated with potential future oil and gas exploration, development, and production activities on the Beaufort Sea and Chukchi Sea Outer Continental Shelf. The elements of this scenario are included for the purpose of analysis and do not necessarily represent expected activities.

May be cited as: Stoeckenius et al., 2017. *Arctic Air Quality Modeling Study Photochemical Modeling Report*, BOEM Arctic Air Quality Impact Assessment Modeling Study. By Ramboll Environ, Novato, CA.

Authors:

Till Stoeckenius

Jaegun Jung

Bonyoung Koo

Tejas Shah

Ralph Morris

Abbreviations and Acronyms

ADEC	Alaska Department of Environmental Conservation
AMSL	Above Mean Sea Level
AKOCSR	Alaska Outer Continental Shelf Regional Office
AQRP	air quality regulatory program
AQRV	air quality-related value
BC	boundary condition
BOEM	Bureau of Ocean Energy Management
CAA	Clean Air Act
CMAQ	Community Multi-Scale Air Quality model
CAMx	Comprehensive Air Quality Model with eXtensions
ERG	Eastern Research Group, Inc.
GCM	Global Chemical Model
GIRAS	Geographic Information Retrieval and Analysis System
H4MDA8	Annual 4th highest maximum daily 8-hour average ozone concentration
H1MDA8	Annual highest maximum daily 8-hour average ozone concentration
IMPROVE	Interagency Monitoring of Protected Visual Environments
MCIP	Meteorology-Chemistry Interface Processor
MOU	memorandum of understanding
MOVES	Mobile Vehicle Emission Simulator
NA	Modeled sodium (Na)
NAA	nonattainment area
NAAQS	National Ambient Air Quality Standards
NEPA	National Environmental Policy Act
NSB	North Slope Borough
O&G	Oil and gas
OCS	Outer Continental Shelf
OCSLA	OCS Lands Act
PCL	Particulate chloride species in CAMx CB6r2 chemical mechanism
PGM	Photochemical Grid Model
PNO3	Particulate nitrate species in CAMx CB6r2 chemical mechanism
PSD	prevention of significant deterioration
RHR	Regional Haze Rule
SIP	State Implementation Plan
SMOKE	Sparse Matrix Operator Kernel Emissions processor
SSA	sea salt aerosol
U.S. EPA	U.S. Environmental Protection Agency
USDOI	U.S. Department of the Interior
USGS	United States Geological Service
USFWS	United States Fish and Wildlife Service
WRF	Weather Research and Forecasting model

Pollutants and Chemical Species

Cl	chlorine
CO	carbon monoxide
Na	sodium species in CAMx CB6r2 chemical mechanism
NO	nitric oxide
NO_2	nitrogen dioxide
NO_x	mono-nitrogen oxides (i.e., the sum of NO and NO_2)
O_3	ozone
Pb	lead
PM	particulate matter
$PM_{2.5}$	particulate matter with an aerodynamic diameter of less than or equal to 2.5 micrometers
PM_{10}	particulate matter with an aerodynamic diameter of less than or equal to 10 micrometers
SO_x	sulfur oxides (e.g., SO_2, SO_3)
SO_2	sulfur dioxide

Units of Measure

dv	deciview(s)
ha	hectare(s)
kg	kilogram(s)
km	kilometer(s)
m	meter(s)
ppb	parts per billion
ppm	parts per million
tpy	tons per year
$\mu g/m^3$	micrograms per cubic meter

Table of Contents

List of Tables

List of Figures

1.0 INTRODUCTION

The Bureau of Ocean Energy Management (BOEM) Alaska Outer Continental Shelf Regional Office (AKOCSR) has the delegated authority to regulate stationary sources of emissions from oil and gas (O&G) activities proposed within the Chukchi Sea and Beaufort Sea Outer Continental Shelf (OCS) Planning Areas that may adversely affect onshore air quality. The planning areas are adjacent to the North Slope Borough (NSB) of Alaska. Proposed operators on the Arctic OCS are required to comply with the U.S. Department of the Interior (USDOI)/BOEM Air Quality Regulatory Program (AQRP), established under 30 CFR Part 550, Subpart C, and BOEM has the obligation to implement the authority provided in OCS Lands Act (OCSLA) Section 5(a)(8). Figure 1-1 shows the Alaska OCS area and NSB of Alaska.

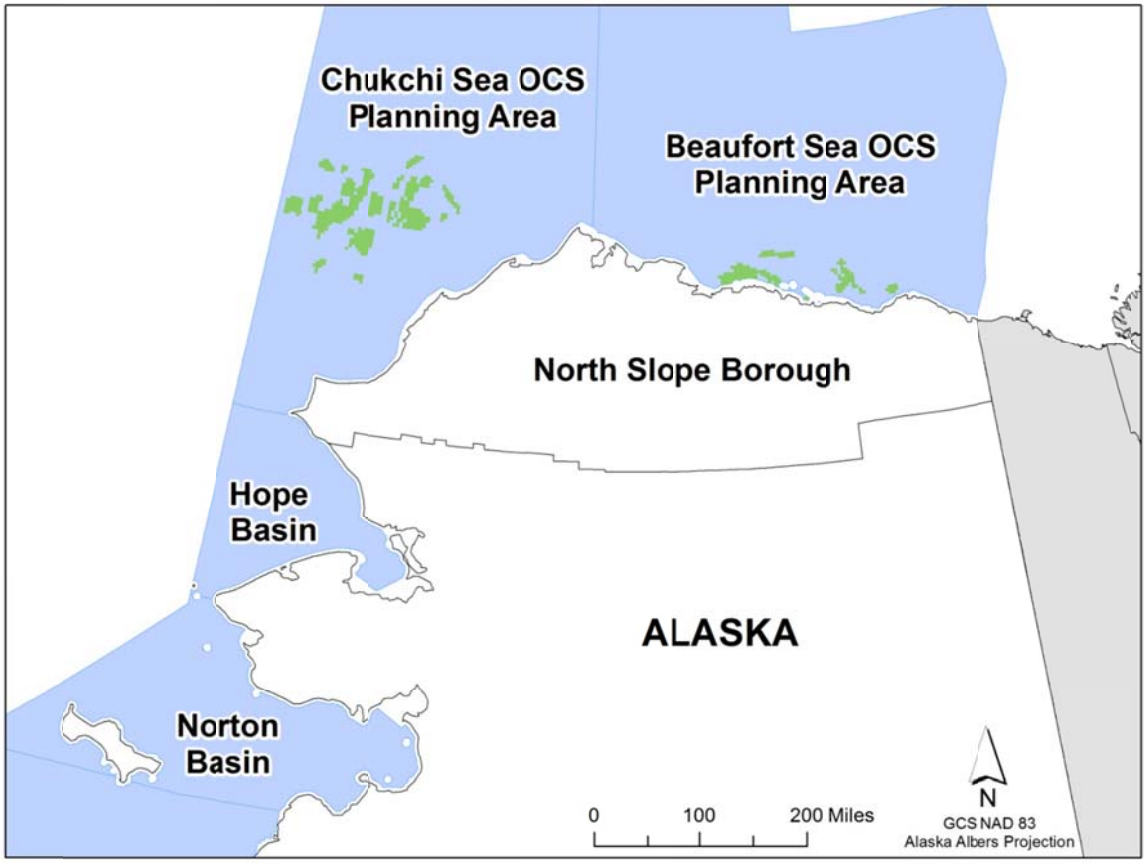

Figure 1-1. Regional map depicting OCS planning areas, including the location of the Arctic Air Quality Modeling Study. (Green areas represent select historical leased areas.)

1.1 Objectives

1.1.1 *Arctic Air Quality Modeling Study Objectives*

The overall objective of the BOEM Arctic Air Quality Impact Assessment Modeling Study (Arctic AQ Modeling Study) is to enable BOEM to assess potential air quality impacts from oil and gas exploration, development, and production on the Alaska OCS and related onshore activities.

1.1.2 *Arctic Air Quality Modeling Study Atmospheric Photochemical Modeling Objectives*

BOEM recognizes that OCS sources and associated activities have the potential to impact air quality, not just on a local scale (within approximately 50 kilometers [km] of the source) but also over a regional scale (greater than 50 km from the source). This report presents results of a photochemical grid modeling study which addresses impacts of existing and potential future sources at the regional scale (i.e., far-field impacts).

The far-field photochemical grid modeling (PGM) performed for this study supports the National Environmental Policy Act (NEPA) environmental impact air quality assessments by estimating the regional-scale impacts from projected oil and gas production on onshore pollution levels for both primary pollutants (those that are directly emitted from sources) and secondary pollutants (pollutant species including ozone and some types of particulate matter that are formed in the atmosphere from primary pollutants).

1.1.3 *Air Quality Standards and Air Quality Related Values*

The U.S. EPA sets National Ambient Air Quality Standards (NAAQS) for seven regulated air quality pollutants. These pollutants, collectively known as the criteria pollutants, include: ground-level ozone (O_3), sulfur dioxide (SO_2), nitrogen dioxide (NO_2), carbon monoxide (CO), lead (Pb), and particulate matter. The particulate matter (PM) NAAQS are set with respect to either the concentration of PM with an aerodynamic diameter of less than or equal to 10 micrometers (PM_{10}) and for PM with an aerodynamic diameter less than or equal to 2.5 micrometers ($PM_{2.5}$). After promulgation of a NAAQS, U.S. EPA designates nonattainment areas (NAAs) and states are required to submit State Implementation Plans (SIPs) to U.S. EPA that contain emission control plans and a demonstration that the NAA will achieve the NAAQS by the required date. Table 1-1 summarizes the current levels of the NAAQS.

There is currently only one designated nonattainment area in Alaska—the Fairbanks North Star Borough, which is a NAA for $PM_{2.5}$. This area is over 200 miles from the NSB and is located south of the Brooks Range which separates North Slope from the rest of Alaska. Alaska also has three maintenance areas—Anchorage Municipality (CO and PM_{10}), Fairbanks North Star Borough (CO), and Juneau City and Borough (PM_{10}), all of which are at least 200 miles from the southern border of the NSB.

There are currently no regulatory ozone or $PM_{2.5}$ monitors operating in the NSB, which will result in an "unclassifiable" designation for any future ozone or $PM_{2.5}$ NAAQS. In February 2010, U.S. EPA issued a new 1-hour NO_2 NAAQS with a threshold of 100 ppb and a new 1-hour SO_2 NAAQS was promulgated in June 2010 with a threshold of 75 ppb. In 2015, U.S. EPA issued a new 8-hour ozone NAAQS set at a level of 70 ppb. The U.S. EPA designated all of Alaska as "unclassifiable/attainment" for the 1-hour NO_2 NAAQS and deferred designation for the 1-hour SO_2 NAAQS. Designations for the new 70 ppb ozone NAAQS are due to be completed in October, 2017.

While a lead NAAQS exists, the total lead emissions in the study area are less than one ton per year, with only 0.135 tons per year from the projected offshore sources (Fields Simms, et al., 2014). This level of emissions should not have a significant impact on air quality in the NSB.

The U.S. EPA categorizes attainment areas into Class I, Class II, and Class III Areas. The Clean Air Act (CAA) designated 156 Class I areas consisting of National Parks and Wilderness Areas

that warrant special protection for air quality and air quality related values (AQRVs). The Class I areas, compared to Class II areas, have lower prevention of significant deterioration (PSD) air quality increments that new sources may not exceed, and are protected against excessive increases in several AQRVs, including visibility impairment, acid (sulfur and nitrogen) deposition, and nitrogen eutrophication. There are currently no Class III areas in the U.S., and areas that are not designated as Class I areas are by default designated as Class II areas. Table 1-1 summarizes the PSD increments for Class I and Class II areas, including the North Slope, along with the related NAAQS.

The Regional Haze Rule (RHR) has a goal of achieving natural visibility conditions by 2064 at Class I areas, and states must submit RHR SIPs that demonstrate progress towards that goal. Figure 1-2 displays the locations of the mandatory Class I areas in Alaska, together with all nonattainment and maintenance areas. The nearest Class I area to the NSB, Denali National Park, is located approximately 900 km south of Barrow.

A complete set of Class I and specified Class II areas designated as national parks, national preserves, and national wildlife refuges falling within the modeling domain analyzed in this study is shown in Figure 1-3 and Table 1-2 (see Section 4 for a description of the modeling domain).

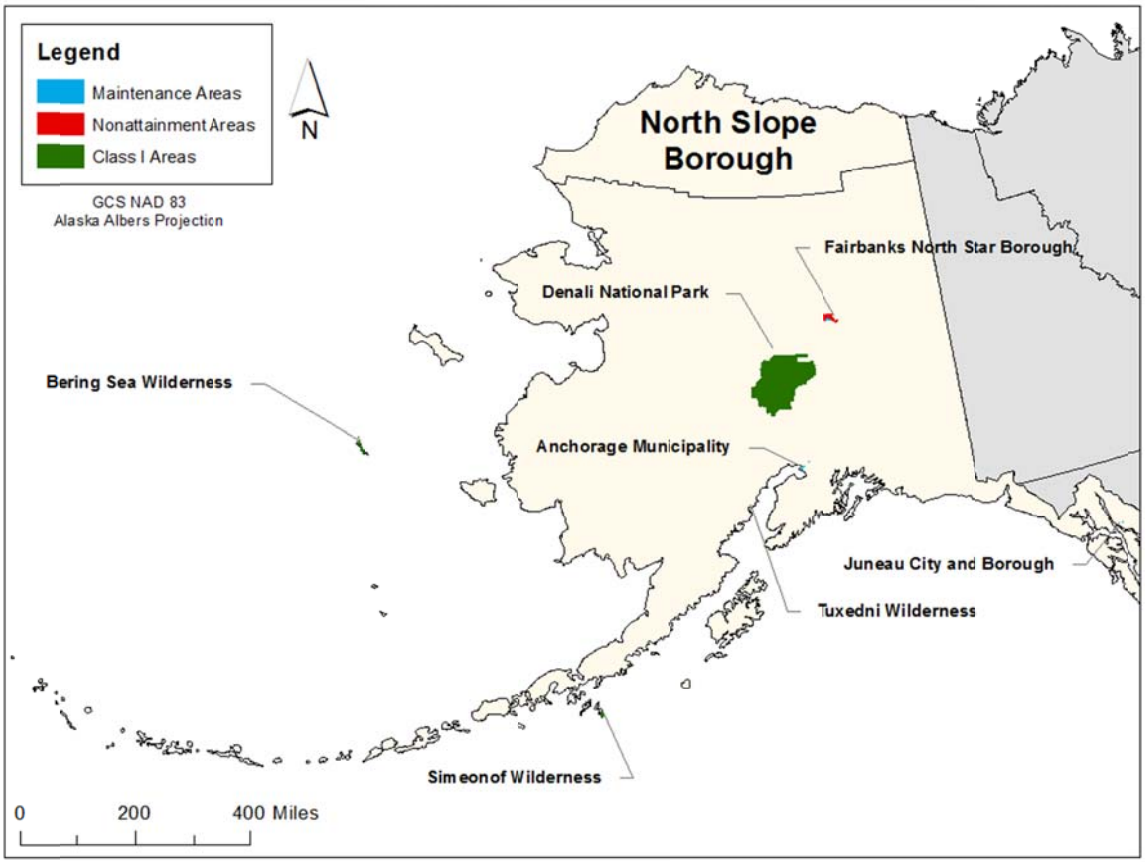

Figure 1-2. Alaska Maintenance, Nonattainment, and Mandatory Class I Areas.

Table 1-1. Current NAAQS and PSD increments.

Pollutant/Indicator		Averaging Time	NAAQS Level[a]	Class I Area PSD Increment[b]	Class II Area PSD Increment[b]
Photochemical Oxidants/Ozone		8-hour	0.070 ppm 137 µg/m^3	-	
Carbon Monoxide		1-hour	35 ppm 40,000 µg/m^3	-	-
		8-hour	9 ppm 10,000 µg/m^3	-	-
Lead/Pb in Total Suspended PM		Rolling 3-month avg.	0.15 µg/m^3	-	-
Nitrogen Oxides/NO_2		1-hour	100 ppb 188 µg/m^3	-	-
		Annual	53 ppb 100 µg/m^3	2.5 µg/m^3	25 µg/m^3
Particulate Matter	$PM_{2.5}$	24-hour	35 µg/m^3	2 µg/m^3	9 µg/m^3
		Annual	12 µg/m^3	1 µg/m^3	4 µg/m^3
	PM_{10}	24-hour	150 µg/m^3	8 µg/m^3	30 µg/m^3
		Annual	-	4 µg/m^3	17 µg/m^3
Sulfur Oxides/SO_2		1-hour	75 ppb 196 µg/m^3	-	-
		3-hour	-	25 µg/m^3	512 µg/m^3
		24-hour	-	5 µg/m^3	91 µg/m^3
		Annual	-	2 µg/m^3	20 µg/m^3

[a] Source:40 CFR 50

[b] Source:40 CFR 51.166

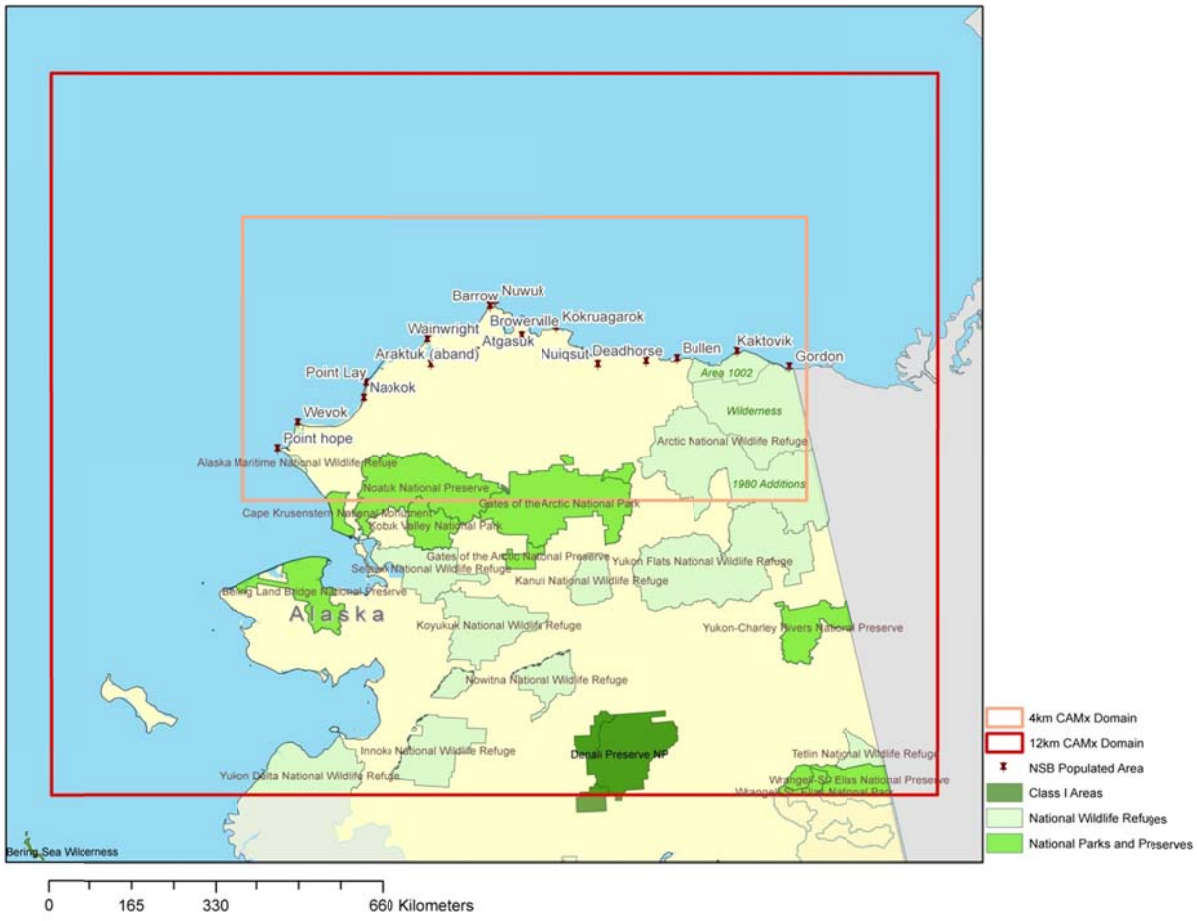

Figure 1-3. Class I and specified Class II areas designated as national parks, national preserves, and national wildlife refuges within the 4 and 12 km modeling domains (see discussion of domains in Section 4).

Table 1-2. Class I and specified Class II areas designated as national parks, national preserves, and national wildlife refuges.

Area	Administrative Agency	Type	Modeling Domain
Denali National Park	NPS	ClassI	12 km
Denali National Preserve	NPS	ClassI	12 km
Bering Land Bridge National Preserve	NPS	Class II	12 km
Cape Krusenstern National Monument	NPS	Class II	12 km, 4 km

Area	Administrative Agency	Type	Modeling Domain
Gates of the Arctic National Park	NPS	Class II	12 km, 4 km
Gates of the Arctic National Preserve	NPS	Class II	12 km, 4 km
Kobuk Valley National Park	NPS	Class II	12 km, 4 km
Noatak National Preserve	NPS	Class II	12 km, 4 km
Wrangell-St. Elias National Park	NPS	Class II	12 km
Wrangell-St. Elias National Preserve	NPS	Class II	12 km
Yukon-Charley Rivers National Preserve	NPS	Class II	12 km
Alaska Maritime National Wildlife Refuge	USFWS	Class II	12 km, 4 km
Arctic National Wildlife Refuge - Area 1002	USFWS	Class II	12 km, 4 km
Arctic National Wildlife Refuge - Wilderness	USFWS	Class II	12 km, 4 km
Arctic National Wildlife Refuge - 1980 Additions	USFWS	Class II	12 km, 4 km
Innoko National Wildlife Refuge	USFWS	Class II	12 km
Kanuti National Wildlife Refuge	USFWS	Class II	12 km
Koyukuk National Wildlife Refuge	USFWS	Class II	12 km
Nowitna National Wildlife Refuge	USFWS	Class II	12 km
Selawik National Wildlife Refuge	USFWS	Class II	12 km
Tetlin National Wildlife Refuge	USFWS	Class II	12 km
Yukon Delta National Wildlife Refuge	USFWS	Class II	12 km
Yukon Flats National Wildlife Refuge	USFWS	Class II	12 km, 4 km

2.0 METEOROLOGY

Meteorological datasets required to determine the rate that pollutants disperse and react in the atmosphere include spatially and temporally varying parameters such as wind speed, wind direction, air temperature, and humidity, among others. Sources of meteorological information include datasets of measurements gathered at various locations within the study area. However, the spatial coverage of measurements is insufficient to describe the three-dimensional structure of the atmosphere away from measurement locations. Using measurement data as inputs, gridded meteorological models capable of simulating the fluid dynamics of the atmospheric can be used to estimate meteorological conditions over a complete modeling domain—including regions far from measurement sites—in a physically consistent fashion. Results of these meteorological models provide the inputs needed to exercise the photochemical grid air quality dispersion models used in this Study. For this Study, the Advanced Research version of the Weather and Research Forecasting (WRF) model (version 3.6.1) was applied over a system of nested modeling grids. Figure 2-1 shows the WRF modeling grids at horizontal resolutions of 36, 12, and 4 km. All WRF grids were defined on a Polar secant Stereographic projection (PSP) centered at 70°N, 155°W with true latitudes at 70°N. The 4 km resolution domain is centered on the Northern Alaska coast, the 12 km domain encompasses most of Alaska and the Beaufort and Chukchi Seas and the extended 36 km domain is designed to capture synoptic scale features.

WRF was run on the 36, 12 and 4 km grids simultaneously with one-way nesting, meaning that meteorological information flows down-scale via boundary conditions (BCs) introduced from the respective coarser grid. The WRF modeling domain was defined to be slightly larger than the CAMx/CMAQ PGM modeling domains (described in Section 4) to eliminate boundary artifacts in the meteorological fields. Such boundary artifacts occur for both numerical reasons (the 3:1 grid spacing ratio) and because the imposed BCs require some time/space to come into dynamic balance with WRF's atmospheric equations. All meteorological modeling domains, techniques, inputs, vertical resolution, parameters, nudging, physics options, and application strategy along with quantitative and qualitative evaluation procedures and statistical benchmarks are discussed in the WRF modeling analysis conducted for the Arctic Air Quality Modeling Study (Brashers et al., 2015).

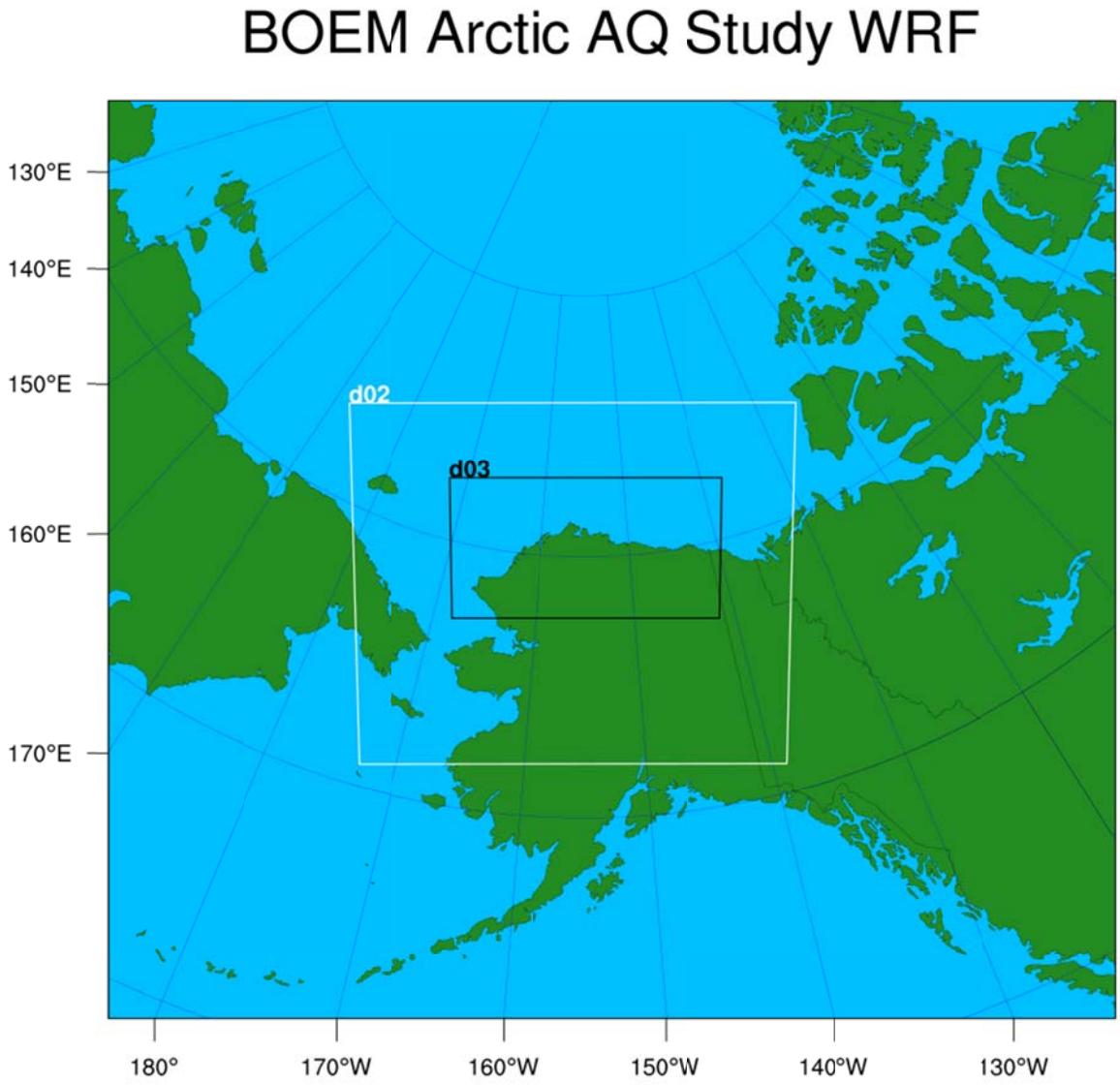

Figure 2-1. BOEM Arctic WRF Domains, 36 km (full plot), 12 km (d02) and 4 km (d03) grid resolution.

3.0 EMISSIONS INVENTORY

3.1 NSB, Chukchi and Beaufort Sea Anthropogenic Emissions

Anthropogenic emissions data for the NSB and adjacent State and Federal waters used in the photochemical modeling were obtained from the Arctic AQ Study Emissions Inventory which was developed under Task 3 of the Arctic AQ Modeling Study (Fields Simms et al., 2014). Anthropogenic sources of emissions include stationary point and area sources located in North Slope communities and oil fields, on-road motor vehicles, nonroad equipment, marine vessels and other offshore (oil and gas-related) sources in near shore (State) waters and in the Alaska OCS region, airports, and unpaved road dust for portions of the Dalton Highway and other roads located in communities and the oil fields. Point source locations are defined in the inventory by latitude and longitude coordinates. All other sources are attributed to an area or lines and will be documented in GIS shapefiles. This inventory is described in detail in the Arctic Air Quality Modeling Study: Emissions Inventory – Final Task Report (Fields Simms et al., 2014).

Under Task 3, ERG estimated emissions for a base case and a future year scenario. The base case scenario is representative of the emissions from sources for which the most recent credible relatable information was available (generally 2011 or 2012). The future year emissions inventory covers sources and activities that are reasonably foreseeable and may potentially be expected to continue for an extended period of time. The projections reflect a future scenario as defined by BOEM (BOEM, 2014) which represents a "full build-out". This scenario includes anticipated increases in future emissions from all stages of oil production (e.g., seismic surveys, exploratory drilling, platform construction, pipe laying, and active production platforms) that may potentially occur in support of a projected annual production of approximately 200 million barrels of oil (MMbbl) per year from each of the Chukchi and Beaufort Seas. The projections also include potentially anticipated increases in future emissions from certain onshore sources (e.g., construction emissions, new processing plants, and increased fugitive emissions from pipelines). Sources not affected by the full build-out scenario are held constant from the baseline. The future year emissions scenario represents a set of conditions and emissions that are not representative of any specific future year. Because all construction activity emissions are included along with the operational emissions for the new sources, the future year full build-out scenario is truly 'theoretical' and not representative of actual emissions that would occur in any given year.

New sources in the projected inventory include six offshore drilling sites (two sites in the Chukchi Sea, and four sites in the Beaufort Sea) and the construction of Liberty (gravel) Island. The initial estimated locations of these sources, as provided by BOEM (BOEM, 2014), are shown in Figure 3-1. The placement of onshore sources was determined by ERG in consultation with BOEM.

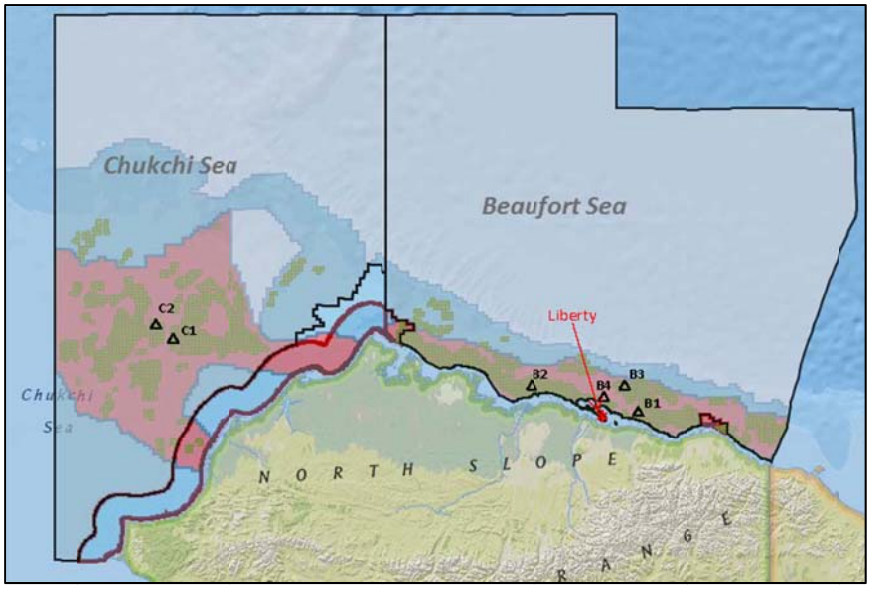

Figure 3-1. Initial placement of new offshore sources.

3.2 Anthropogenic Emissions outside the NSB

Anthropogenic emissions for all of Alaska except the areas covered by the Arctic AQ Emission Inventory described in Section 3.1 above were obtained from the 2011 National Emissions Inventory (NEI) version 2 (U.S. EPA, 2015). On-road annual emissions were pre-calculated and obtained directly from the NEI (i.e., no detailed SMOKE-MOVES[1] processing was performed). These year-2011 emissions were used without modification in both the base case and future year scenarios. Ancillary inputs for emissions processing were based on the U.S. EPA's 2011 NEI modeling platform version 6.2 (2011v6.2 platform) with modifications as needed. For example, spatial surrogates were recreated in the required Polar Stereographic projection for emissions modeling.

Anthropogenic emissions for portions of Canada included in the modeling domain were obtained from the U.S. EPA 2011-based modeling platform version 6.2 (2011v6.2). The Canadian emissions are for year 2010 and were originally generated by Environment Canada. The inventory consists of area, point and on-road source categories. Ancillary inputs were based on the U.S. EPA's 2011v6.2 modeling platform.

Anthropogenic emissions outside of the United States and Canada were obtained from the GEOS-Chem global model. These emissions are based on various inventories (e.g., anthropogenic volatile organic compound [VOC] emissions are based on RETRO inventory[2] and

[1] SMOKE-MOVES is a version of EPA's MOVES on-road mobile source emissions model that is integrated with the SMOKE emissions processing system (http://www.smoke.model.org) used to prepare model-ready emissions for this study.

[2] http://wiki.seas.harvard.edu/geos-chem/index.php/Implementation_of_RETRO_Anthropogenic_Emissions

other pollutants are based on EDGAR inventory.[3]) These inventories provide global anthropogenic emissions by sector, both at country and regional levels, as well as in gridded format. The global gridded inventories were re-projected to the modeling grids used for this study.[4] Available scaling factors[5] were applied to project the 2005 EDGAR emissions to 2010; no projections were applied to the 2000 RETRO inventory as projection factors are not available. Emissions were temporally allocated to get hourly emissions using temporal profiles from GEOS-Chem. Since the EDGAR and RETRO inventories did not provide any information about vertical distribution, Ramboll Environ used vertical layer distribution profiles for each source sector from the AQMEII study (Nopmongcol, et al., 2011). Next, the SMOKE LAYALLOC utility was used to allocate emissions vertically into modeling layers using these profiles.

3.3 Biogenic Emissions

Biogenic emissions were generated using MEGAN version 2.03, developed at the National Center for Atmospheric Research (Sakulyanontvittaya et al., 2008). The MEGAN model is preferable to the U. S. EPA BEIS biogenic emissions model for use in photochemical modeling because it incorporates more recent information (as explained in the next paragraph) and has a better classification of plant species. MEGAN is publicly available and can be downloaded from the Washington State University website (http://lar.wsu.edu/megan/guides.html) with no costs or restrictions.

Biogenic emissions depend critically upon landuse/landcover input data. Biogenic VOC and NO_x emissions vary considerably on spatial scales ranging from a few meters to thousands of kilometers. The MEGAN model accounts for this variability with high resolution estimates of vegetation type and quantity. The MEGAN landcover variables include total Leaf Area Index (LAI), tree fraction and plant species composition. These variables are determined based on satellite observations, such as 2003 1 km^2 Moderate Resolution Imaging Spectroradiometer (MODIS) and 30 m resolution LANDSAT data (Guenther et al., 2006; Sakulyanontvittaya et al., 2008). Additionally, biogenic VOC and nitric oxide (NO) emissions vary considerably on spatial scales ranging from a few meters to thousands of kilometers. The MEGAN model accounts for this variability with high resolution estimates of vegetation type and quantity. MEGAN driving variables are weather data, LAI, plant functional type (PFT) cover and compound-specific emission factors that are based on plant species composition. The data for all of these variables are available at various temporal scales and are provided in a geo-referenced gridded database in several formats (e.g., netcdf, ESRI GRID). The MEGAN database has global coverage at 30 seconds (roughly 1 km) spatial resolution.

Ramboll Environ applied the MEGAN model using the specific hourly meteorology (e.g., temperature and solar radiation) extracted from the 2012 WRF model outputs to generate day-specific biogenic emissions for the 2012 calendar year in the 36, 12 and 4 km PGM modeling

[3] http://wiki.seas.harvard.edu/geos-chem/index.php/EDGAR_v4.2_anthropogenic_emissions

[4] The RETRO inventory has a horizontal grid resolution of 0.5 x 0.5 degrees; the EDGAR inventory has a horizontal grid resolution of 0.1 x 0.1 degrees.

[5] http://wiki.seas.harvard.edu/geos-chem/index.php/Organics_Working_Group#GEIA_anthropogenic_scaling_factors

domains. Total biogenic VOC emissions over the 4 km domain were calculated to be 150,967 tons per year (tpy) or an average of 0.6 tpy/km^2 when averaged over all grid cells with non-zero biogenic emissions (i.e., ignoring water areas). Of this total, 45% by mass was methanol, 21% isoprene, 19% terpene, and 14% other VOCs. This is in contrast to, for example, the composition of biogenic VOCs recently estimated using MEGAN for the western Gulf of Mexico coastal area including southeast Texas, Louisiana and southern portions of Mississippi and Alabama along with a portion of the Florida Panhandle. For this region, biogenic VOC emissions averaged 8.6 tpy/km^2 of which isoprene was the most abundant VOC at 49%, and methanol was the second most abundant at 18%, and terpene was 16%. Thus, the biogenic VOC emissions density is more than 10 times lower in Alaska than in the Gulf of Mexico region and emissions in Alaska are substantially less reactive given the much greater reactivity of isoprene as compared to methanol.

3.4 Fire Emissions

Wildfire emissions are highly episodic and very location specific. Using annual average fire emissions and temporally and spatially allocating these emissions using generic allocation schemes would result in considerable inaccuracies in the modeling results. For this study, forest fire emissions were based on 2012 calendar year estimates of fire emissions from the National Center for Atmospheric Research (NCAR) derived from analysis of fire locations determined by satellite borne detectors. Ramboll Environ processed the day-specific Fire INventory from NCAR (FINN)[6] to develop "point sources" of fire emissions using plume rise estimates as a function of fire size from the Western Regional Air Partnership's (WRAP) Joint Fire Science Program's Deterministic and Empirical Assessment of Smoke's Contribution to Ozone ($DEASCO_3$) project. A description of the WRAP 2002 fire plume rise approach can be found in Mavko and Morris (2013).

MODIS instruments fly aboard two polar-orbiting satellites, Terra and Aqua. As these two satellites orbit the Earth, traveling from pole to pole while the earth rotates beneath them, a given area of the Earth will experience an overpass from Terra and Aqua approximately twice a day. MODIS instruments detect fires as thermal anomalies (i.e., hot spots seen against a cooler background) at a spatial resolution of approximately 1 km. Fire emissions derived from the MODIS data include NO_x, CO, VOC and PM species. The NCAR fire emissions inventory development is described by Wiedinmyer et al., 2006; 2011, and Wiedinmyer and Friedli, 2007.

The NCAR satellite-derived fire emissions data for 2012 contains daily fire emission locations, acreage burned and fuel loading at a resolution of 1 km^2, representing the size of each satellite pixel. SMOKE does not have the capability to handle this type of inventory. Therefore, the fire inventory was processed using the Emissions Processing System version 3 (EPS3). Similar to SMOKE, the EPS model can perform the intensive data manipulations required to incorporate spatial, temporal, and chemical resolution into an emissions inventory used for photochemical modeling. Two EPS modules, PREFIR and PSTFIR, were developed specifically to handle point source fire emissions. These modules allow EPS to treat fire emissions from many data sources including satellite-derived fire emissions. Fire emissions modeling has been conducted using this approach for a number of regional modeling studies e.g. Texas Commission on

[6] https://www2.acom.ucar.edu/modeling/finn-fire-inventory-ncar

Environmental Quality (TCEQ; Tai et al., 2008).

Each fire record was treated as a point source and emissions were distributed vertically into multiple model layers to better represent each fire plume. The chemical speciation profile for the MODIS fire emissions was derived from a study on biomass burning (Karl et al., 2007).

3.5 Sea Salt Emissions

Ramboll Environ used an emissions processor that integrates published sea spray flux algorithms to estimate sea salt PM emissions for input to CAMx. The gridded data for input to the sea salt emissions model are a land-water mask file that identifies each modeling domain grid cell as either open ocean, surf zone, or land (Morris et al., 2012) which originated from the shape file that CMAQ uses to maintain consistency between the two models. The CAMx sea salt emissions processor was used with the 2012 WRFCAMx 3D data to calculate wind speed at the 10 m reference height. To account for the presence of sea ice, WRFCAMx 2D data were used to identify sea ice coverage in each model grid cell and the sea salt processor was modified to reduce emissions proportional to the fractional ice coverage.

The CMAQ model includes inline calculation of sea-salt emissions from the open ocean and coastal surf zone so no pre-processing of sea salt emissions is needed but CMAQ requires an ocean mask file that indicates areas of open ocean and surf zone. For modeling domains without sea ice, a single ocean mask file can be used. For this project, however, it was necessary to produce a different ocean mask file for each day of the year to properly represent sea ice coverage. Each ocean mask file was made by reading the SEAICE variable provided by MCIP METCRO2D file to allow for the impact of sea ice on sea salt emissions to be taken into account.

The sea salt emissions developed by Ramboll Environ using the above methods were used to generate the model results described in Section 7. However, there are considerable uncertainties in these sea salt emission estimates which are potentially important in mediating certain atmospheric chemistry processes in the relatively pristine coastal and near-coastal environments characterizing much of the Arctic modeling domain. Therefore, Ramboll Environ also conducted a sensitivity analysis designed to evaluate the influence of sea salt emission uncertainties on modeled anthropogenic source impacts. The sea salt uncertainty analysis is described in Section 8.

3.6 Lightning

NO_x is formed in lightning channels as the heat released by the electrical discharge causes the conversion of nitrogen (N_2) and oxygen (O_2) to NO. Modeling of lightning and its emissions is an area of active research. For example, the mechanism for the buildup of electric potential within clouds is not well understood, and modeling the production, transport and fate of emissions from lightning is complicated by the fact that the cumulus towers where lightning occurs may be sub-grid scale depending on the resolution of the model. Given the importance of lightning NO_x in the tropospheric NO_x budget and in understanding its effect on upper tropospheric ozone and OH-, lightning NO_x is typically incorporated in global modeling (e.g.; Tost et al., 2007; Sauvage et al., 2007; Emmons et al., 2010), and has also been integrated into many regional modeling studies (e.g., Allen et al., 2012; Koo et al., 2010).

For the CMAQ modeling, Ramboll Environ used in-line lightning NO_x emissions derived from the convective precipitation rate provided in the MCIP files (see Section 4.3). Since the CMAQ

model includes inline calculation of lightning NO_x emissions, no pre-processing of lightning NO_x is needed. The CAMx model requires pre-calculated lightening emissions for input. To better facilitate comparisons with CMAQ, lightning NO_x emissions from the CMAQ modeling were output and converted into a format suitable for use in CAMx.

3.7 Emissions Processing for Preparation of Model-Ready Emissions

Anthropogenic emissions inventories discussed in the previous section and other data were used to prepare PGM model-ready emission files using the Sparse Matrix Operator Kernel Emissions (SMOKE) system version 3.6 and other methods as described below. The inventories were processed through SMOKE to develop hourly, gridded, and speciated emissions required for input to the PGM models at 36, 12 and 4 km grid resolutions. During emissions processing, annual emissions inventories were speciated to model species, temporally allocated to hourly emissions, and spatially allocated to grid cells.

The latest Carbon Bond 6 revision 2 (CB6r2) photochemical mechanism with active local methane emissions chemistry was used for the CAMx modeling whereas the Carbon Bond 5 (CB05) with updated toluene and chlorine chemistry photochemical mechanism was used for the CMAQ modeling, and emissions were processed accordingly. CMAQ versions 5.0 and later contain a thermodynamic equilibrium aerosol mechanism (ISORRPIA v2) that requires detailed speciation of $PM_{2.5}$. This involves splitting PMFINE into additional elemental components.

The SMOKE emissions model was used to perform the following tasks:

- Spatial Allocation: Spatial surrogates contained in the U.S. EPA 2011v6.2 modeling platform were used to spatially distribute emissions to modeling grid cells. Spatial surrogates are generated by overlaying the PGM modeling grid on maps of geospatial indicators appropriate to each source category (e.g., housing units). The Surrogate Tool, a component of U.S. EPA's Spatial Allocator system, was used to calculate the fraction of geospatial indicator coverage in each model grid cell.
- Temporal Allocation: Air quality modeling systems, such as CMAQ and CAMx, require hourly emissions input data. With the exception of a few source types (i.e., Continuous Emissions Monitoring data, biogenic emissions, and some fire inventories), most inventory data are estimated in the form of annual or daily emissions. SMOKE was used to allocate annual emissions to months and across the diurnal cycle to account for seasonal, day-of-week and hour-of-day effects. Temporal profiles and Source Classification Code (SCC) cross references from the 2011v6.2 modeling platform were used to incorporate seasonal and monthly variations into the development of the PGM model-ready emissions.
- Chemical Speciation: The emissions inventories for the Arctic Air Quality Modeling Study included the following pollutants: CO, NO_x, VOC, NH_3, SO_2, PM_{10}, $PM_{2.5}$, and greenhouse gasses (CO_2, CH_4, N_2O; included for reporting purposes). Ramboll Environ used SMOKE to convert inventoried VOC emissions into the CB6r2 photochemical mechanism model species. Chemical speciation profiles were assigned to inventory sources using cross-referencing data that match the profiles and inventory sources using Federal Information Processing System (FIPS) country/state/county codes and source classification codes (SCCs). Ramboll Environ used NO_x, VOC and PM speciation profiles from the 2011v6.2 platform for SMOKE processing. In the 2011v6.2 platform, U.S. EPA generated emissions for Carbon Bond version 6 revision 2 (CB6r2) chemical mechanism used by CAMx. In

addition, this platform generates the $PM_{2.5}$ model species associated with the CMAQ Aerosol Module, version 6 (AE6). SMOKE also applied source-specific speciation profiles to convert inventoried NO_x emissions to NO, SO_2, and HONO components. After SMOKE processing, Ramboll Environ applied necessary species mapping to prepare CMAQ-ready emissions in CB05/AE6 terms and CAMx-ready emissions in CB6r2/CF terms. Note that CB6r2 chemistry also models local excess methane (ECH4) from anthropogenic sources above background concentrations. Sea salt emissions from ocean portions of the modeling domain were also generated for CAMx as described in Section 3.4 above.

3.8 QA/QC

Emissions were processed by major source category in several different processing "streams" to simplify the emissions modeling process and facilitate the QA/QC of results. SMOKE includes QA and reporting features to keep track of the adjustments at each step of emissions processing and to ensure that data integrity is not compromised. Ramboll Environ carefully reviewed the SMOKE log files for noteworthy error messages and ensured that appropriate source profiles are being used. In addition, SMOKE output summary reports were reviewed and compared with input emission totals.

3.9 Development of CMAQ-ready Emissions

Each SMOKE processing stream generates a set of pre-merged model-ready emissions in CMAQ input format (I/O API). As specified in the chemical speciation section, species mapping was applied to convert SMOKE generated model species to the appropriate input for CMAQ. SMOKE modeling generated VOC model species for the CB6 chemical mechanism which were converted into CB05 model species for CMAQ. All pre-merged gridded emissions inputs were merged together to generate the final CMAQ-ready two-dimensional gridded low-level (layer 1) and point source emissions inputs. Distributed sources (mobile sources, area sources, natural emissions) were merged in developing the CMAQ-ready gridded emissions files, and point source emissions files for individual sources were used without being merged as CMAQ allows this.

3.10 Development of CAMx-ready Emissions

CAMx requires two types of emissions files, as described below, for every episode day; both the emission files are UAM-based Fortran binary files.

(1) Surface-level 2D emissions: this file contains two-dimensional gridded fields of low-level (i.e. surface) emissions rates for all emitted species to be modeled.
(2) Elevated point source emissions: the elevated point source emissions file contains stack parameters and emissions rates for all elevated point sources and emitted species to be modeled.

The merged two-dimensional gridded anthropogenic emissions in CMAQ format were converted into CAMx format using the CMAQ2CAMx program. Natural source categories (i.e., sea salt, biogenic, fires, and lightning) were then merged with the surface-level emissions using the MRGUAM processor to develop CAMx model-ready emissions. Model species were first converted from the CMAQ CB05TUCL-AE6 mechanism to the CAMx CB6r2-CF mechanism compatible form, and then the file format changed from CMAQ 2-D and in-line point emissions to CAMx area-/point-source emissions using the CMAQ2CAMx interface program. The point source emissions files in UAM-based binary format were merged together to develop the final

CAMx-ready point-source emissions. The elevated point source file is independent of the modeling grid, because it contains horizontal (X, Y) coordinates for each point source. Therefore, one file includes all point sources in the 12 and 4 km BOEM modeling grids. In addition, separate emissions inputs for source groups were prepared for use with the CAMx source apportionment modeling in the future year scenario to track the individual source groups.

3.11 Emissions Summaries

This section presents 2012 base case and future year scenario emissions summaries for the Arctic AQ Modeling Study area which includes sources in the NSB and sources in the adjacent State and Federal waters. Table 3-1 provides NO_x, VOC, SO_2, and $PM_{2.5}$ air pollutant emissions summary in short tons per year by source category. The summary data are based on SMOKE processing of 2012 base case and future year inventories as described above. With the exception of fires and biogenic sources, emissions are summarized from the SMOKE reports generated by the SMKMRG program. As noted above, biogenic and fire emissions were generated using the MEGAN model and fire emissions processor outside of SMOKE and so are generated directly on the 36, 12, and 4 km grids rather than by state/county. As a consequence, natural emissions in Table 3-1 are for the 4 km domain most of which covers the NSB but which also includes some adjacent areas.

Table 3-2 summarizes the changes in Arctic AQ Study emissions inventory between the base case and future year scenarios by major source category. Small increases are projected between the base case and future year scenarios in Baseline (i.e., existing) oil and gas (O&G) and other anthropogenic sources but by far the largest difference between the future year and base case scenarios is the introduction of new O&G sources in the future year scenario with total emissions that are on par with those from existing sources.

Biogenic and fire emissions representative of the 2012 base year are also used in the future year scenario. It should be recognized that, given the rapidly changing climatic conditions in the Arctic, biogenic and fire emissions based on 2012 conditions may not be reasonably representative of conditions too far into the future. Additional analysis may be needed to account for anticipated future trends in emissions from these natural sources.

Table 3-1. 2012 base case and future year emissions summary for selected pollutants by source category from the Arctic AQ Study emissions inventory (short tons per year).

Simplified Sector	2012 Base Year				Future Year			
	NO_x	$PM_{2.5}$	SO_2	VOC	NO_x	$PM_{2.5}$	SO_2	VOC
Baseline Other Anthropogenic	2,221	3,599	165	818	2,368	3,600	103	826
Baseline O&G	45,509	1,203	1,119	2,241	45,627	1,220	1,130	2,302
New O&G	-	-	-	-	30,751	1,433	1,955	1,769
Biogenic[a]	1,782	-	-	150,967	1,782	-	-	150,967
Fire[a]	482	1,207	88	392	482	1,207	88	392

[a] Biogenic and fire emissions are for the entire 4 km domain and are held constant between the base and future year cases. The assumption that biogenic emissions in future years will be approximately equal to those calculated for 2012 may only be valid for a limited future period given the impacts of current rapid climate change in the Arctic on plant communities and weather conditions.

Table 3-2. Changes in emissions between the 2012 base case and future year emissions (short tons per year) by source category.

Simplified Sector	Future Year - Base Year (TPY)				Future Year - Base Year (%)			
	NO_x	$PM_{2.5}$	SO_2	VOC	NO_x	$PM_{2.5}$	SO_2	VOC
Baseline Other Anthropogenic	146	1	-63	8	6.6%	0.0%	-37.9%	0.9%
Baseline O&G	117	17	12	61	0.3%	1.4%	1.0%	2.7%
New O&G	30,751	1,433	1,955	1,769	N/A	N/A	N/A	N/A
Biogenic[a]	-	-	-	-	-	-	-	-
Fire[a]	-	-	-	-	-	-	-	-

[a] Biogenic and fire emissions for the entire 4 km domain.

Figure 3-2 presents spatial plots over the 4 km domain of total NO_x, VOC, $PM_{2.5}$ and SO_2 emissions for the 2012 base year in short tons per year. The color scale on these figures was chosen to highlight key emission sources; small and diffuse (area) sources fall within the white range of the scale. The Dalton Highway is clearly visible in the $PM_{2.5}$ emissions map and the shipping lanes used by support vessels are visible in the SO_2 emissions map. The regular array of small sources in the NO_x emissions map reflects the spatial allocation of lightning NO_x emissions generated by the CMAQ in-line lightning NO_x processor. Anthropogenic NO_x sources can also be seen, especially in the area of Prudhoe Bay.

Figures 3-3a-d present, respectively, spatial distributions of NO_x, $PM_{2.5}$, SO_2, and VOC in short

tons per year for the future year scenario over the 4 km domain along with emissions difference plots between the future year and base case scenarios. Most of the emissions differences between the future and base year scenarios represent projected new offshore oil and gas sources included in the future year scenario. As in Figure 3-2, color scales have been chosen to best identify key features. In particular, the color scale for the future year NO_x emissions plot (top panel of Figure 3-3a) was chosen to make certain source categories which are represented as area sources visible. Note in particular that survey vessel emissions, which are represented as a mesh of line sources traversing the Beaufort Sea waters in the base year inventory (for which their transect line positions are known), are represented as a broad area source in the future year inventory because locations of future survey transects are not known. This results in the negative NO_x emissions seen in the difference plot in the bottom panel of Figure 3-3a – the more diffuse future year area source survey vessel emissions fall within the white portion of the color scale of the difference plot.

Figure 3-4 shows the spatial distribution of emissions from baseline (i.e., existing) oil and gas sources in the Arctic AQ Study inventory under the future year scenario. Most of the existing oil and gas activities are concentrated in the vicinity of Prudhoe Bay (including some offshore activity) with a few point sources in other locations in the NSB and some offshore survey and exploratory drilling activity in the Chukchi Sea northwest of Wainwright. Figure 3-5 shows the spatial distribution of emissions from non-oil and gas (i.e., other anthropogenic) baseline sources under the future year scenario. Offshore emissions from these sources represent vessel traffic such as fishing boats which are not part of any oil and gas activities. Figure 3-6 shows emissions for projected new oil and gas sources under the future year scenario. This primarily shows the locations of projected new offshore oil and gas activities. Common features between the bottom panels in Figure 3-3 and the corresponding panels in Figure 3-6 underscore the fact that nearly all of the emissions differences between the base year and future year scenarios are due to the new oil and gas sources.

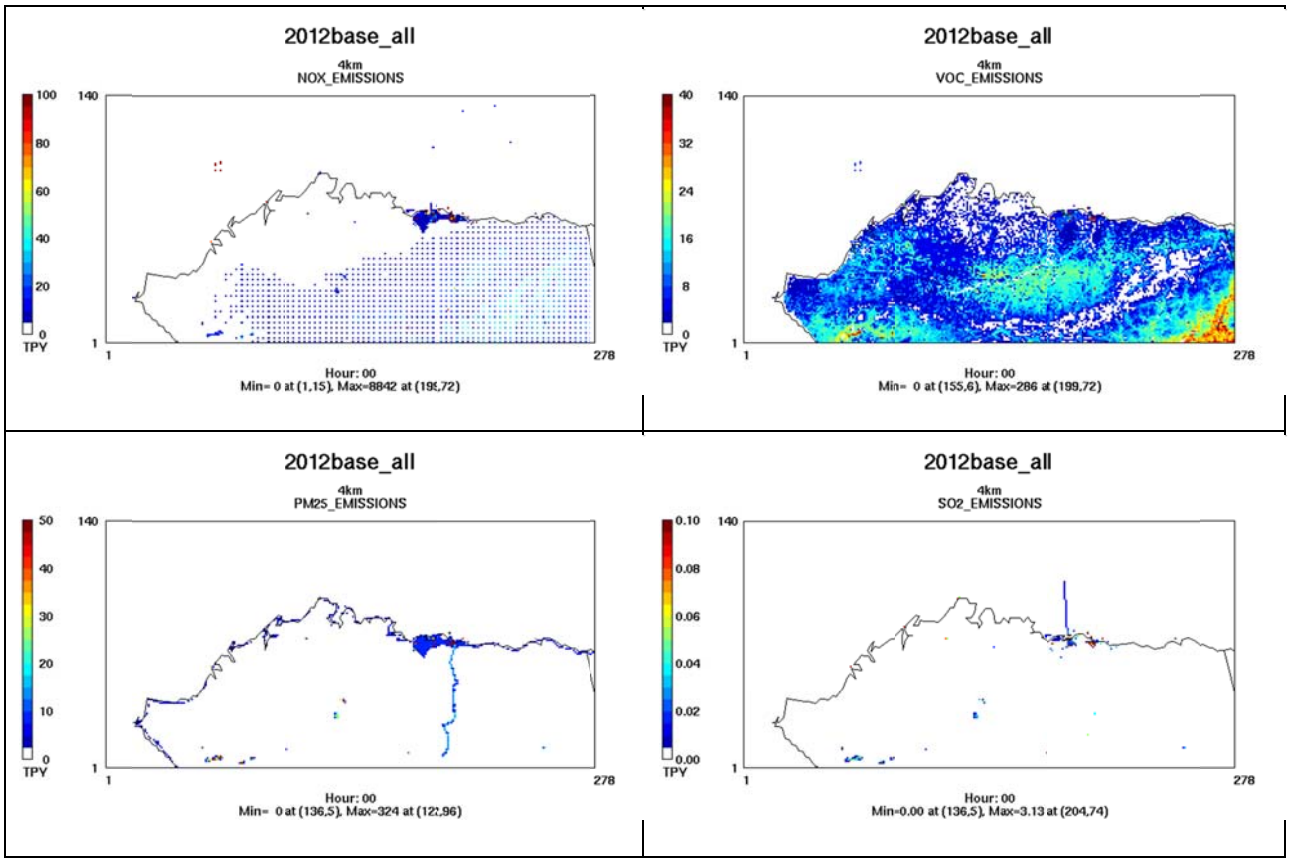

Figure 3-2. Spatial distribution of (clockwise starting from top left) NO_x, VOC, SO_2 and $PM_{2.5}$ emissions from all sources (tons per year) for the 2012 base case.

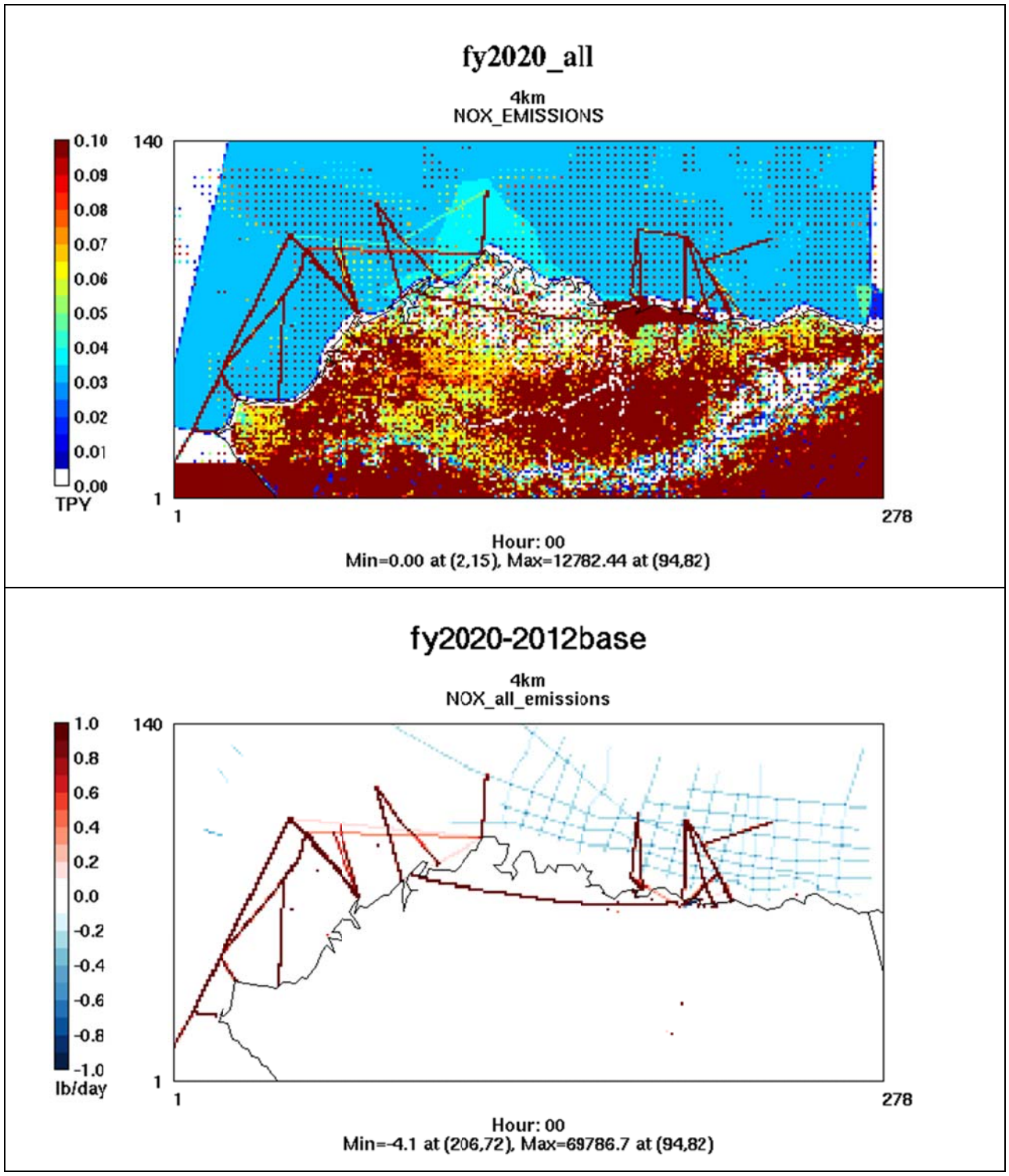

Figure 3-3a. Spatial distribution of NO_x emissions for the future year (top) and differences between the future year and 2012 base case scenarios (bottom).

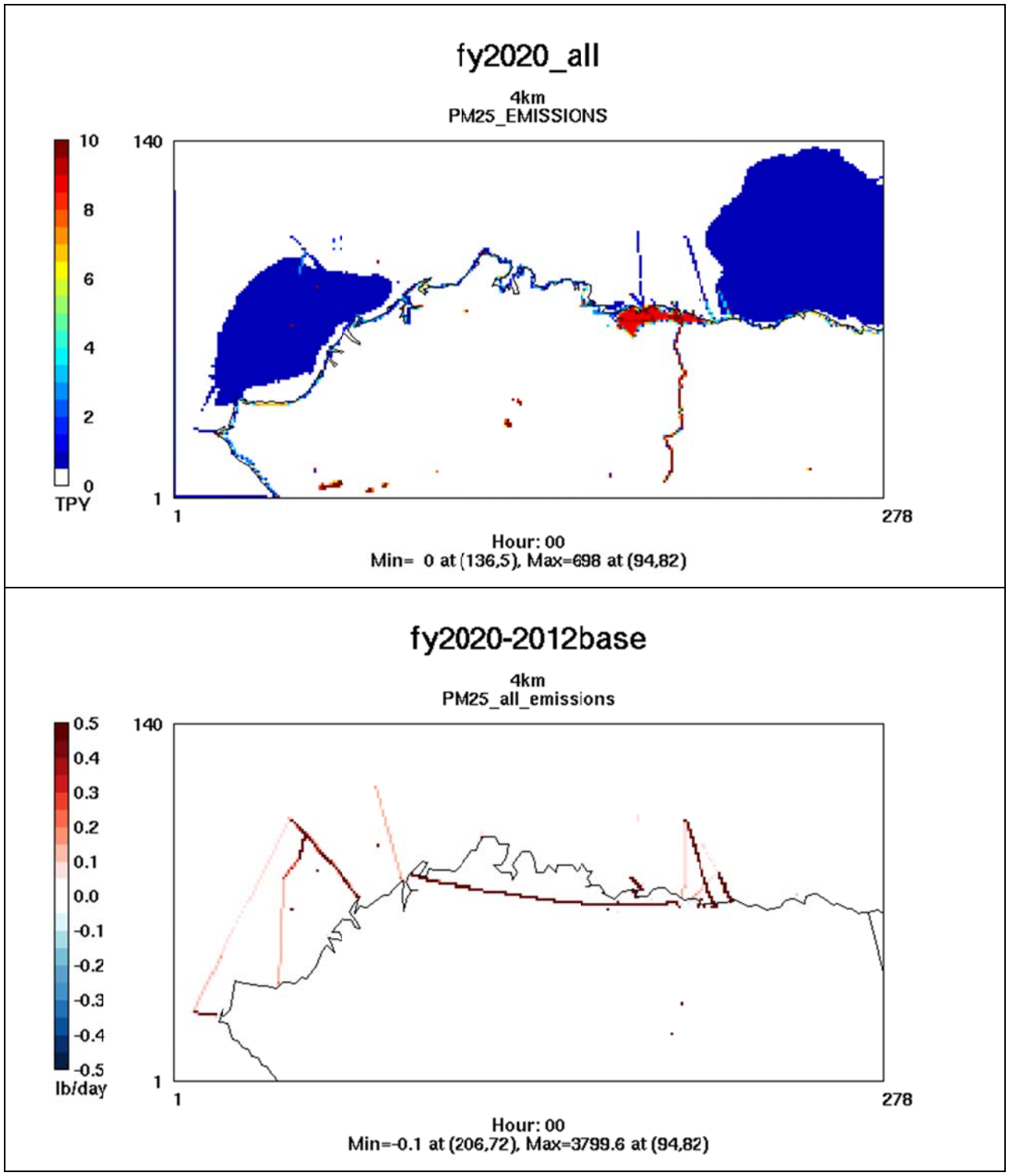

Figure 3-3b. Spatial distribution of $PM_{2.5}$ emissions for the future year (top) and differences between the future year and 2012 base case scenarios (bottom).

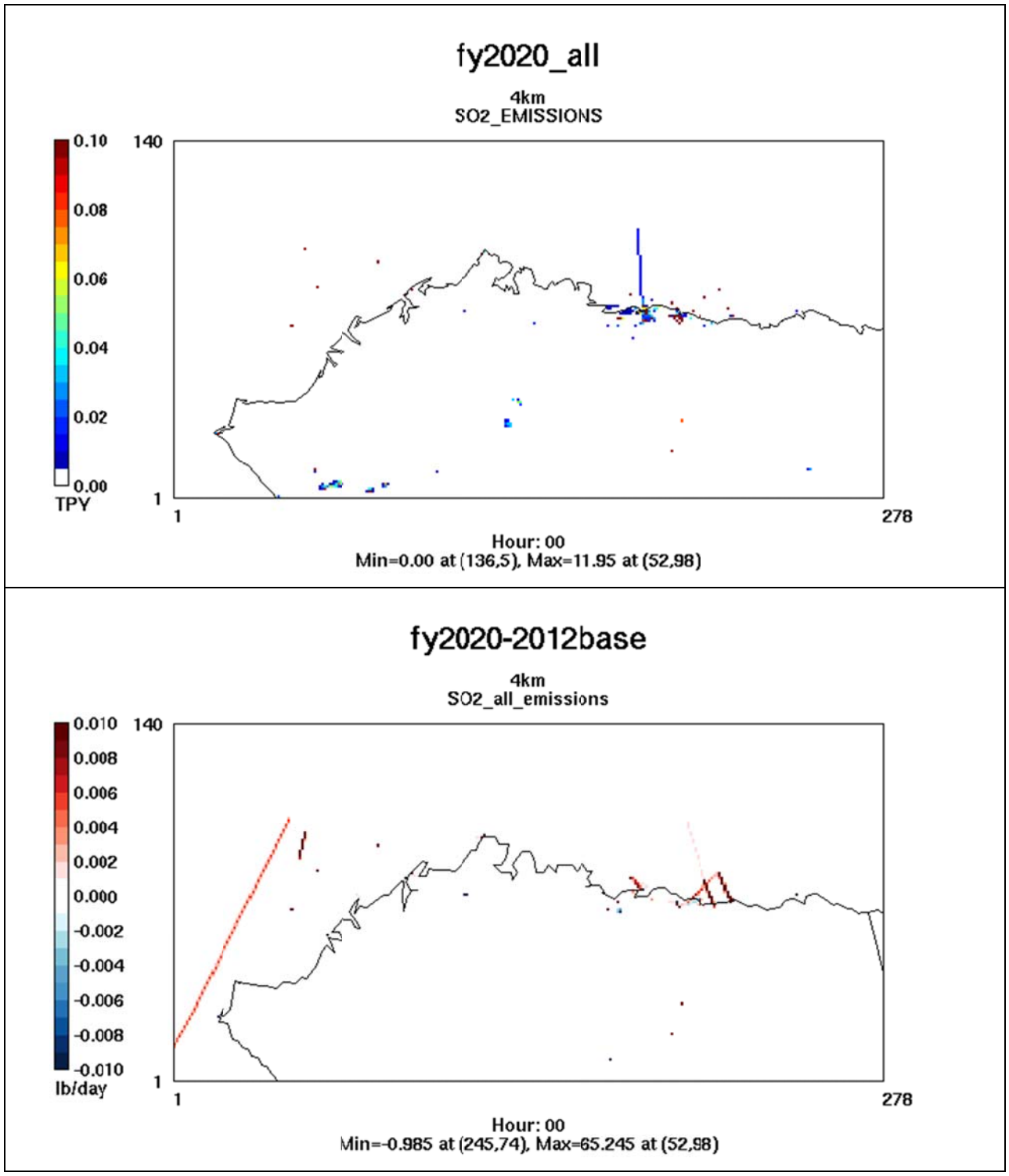

Figure 3-3c. Spatial distribution of SO_2 emissions for the future year (top) and differences between the future year and 2012 base case scenarios (bottom).

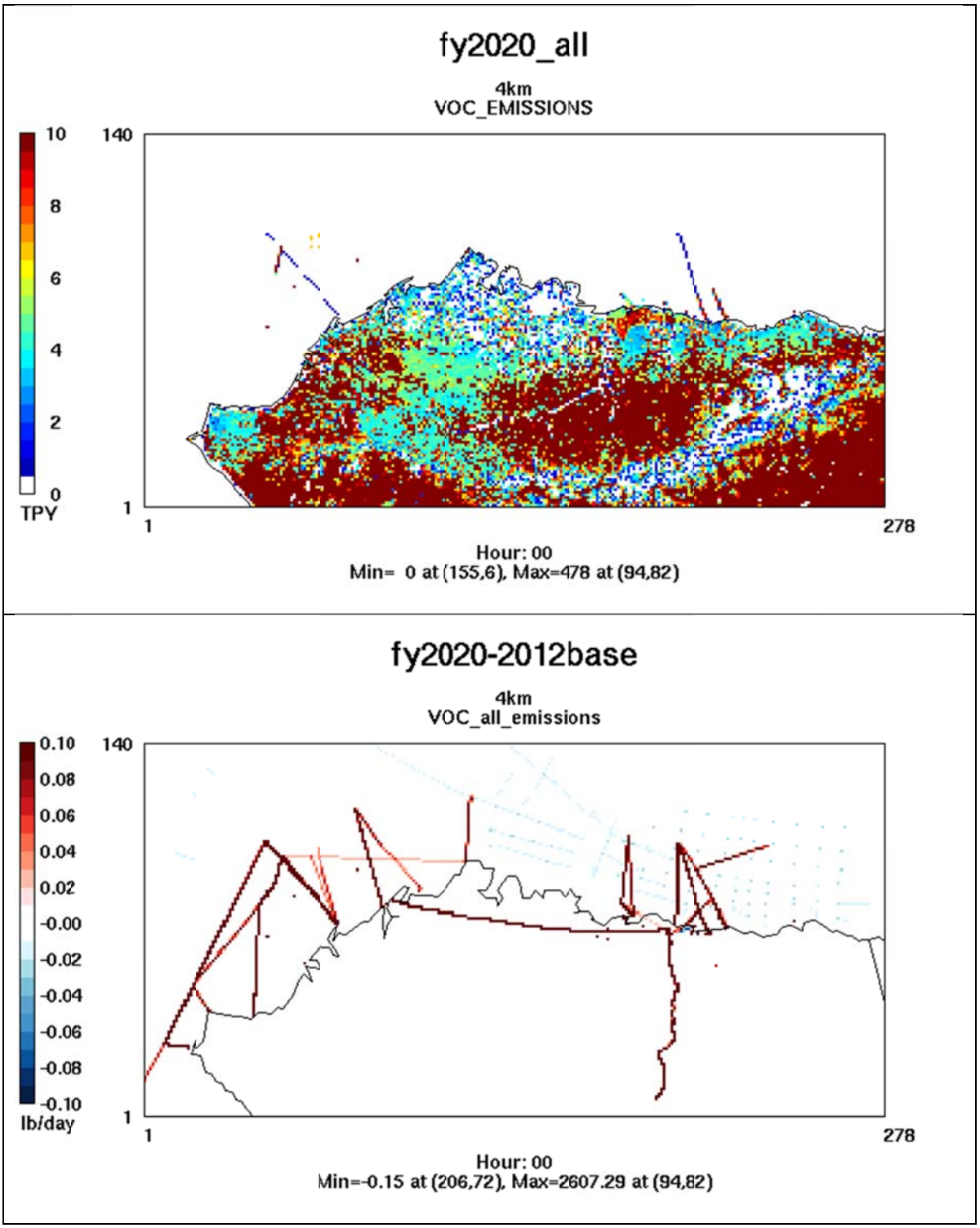

Figure 3-3d. Spatial distribution of VOC emissions for the future year (top) and differences between the future year and 2012 base case scenarios (bottom).

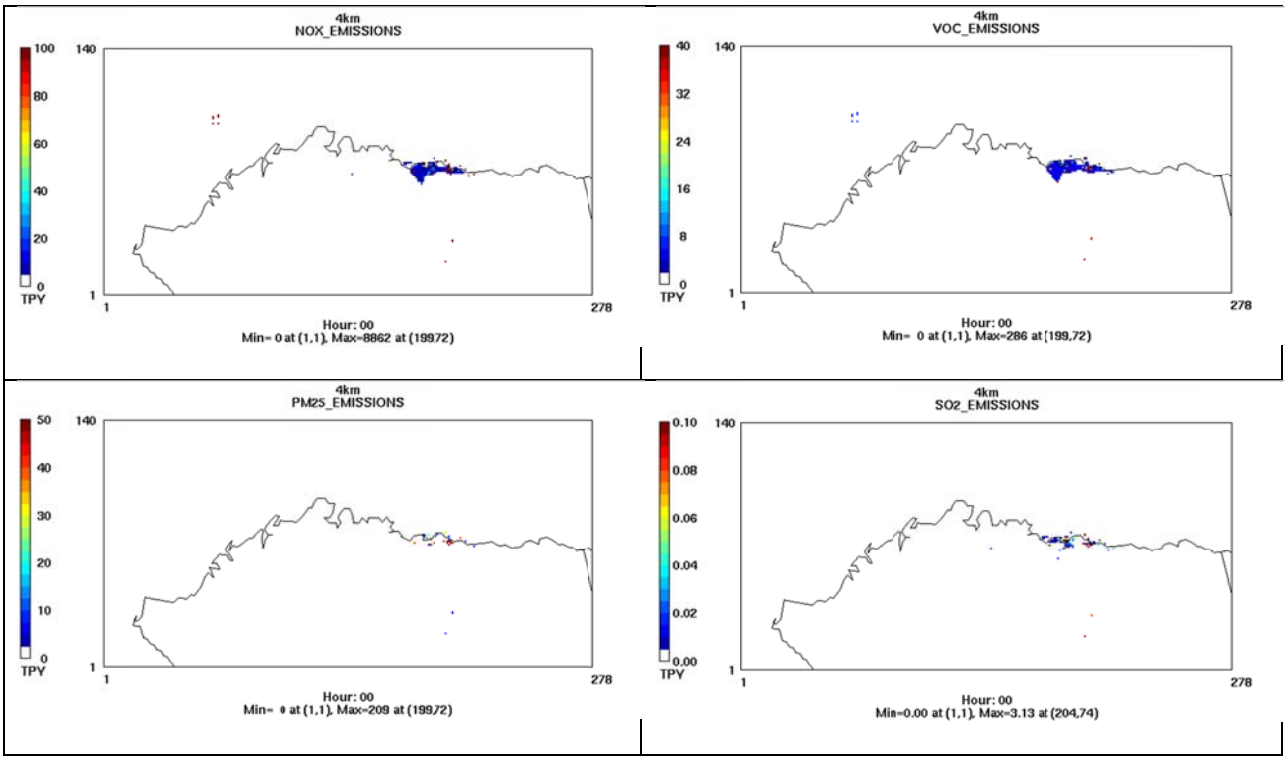

Figure 3-4. Spatial distribution of (clockwise starting from top left) NO_x, VOC, SO_2 and $PM_{2.5}$ emissions (tons per year) from baseline O&G sources under the future year scenario.

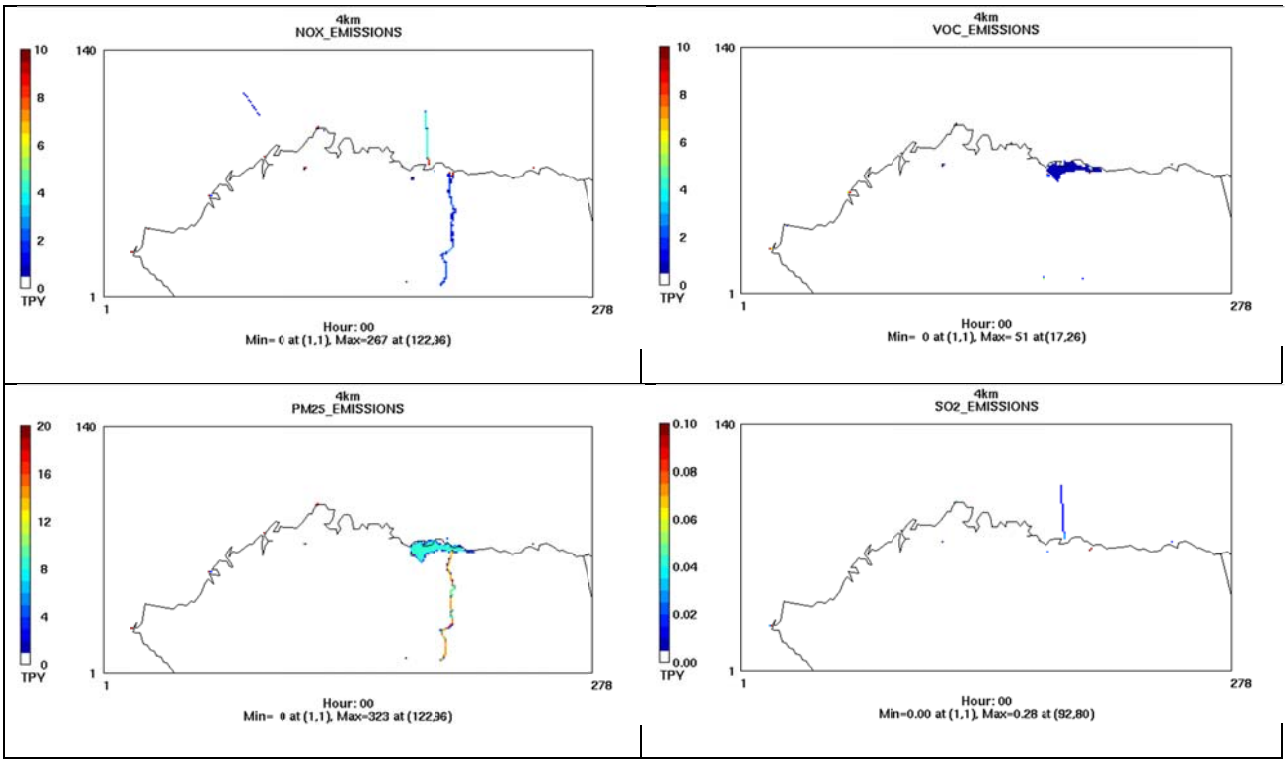

Figure 3-5. Spatial distribution of (clockwise starting from top left) NO_x, VOC, SO_2 and $PM_{2.5}$ emissions (tons per year) for baseline non-O&G (i.e., other anthropogenic) sources under the future year scenario.

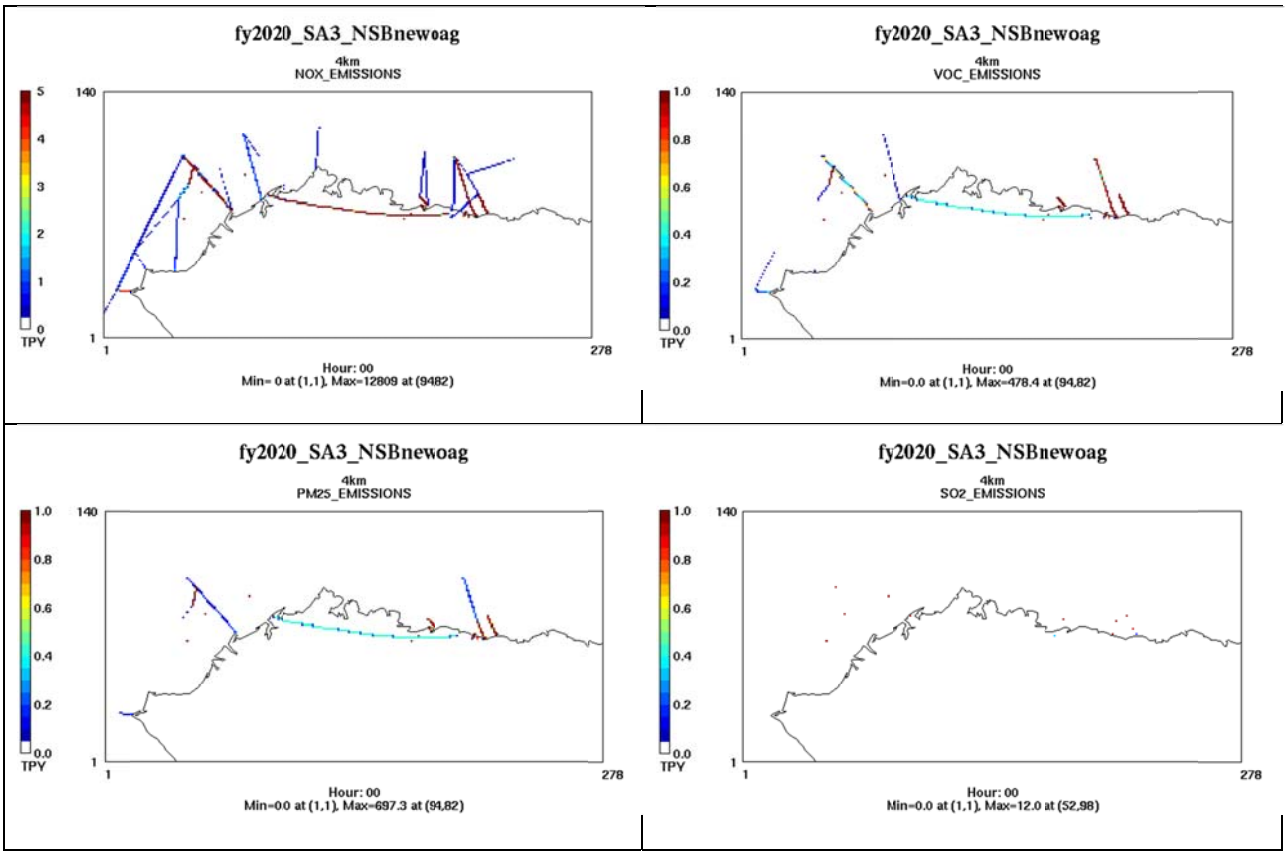

Figure 3-6. Spatial distribution of (clockwise starting from top left) NO_x, VOC, SO_2 and $PM_{2.5}$ emissions (tons per year) for new O&G sources in the future year scenario.

4.0 BASE CASE PHOTOCHEMICAL GRID MODELING

4.1 Overview

The CAMx Photochemical Grid Model (PGM) was applied on a set of nested domains with horizontal resolutions of 36, 12 and 4 km centered on the NSB (Figure 4-1). For the 2012 base case analysis, CAMx was run with the 2012 base case emissions described in Section 3. Meteorological fields required by CAMx were obtained from the WRF meteorological model results for 2012 which were developed as described in Section 2. Modeling procedures were based on the U.S. EPA's current and revised draft modeling guidance procedures (U.S. EPA, 2007; 2014). Additional features of the modeling approach used by Ramboll Environ are:

- Anthropogenic and non-anthropogenic model-ready emissions for the 2012 base case were developed as described in Section 3 and the Arctic Air Quality Modeling Study Emissions Inventory Report (Fields Simms et al., 2014).
- Photochemical grid modeling was based on CAMx version 6.20 with the Carbon Bond 6 revision 2 (CB6r2) photochemical mechanism including active excess methane emissions.
- An alternative PGM simulation was conducted using CMAQ version 5.0.2 with the Carbon Bond 2005 version with toluene and chlorine chemistry updates (CB05TUCL).
- Day-specific boundary conditions (BCs) for the lateral boundaries of the 36 km modeling domain were based on 2012 GEOS-Chem global chemistry model (GCM) output. A CMAQ test simulation using BCs derived from the MOZART-4/GEOS5 GCM was also conducted, and results compared with a CMAQ simulation using GEOS-Chem BCs.
- A model performance evaluation was conducted using available ambient monitoring data to assess the reliability of model results over areas without monitoring data in the base case and predicted impacts of changes in emission in the future year scenario. Results of the model performance evaluation are presented in Section 5.

4.2 Model Grid Configuration

The PGM domain configuration is comprised of a system of nested grids with 36, 12, and 4 km horizontal resolution as shown in Figure 4-1. Table 4-1 provides the modeling grid definitions for the PGM simulations. A more detailed view of the 4 km resolution grid is shown in Figure 4-2, together with information about the spatial locations of sources in the Arctic Air Quality Study emissions inventory. As shown in this figure, the 4 km domain encompasses all of the onshore NSB sources and also includes offshore sources out to a distance of roughly 200 km or more from shore.

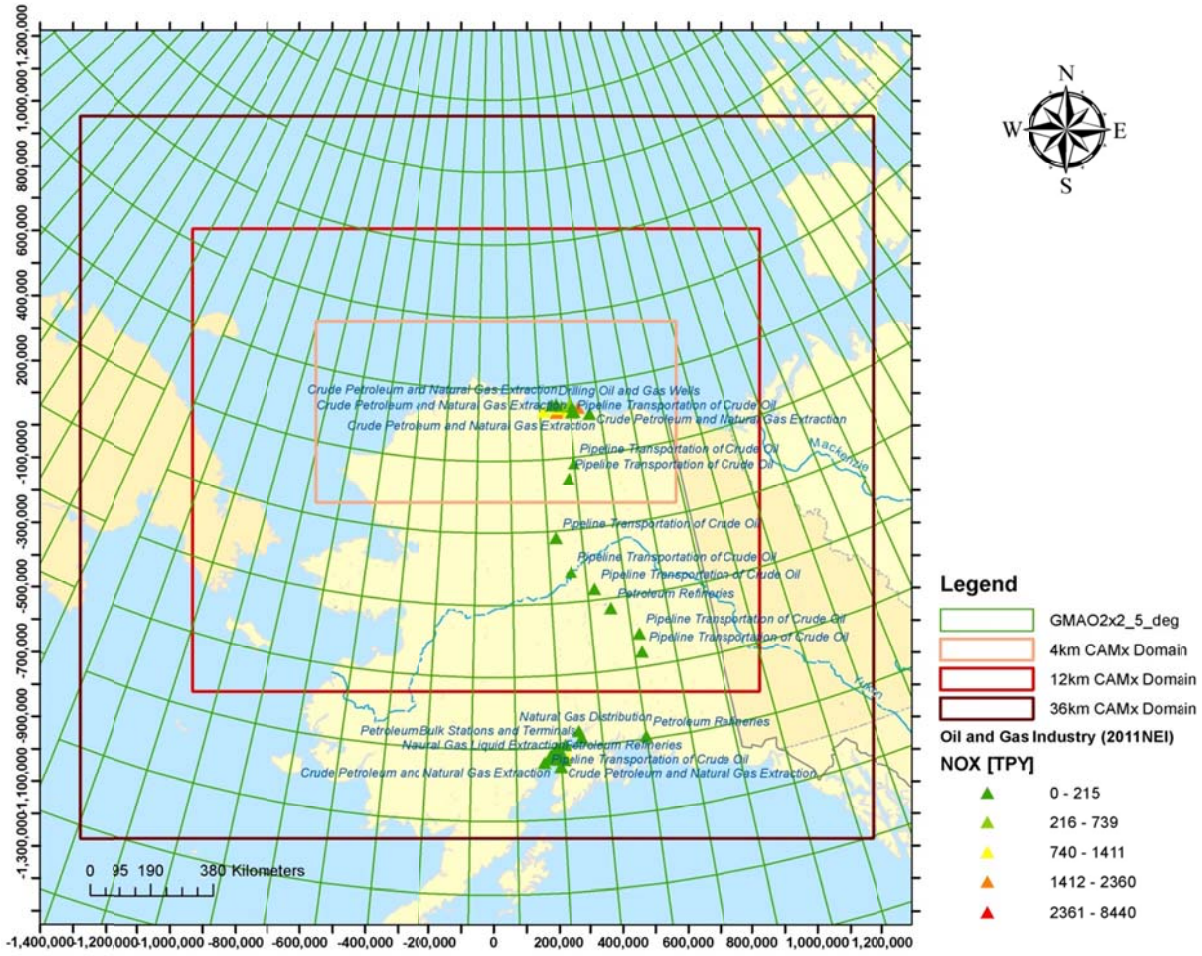

Figure 4-1. CAMx nested modeling domains at horizontal resolutions of 36 km, 12 km, and 4 km horizontal resolutions: green grid lines represent the GEOS-Chem 2 x 2.5 degree global modeling grid.

Table 4-1. PGM domain definitions (polar stereographic projection; projection plane secant 70 deg. N with origin at 70 deg. N, 155 deg. W).

Resolution	Origin (lower-left corner)	Dimension
36 km	(-1278 km, -1278 km)	68 x 62
12 km	(-930 km, -822 km)	146 x 119
4 km	(-550 km, -238 km)	278 x 140

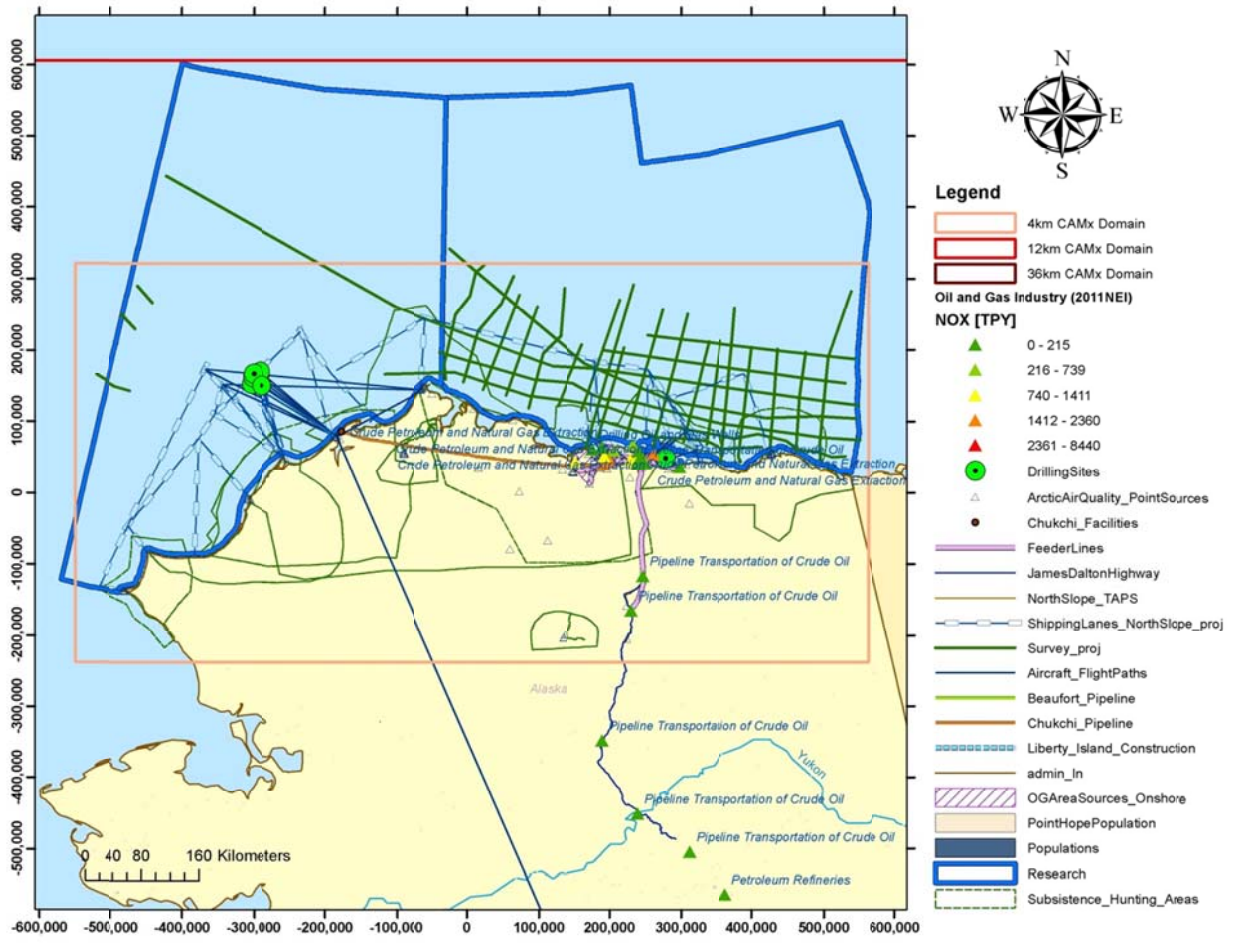

Figure 4-2. Alaska North Slope with PGM 4 km resolution domain (orange rectangle) with locations of emission sources included in the Arctic AQ Study emission inventory (circles and triangles represent point sources; linear features represent roads, pipelines, shipping lanes, offshore survey routes and aircraft flight paths).

For CAMx, BCs for the 12 km domain were extracted from the 36 km simulation results and the 12 and 4 km grids were modeled using 2-way nesting (allowing interactions between the two grids in both inbound and outbound directions).

Specification of the PGM vertical domain structure was based on the definition of the WRF vertical layers structure. The WRF simulation was run with 34 vertical layer interfaces (which is equivalent to 33 vertical layers) from the surface up to 100 mbar (approximately 16 km above mean sea level [AMSL]). The WRF model employs a terrain following coordinate system called eta (η) coordinate which is defined by relative pressure differences between layers. As shown in Table 4-2, the WRF levels are more finely stratified near the surface in an attempt to improve simulation of the atmospheric boundary layer structure and processes. A layer collapsing scheme is adopted for the PGM simulations whereby multiple WRF layers are combined into single PGM layer to improve the PGM computational efficiency. Table 4-2 also shows the layer collapsing from the 33 WRF layers to 24 PGM layers. The mixing heights over the study domain

are typically below 2 km. Therefore, the WRF modeling layers up to the 15th layer (approximately 1.2 km) are directly mapped to the PGM layers (no layer-collapsing) to better simulate the stable thermal stratification of the boundary layer and avoid errors potentially introduced by layer collapsing. Above the 15th WRF layer, two WRF layers were combined into a single PGM layer up to the 100 mbar region top.

Table 4-2. Vertical layer interface definition for WRF simulations (left most columns) and the layer-collapsing scheme for the CAMx/CMAQ layers (right columns).

WRF					CAMx/CMAQ		
Layer Interface	**Eta (η)**	**Pressure (mb)**	**Height (m)**	**Thickness (m)**	**Layer**	**Height (m)**	**Thickness (m)**
33	0	100	15725.8	1208.7	24	15725.8	2449.2
32	0.027	124	14517	1240.5			
31	0.06	154	13276.6	1266.3	23	13276.6	2600.3
30	0.1	190	12010.2	1333.9			
29	0.15	235	10676.3	1140.8	22	10676.3	2141.6
28	0.2	280	9535.5	1000.8			
27	0.25	325	8534.8	894.2	21	8534.8	1704.2
26	0.3	370	7640.6	810			
25	0.35	415	6830.5	741.8	20	6830.5	1492.7
24	0.4	460	6088.8	750.9			
23	0.455	510	5337.9	814.8	19	5337.9	1508.6
22	0.52	568	4523.1	693.8			
21	0.58	622	3829.3	646.7	18	3829.3	1252.7
20	0.64	676	3182.6	606.1			
19	0.7	730	2576.5	384.2	17	2576.5	754
18	0.74	766	2192.3	369.8			
17	0.78	802	1822.5	356.6	16	1822.5	616
16	0.82	838	1465.9	259.4			
15	0.85	865	1206.5	252.9	15	1206.5	252.9
14	0.88	892	953.6	165.2	14	953.6	165.2

WRF					CAMx/CMAQ		
Layer Interface	**Eta (η)**	**Pressure (mb)**	**Height (m)**	**Thickness (m)**	**Layer**	**Height (m)**	**Thickness (m)**
13	0.9	910	788.4	122.2	13	788.4	122.2
12	0.915	924	666.2	120.7	12	666.2	120.7
11	0.93	937	545.5	79.7	11	545.5	79.7
10	0.94	946	465.8	79.1	10	465.8	79.1
9	0.95	955	386.7	78.5	9	386.7	78.5
8	0.96	964	308.2	77.9	8	308.2	77.9
7	0.97	973	230.3	77.3	7	230.3	77.3
6	0.98	982	152.9	53.8	6	152.9	53.8
5	0.987	988	99.2	38.2	5	99.2	38.2
4	0.992	993	60.9	22.9	4	60.9	22.9
3	0.995	996	38	15.2	3	38	15.2
2	0.997	997	22.8	11.4	2	22.8	11.4
1	0.9985	999	11.4	11.4	1	11.4	11.4
0	1	1000	0				

4.3 Meteorology

Given the objectives of the BOEM Arctic AQ Modeling Study analysis and the availability of full annual WRF simulations for 2009 through 2013, the CAMx and CMAQ models were exercised for a full calendar year. The decision to model for an entire calendar year rather than just a single season is consistent with the need to address ozone, $PM_{2.5}$, visibility and annual deposition. For reasons described in the Emission Inventory Report (Fields Simms, 2014), meteorological data and emissions data were developed for the 2012 calendar year to represent the base case modeling scenario.

Meteorological inputs for the PGM simulations were generated by processing the WRF outputs using appropriate meteorological input preprocessors. WRFCAMx Version 4.4 was used to translate WRF output meteorological fields to daily CAMx meteorological inputs. For a single day, 25 hours of meteorology must be present (midnight through midnight, inclusive) as these fields represent hourly instantaneous conditions and CAMx internally time-interpolates these fields to each model time step. Precipitation fields are not time-interpolated but rather time-accumulated, so cloud/precipitation files contain one less hour than other met files (e.g., 24 hours of clouds/precipitation vs. 25 hours for other meteorology fields).

Several methodologies are available in WRFCAMx to derive vertical diffusivity (Kv) fields from WRF output. For this modeling, a method consistent with the Yonsei University (YSU) bulk boundary layer scheme (Hong and Noh, 2006; a default option in WRF) was used to generate the Kv profile. The KVPATCH method sets lower bound Kv values by land-use type and calculates minimum Kv values based on landuse fractions for each grid cell. Deep cumulus convection is difficult to simulate in a grid model because of the small horizontal spatial scale of the cumulus tower. Inadequate characterization of this convective mixing can cause ozone and precursor species to be overestimated in the boundary layer. KVPATCH increases transport of air from the planetary boundary layer into the free troposphere and up to the cloud top within cloudy grid cells when there is cumulus convection within a grid cell (ENVIRON, 2012). Use of KVPATCH was shown to improve surface layer ozone in a recent modeling study in Texas (Kemball-Cook et al., 2015) and thus was also employed in this modeling study. It must be recognized, however, that convective conditions in the Arctic environment are likely to differ substanially from those encountered in the southeastern United States.

WRFCAMx provides an option to process sub-grid cloud data from WRF fields. Selecting the "DIAG" sub-grid cloud method diagnoses sub-grid cloud fields from WRF gridded thermodynamic fields. The DIAG option is generally selected for the 36 and 12 km WRF output extraction, but not for grid spacing less than about 10 km, as at these smaller scales, small-scale convection is likely generated by the grid-resolved cloud physics in WRF. Therefore, the DIAG option was selected for the 36 and 12 km WRF output extraction, but not for the 4 km conversion.

The Meteorology-Chemistry Interface Processor (MCIP) version 4.2 was used to prepare the meteorological inputs for CMAQ from the WRF outputs. The lower bound Kv value is set based on urban land use fraction of each grid cell in CMAQ: grid cells that are predominantly urban use a minimum Kv value of 1.0 m^2/s and nonurban cells use 0.01 m^2/s. In CMAQ, sub-grid cloud is simulated when the meteorological model uses a convective cloud parameterization.

4.4 Configuration of Model Input Parameters

Configuration of the CAMx model setup is summarized in Table 4-3. Key configuration selections include:

Chemical Mechanism: Gas phase chemistry using the Carbon Bond 6 revision 2 (CB6r2) photochemical mechanism including active local excess methane emissions was used. For particles, CAMx was configured to use the Coarse-Fine (CF) aerosol scheme in which primary species are modeled using two static modes (coarse and fine) while all secondary species are modeled as fine particles only.

Photolysis Rates: CAMx requires a lookup table of photolysis rates as well as gridded albedo/haze/ozone/snow as input. Day-specific ozone column data are based on the Total Ozone Mapping Spectrometer (TOMS) data measured using the satellite-based Ozone Monitoring Instrument (OMI). Albedo is based on land use data, which includes enhanced albedo values when snow cover is present. For CAMx there is an ancillary snow cover input that is based on WRF output that overrides the land use based albedo input to use an enhanced snow cover albedo value. The Tropospheric Ultraviolet and Visible (TUV) Radiation Model photolysis rate processor was used. CAMx is configured to use the in-line TUV to adjust for cloud cover and account for the effects of aerosol loadings on photolysis rates; this latter effect on photolysis may be especially important

in adjusting the photolysis rates due to the occurrence of PM concentrations associated with emissions from fires. Note that the same clear-sky photolysis rates are used in the 2012 base case and future year scenario model runs.

Landuse: Fractional landuse fields and hourly varying snow and ice cover and data were obtained from the WRF simulation. The Leaf Area Index (LAI), which accounts for enhanced surface area for pollutant deposition provided by trees or other vegetation types, was obtained from the MEGAN inputs for use in CAMx since LAI values from the U.S. Geological Survey (USGS) Geographic Information Retrieval and Analysis System (GIRAS)[7] are not available for the full extent of the modeling domain.

Advection/Diffusion Methods: The piecewise parabolic method advection solver was used for horizontal transport (Colella and Woodward, 1984) along with the spatially varying (Smagorinsky) horizontal diffusion approach. CAMx used K-theory for vertical diffusion using the vertical diffusivities from WRFCAMx and KVPATCH.

Initial and Boundary Conditions: The initial and lateral boundary conditions (ICs and BCs) for the final 36 km grid simulation were based on results from a GEOS-Chem GCM simulation for year 2012. The GEOS2CAMx processor was used to interpolate from the GEOS-Chem horizontal and vertical coordinate system to the CAMx coordinate system and to map the GEOS-Chem chemical species to the chemical mechanisms being used by CAMx. A 10-day spin-up period was then used to eliminate any notable influence of the ICs. ICs and BCs for the nested (12/4 km) grid simulations were extracted from the parent grid simulation outputs with a shorter (3 day) spin-up period. The use of an alternative global model (MOZART-4/GEOS5; available at http://www.acd.ucar.edu/wrf-chem/mozart.shtml) as a source for the BCs was explored via a test simulation on the 36 km domain with BCs derived from MOZART. Comparisons of CMAQ simulations based on MOZART BCs with CMAQ simulations based on GEOS-Chem BCs showed generally similar results for ozone and PM over northern Alaska. Based on these results and the fact that, in contrast to GEOS-Chem, MOZART does not use day-specific values for dust emissions, BCs based on the GEOS-Chem model were selected for use in the final model simulations.

Table 4-3. CAMx model configuration.

Science Options	Configuration	Notes
Model Codes	CAMx V6.20	Released March 2015
Horizontal Grid	36/12/4 km	See Section 4.2; the 36-km grid dimension gives a buffer of at least 10 grid cells between the WRF and CAMx modeling grid boundaries
36 km grid	68 x 62 cells	
12 km grid	146 x 119 cells	
4 km grid	278 x 140 cells	

[7] http://pubs.usgs.gov/ds/2006/240

Science Options	Configuration	Notes
Vertical Grid	24 vertical layers (layer-collapsed from 33 WRF layers)	See Section 4.2; layer 1 thickness ~12 m; model top at ~16 km above AMSL
Grid Interaction	36/12 km one-way nesting 12/4 km two-way nesting	
Initial Conditions	36 km from GCM simulation	10-day spin-up for the 36 km grid; 3-day spin-up for the nested (12/4 km) grids
Boundary Conditions	36 km from GCM simulation	Final configuration used 2012 GEOS-Chem simulation results
Meteorological Input Preprocessor	WRFCAMx V4.4	Compatible with CAMx V6.20 and updated for the polar stereographic coordinate system
Land-use Data	WRF fractional landuse; LIA data from USGS GIRAS	
Photolysis Rate	TUV V4.8 Preprocessor	Clear-sky photolysis rates based on day-specific Total Ozone Mapping Spectrometer (TOMS) data; CAMx in-line adjustment based on modeled aerosol loading
Chemistry		
Gas-phase	CB6r2	Updated isoprene chemistry; heterogeneous hydrolysis of organic nitrates; active methane chemistry and ECH4 excess methane tracer species (Ruiz and Yarwood, 2013)
Aerosol-phase	CF	Coarse and fine mode aerosols
Diffusion Scheme		
Horizontal-grid	Explicit horizontal diffusion	Spatially varying horizontal diffusivities determined based on the methods of Smagorinsky (1963)
Vertical-grid	K-theory 1st-order closure	Vertical diffusivities from WRFCAMx and KVPATCH; land-use dependent minimum diffusivity (minimum Kv = 0.1 to 1.0 m^2/s)
Deposition Scheme		
Dry deposition	ZHANG03	Dry deposition scheme by Zhang et al. (2001; 2003)
Wet deposition	CAMx-specific formulation	Scavenging model for gases and aerosols (Seinfeld and Pandis, 1998)

Science Options	Configuration	Notes
Numerical Solvers		
Gas-phase chemistry	Euler Backward Iterative (EBI) solver	Hertel et al., 1993
Horizontal advection	Piecewise Parabolic Method	Colella and Woodward, 1984
Vertical advection	Implicit scheme w/ vertical velocity update	

Configuration settings used for the CMAQ model are shown in Table 4-4.

Table 4.4. CMAQ model configuration.

Science Options	Configuration	Notes
Model Codes	CMAQ V5.0.2	Released May 2014
Horizontal Grid	36 km (68 x 62 cells)	See Section 4.2
Vertical Grid	24 vertical layers (layer-collapsed from 33 WRF layers)	See Section 4.2
Initial Conditions	36 km from GCM simulation	10-day spin-up period
Boundary Conditions	36 km from GCM simulation	Used 2012 GEOS-Chem simulation results
Land-use Data	WRF fractional land-use	
Photolysis Rate	In-line	In-line calculation based on surface albedo and predicted aerosol loading
Chemistry		
Gas-phase	CB05TUCL	Updated toluene chemistry; updated chlorine chemistry (Sarwar et al., 2011)
Aerosol-phase	AERO6	Modal representation of aerosol size distribution; explicitly models elemental species (Al, Ca, Fe, K, Mg, Mn, Si, and Ti)
Meteorological Input Preprocessor	MCIP V4.2	
Diffusion Scheme		
Horizontal-grid	Single eddy diffusion algorithm	Uniform horizontal eddy diffusivity which depends on grid resolution

Science Options	Configuration	Notes
Vertical-grid	ACM2	Calculate vertical diffusion using the Asymmetric Convective Model version 2; Minimum Kv = 0.01 to 1.0 m^2/s depending on urban land-use fraction
Deposition Scheme		
Dry deposition	M3DRY	Updated with mesophyll resistance (Wesely, 1989)
Wet deposition	RADM	Chang et al., 1987
Numerical Solvers		
Gas-phase chemistry	Euler Backward Iterative (EBI) solver	Hertel et al., 1993
Horizontal advection	Piecewise Parabolic Method	Colella and Woodward, 1984
Vertical advection	Piecewise Parabolic Method	

5.0 MODEL PERFORMANCE EVALUATION

5.1 Comparison of CAMx and CMAQ Results

Both CAMx and CMAQ were run for the Base Year scenario at 36 km resolution with the configurations described above. Both runs used boundary conditions extracted from the GEOS-Chem GCM output.

Predicted annual 4th highest daily maximum 8-hour average ozone concentrations (H4MDA8) are shown in Figure 5-1. Predicted maximum values within the domain differ by just 1.2% and the spatial patterns are very similar between the two models.

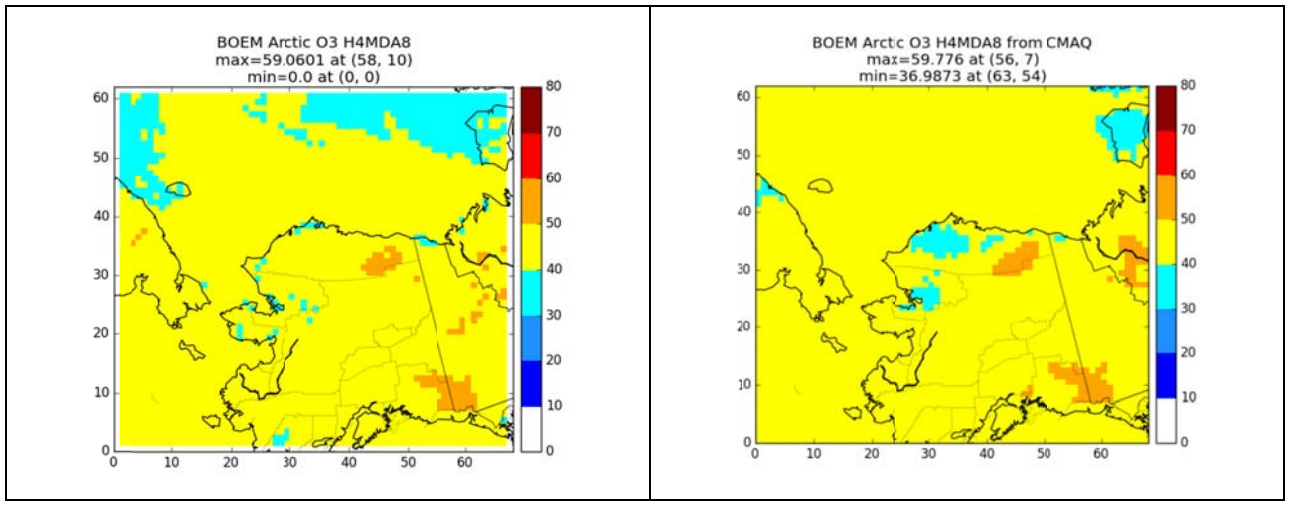

Figure 5- 1. Predicted annual 4th highest daily maximum 8-hour average ozone concentrations (H4MDA8) from CAMx (left) and CMAQ (right).

Comparisons of predicted highest daily maximum 8-hour average (H1MDA8) ozone were also made for each calendar quarter as shown in Figure 5-2. The pattern and overall level of predicted values are similar although CMAQ predictions tend to be a bit higher than those from CAMx throughout the year in most portions of the domain. An exception to this pattern is the slightly lower CMAQ predictions in coastal portions of the NSB in Q3 (July – September).

CAMx	CMAQ
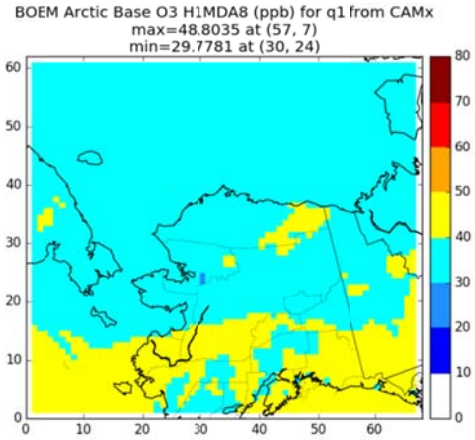 BOEM Arctic Base O3 H1MDA8 (ppb) for q1 from CAMx max=48.8035 at (57, 7) min=29.7781 at (30, 24)	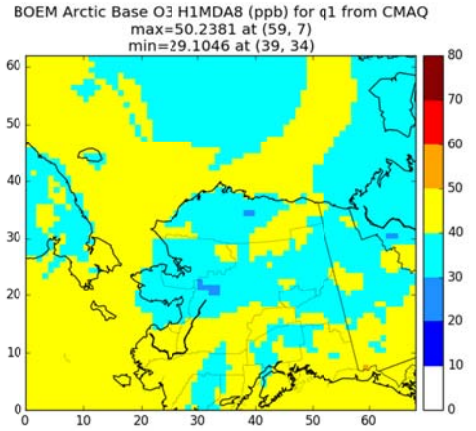 BOEM Arctic Base O3 H1MDA8 (ppb) for q1 from CMAQ max=50.2381 at (59, 7) min=29.1046 at (39, 34)
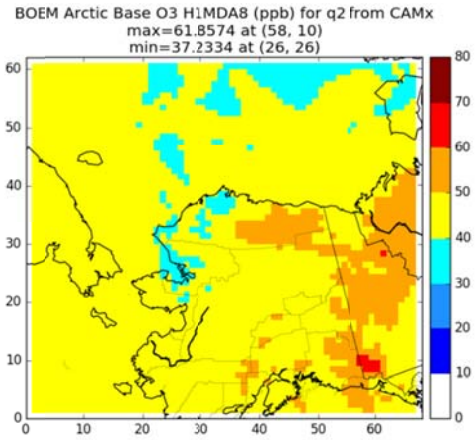 BOEM Arctic Base O3 H1MDA8 (ppb) for q2 from CAMx max=61.8574 at (58, 10) min=37.2334 at (26, 26)	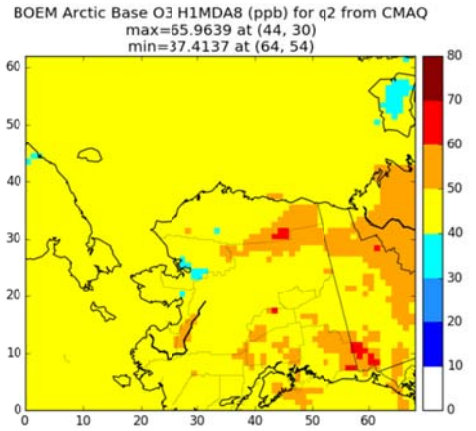 BOEM Arctic Base O3 H1MDA8 (ppb) for q2 from CMAQ max=55.9639 at (44, 30) min=37.4137 at (64, 54)
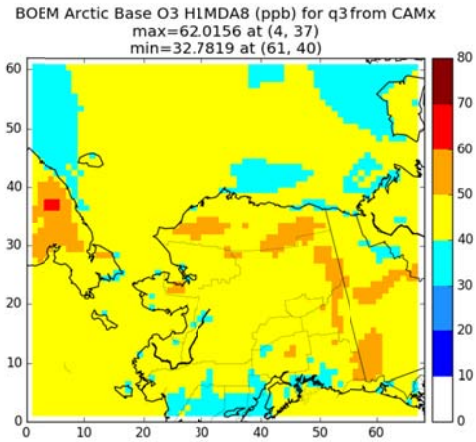 BOEM Arctic Base O3 H1MDA8 (ppb) for q3 from CAMx max=62.0156 at (4, 37) min=32.7819 at (61, 40)	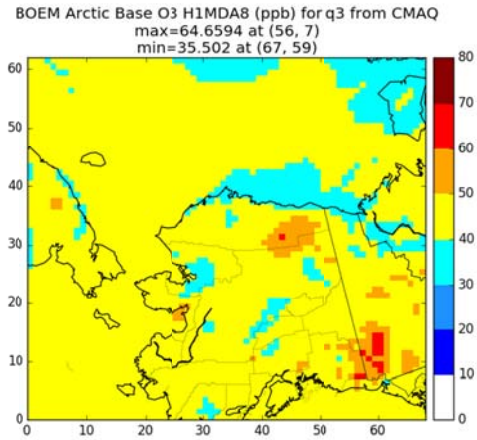 BOEM Arctic Base O3 H1MDA8 (ppb) for q3 from CMAQ max=64.6594 at (56, 7) min=35.502 at (67, 59)

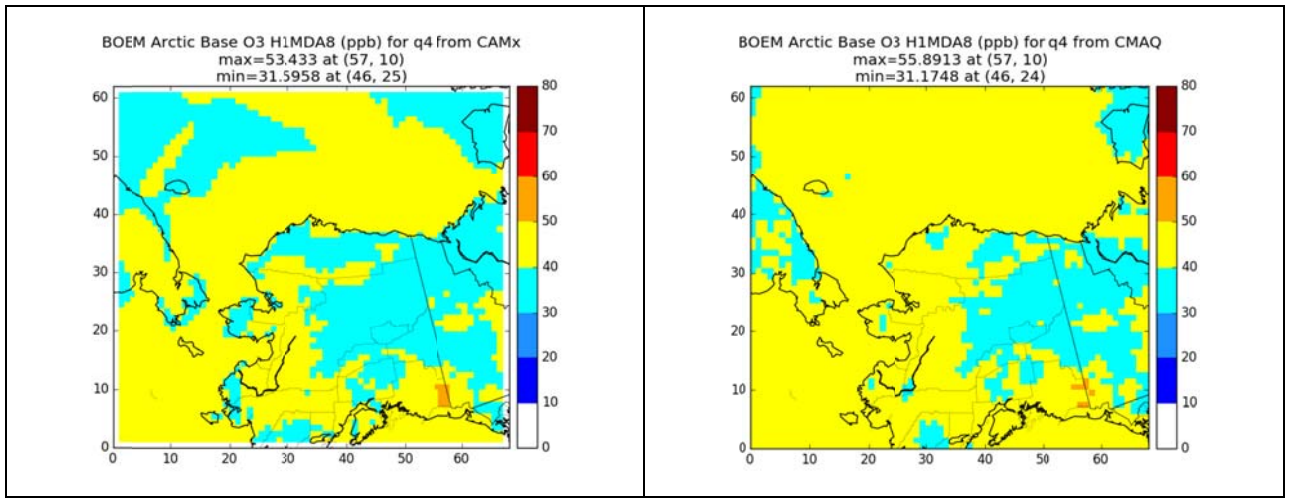

Figure 5-2. Predicted highest daily maximum 8-hour average (H1MDA8) ozone concentrations in each calendar quarter (Q1 in top row through Q4 in bottom row) from CAMx (left) and CMAQ (right).

Comparisons of annual average $PM_{2.5}$ predicted by CAMx and CMAQ are shown in the top row of Figure 5-3. CAMx predicts much higher amounts of $PM_{2.5}$ over the oceans and especially in coastal areas as a result of the much higher sea salt emissions generated by the CAMx sea salt preprocessor as compared to the in-line sea salt emissions calculator used by CMAQ. This is shown by the predicted annual average sea salt concentrations in the middle row of Figure 5-3. Subtracting sea salt from the $PM_{2.5}$ predictions, by subtracting out all particulate sodium and chloride, results in better agreement between the two models as shown in the bottom row of Figure 5-3. Nevertheless, CAMx non-sea salt $PM_{2.5}$ is still higher than CMAQ outside of the Fairbanks and Anchorage urban areas. This is likely due at least in part to higher predicted particulate nitrate in CAMx due to greater substitution of chloride by nitrate ions in the more abundant CAMx sea salt particles. As measurements of sea salt concentrations are not available, it is not possible to determine which model produces the more accurate sea salt estimates. However, in other studies where observations of sea salt concentrations were available, CAMx was found to widely overestimate sea salt emissions whereas CMAQ has been found to underestimate sea salt emissions (Ramboll Environ, 2016; Gantt, et al., 2015). Additional evaluations of the sea salt emissions modules used in both models for application in the Arctic are needed to improve sea salt emission estimates.

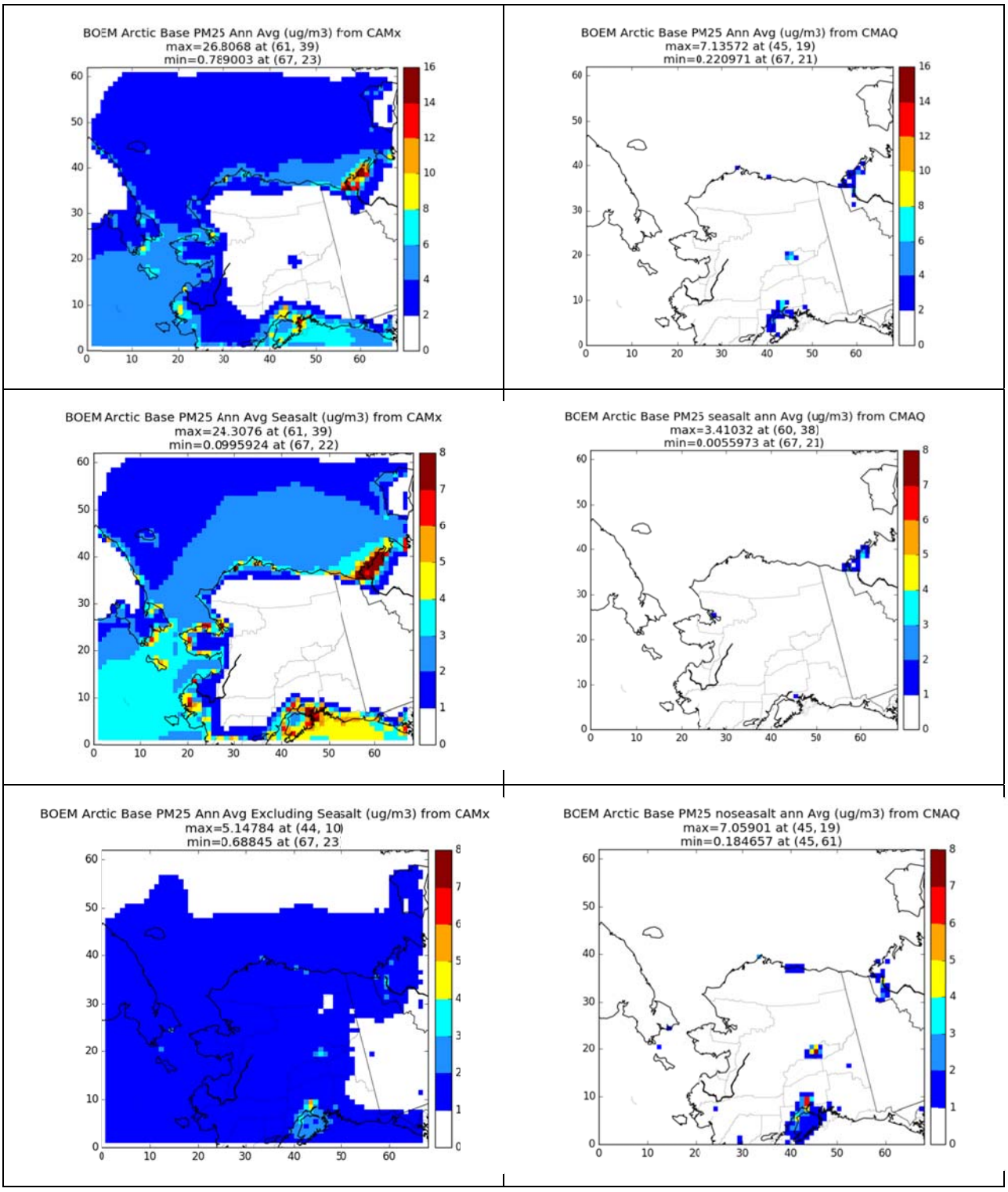

Figure 5-3. Predicted annual average $PM_{2.5}$ concentrations from CAMx (left) and CMAQ (right) for total $PM_{2.5}$ (top), sea salt (middle), and $PM_{2.5}$ with sea salt subtracted out (bottom).

Similar comparisons of CAMx with CMAQ results were also carried out for individual $PM_{2.5}$ components (sulfate, organic aerosols, and other $PM_{2.5}$) as shown in Figure 5-4. CAMx predicts slightly higher sulfate than CMAQ overall, slightly higher organic aerosols over wide portions of the domain (but lower organic aerosols than CMAQ in the Fairbanks and Anchorage areas), and lower concentrations of other PM. The higher sulfate predictions from CAMx are expected as a result of the much higher sea salt emissions calculated by the CAMx sea salt preprocessor since emitted species from the sea salt processor include sulfates of marine origin. Analysis of organic aerosols (OA) components shows that differences in OA seen in Figure 5-4 are largely due to differences in secondary organic aerosols (SOA) between the two models. These SOA differences are likely due to different SOA formation parameterizations in the two models (Emery et al., 2016).

Results from the above comparisons of CAMx and CMAQ, provide no definitive reasons to prefer one model over the other. Both models predict generally similar ozone levels and PM prediction differences are mostly attributable to the much lower sea salt emissions predicted by the CMAQ in-line sea salt emissions module as compared to the CAMx sea salt emissions preprocessor. In the absence of suitable measurements of PM components related to sea salt emissions; however, it is not possible to definitively determine the accuracy of either approach for estimating sea salt emissions. More generally, the extremely limited availability of air quality measurements within the study area suggests that more detailed intercomparisons of model performance at finer spatial resolutions are unlikely to yield a clear reason to prefer one model over the other. However, the availability of source apportionment technology in CAMx, which allows for the ability to track the relative contributions of different source groups (such as the contributions of anticipated new oil and gas sources to future ozone and PM concentrations) within a single model run, argues in favor of using CAMx for analysis of the future year scenario and, therefore, also for the base year scenario (so as to avoid confounding comparisons of future year and base year results with inter-model biases). We therefore decided to use CAMx for the 12 km and 4 km resolution runs. An evaluation of CAMx base year results against the limited available ambient measurements is presented in Section 5.2.

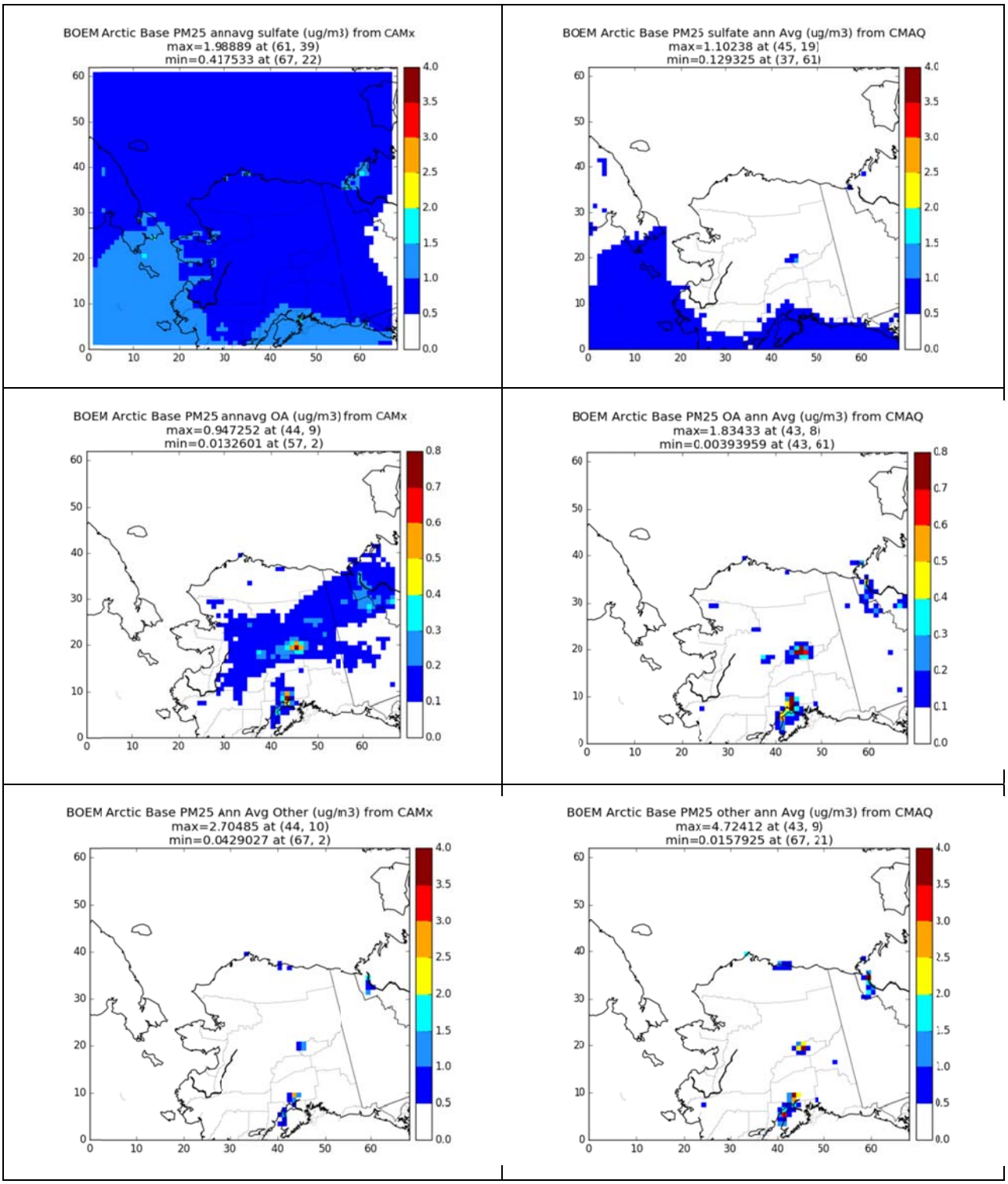

Figure 5-4. Comparisons of CAMx (left) and CMAQ (right) predictions of annual average sulfate (top), organic aerosols (middle), and other PM (bottom).

5.2 Evaluation with Ambient Data

An evaluation of photochemical model performance for the 2012 base year scenario was carried out by comparing model results with ambient air quality observations. In keeping with the objectives of this study, the model evaluation focused on the assessment of model performance over the North Slope and adjacent areas where impacts from the new offshore energy development are likely to be most pronounced. As pointed out in a previous study (ADEC, 2011a), ambient air quality monitoring data suitable for model evaluation are extremely limited in this area. A survey of available data for 2012 was performed by accessing United States and Canadian data repositories and requesting information from the Alaska Department of Environmental Conservation (ADEC). Air monitoring sites with data available for at least portions of 2012 are listed in Table 5-2. Site locations are shown in Figure 5-5. All of these sites are located within either the 4 km or 12 km model domains. Four sites (APAD, DS1F, BRW, CCP) are located in coastal portions of the NSB. The APAD, DS1F and CCP monitoring sites were originally established to satisfy PSD permitting requirements for new major sources. As such they are located close to sources of emissions and thus subject to near-source impacts which may not be well represented by a PGM run on a 4 km grid. While monitoring sites in the Fairbanks area - which is 630 km (392 miles) south of the Beaufort Sea coast - are within the 12 km modeling domain, these monitors are heavily influenced by local sources and thus are not representative of regional air quality in general nor air quality in the NSB in particular. Therefore, data from the Fairbanks monitoring network were not included in our analysis.

U.S. EPA's automated model evaluation tool (AMET[8]) could not be used for this analysis due to the limited availability of ambient data. Instead, model predictions averaged over the 9-grid cell block centered on individual monitoring site were used for comparison with the measurements on a site-by-site basis. Comparisons of results using 9-grid cell averages with results using model predictions from the single grid cell containing the monitoring site for 24-hour $PM_{2.5}$ showed little difference between the two methods, suggesting that use of the 9-grid cell average was adequate for this evaluation.

Standard statistical measures of model performance as recommended in U.S. EPA guidance (U.S. EPA, 2014) were used for this analysis with a focus on the normalized mean bias (NMB) and normalized mean error (NME) which are defined as described in Table 5-1. Generally speaking, in photochemical model performance evaluations for regulatory applications, a NMB with absolute value less than or equal to 15% and a NME less than or equal to 35% is considered acceptable performance for ozone. For PM, which is more difficult to predict, limits of 30% for NMB and 50% for NME are considered a "good performance goal" and limits of 60% for NMB and 75% for NME are considered an "average PM performance criteria" (see for example Adelman et al., 2014).

[8] https://www.cmascenter.org/help/documentation.cfm?MODEL=amet&VERSION=1.1

Table 5-1. Definitions of primary model performance evaluation statistics.

Statistical Measure	Mathematical Expression	Notes
NME: Normalized Mean Error	$\frac{\sum_{i=1}^{N}\lvert P_i - O_i\rvert}{\sum_{i=1}^{N} O_i}$	Reported as %
NMB: Normalized Mean Bias	$\frac{\sum_{i=1}^{N}(P_i - O_i)}{\sum_{i=1}^{N} O_i}$	Reported as %

Table 5-2. Monitoring sites used in the model performance evaluation.

Site Name	Site ID	Source[a]	Lat	Lon	Species
Denali	20680003	IMPROVE	63.72535	-148.966	O_3, PM_{10}, $PM_{2.5}$
APAD	02185APAD	AK Permit Data	70.26667	-148.753	NO_x, O_3
DS1F	02185DS1F	AK Permit Data	70.29739	-149.681	NO_x, O_3
BRW	02185XBRW	NOAA	71.32	-156.61	O_3
CCP	02185XCCP	AK Permit Data	70.32056	-148.502	NO_x, O_3, $PM_{2.5}$
BTT	22909000	AQS	66.93093	-151.492	PM_{10}, $PM_{2.5}$

[a]IMPROVE monitoring network (http://vista.cira.colostate.edu/Improve/); AK Permit Data from ADEC air quality permit files as supplied for use in this study by the ADEC; NOAA ESRL published data for the Barrow Observatory (http://www.esrl.noaa.gov/gmd/obop/brw/); AQS data from U.S. EPA's AirData system (https://www.epa.gov/outdoor-air-quality-data).

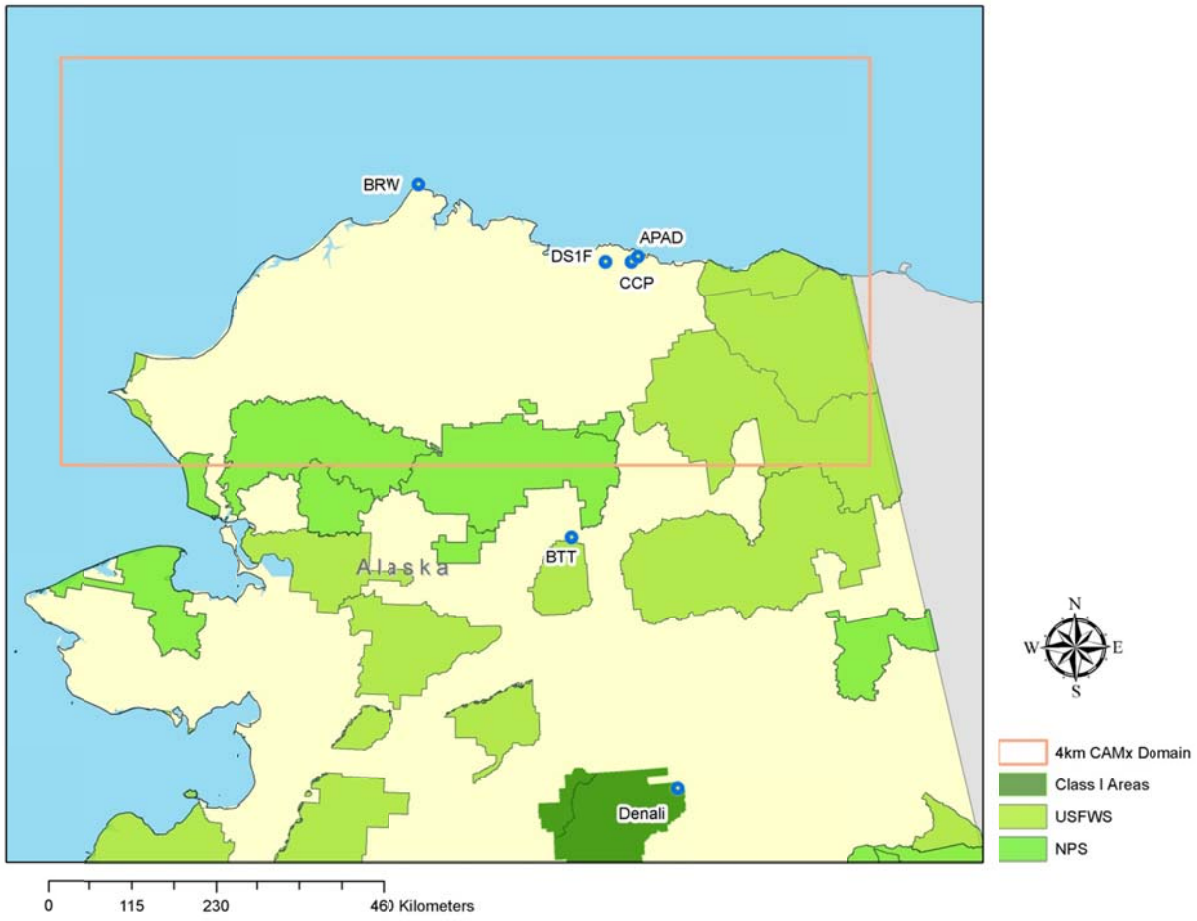

Figure 5-5. Air quality monitoring sites within the 4/12 km modeling domain used for model performance evaluation (shaded areas represent Class I and specified Class II areas designated as national parks, national preserves, and national wildlife refuges – see Figure 1-3).

5.2.1 *Ozone*

Model performance evaluation results for hourly ozone concentrations are summarized for Barrow in Figure 5-6. Both observed and predicted ozone time series at other sites on the North Slope are very similar to the pattern shown here for Barrow. Peak observed ozone concentrations are less than 50 ppb at all of these sites with a seasonal pattern characterized by maximum variability around March – April when both zero or near zero values and values at or near the annual maximum typically occur, a local minimum around late July and August followed by increasing mean values during the fall months, and maximum mean values during November - February. Factors potentially contributing to this seasonal pattern have been described in the literature (Oltmans, et al., 2012) and are unrelated to local anthropogenic emissions. Data for all the other ozone monitoring sites in the North Slope as well as the Inuvik monitoring site in Northwest Territories, Canada exhibit a similar temporal pattern. Predicted ozone concentrations also exhibit a similar seasonal pattern at all of these sites. The model matches the observations reasonably well between June and October and is able to reproduce the

observed August ozone minimum. However, the model consistently over predicts by roughly 10 ppb during November – February and is unable to reproduce the periods of zero or near zero ozone observed during March – April. The overall model performance results for hourly ozone exhibit low bias but high error as shown by the performance statistics in the bottom panel of Figure 5-6. However, the error is still within 35%, which is the limit of acceptable performance.

Seasonal patterns of observed and predicted ozone are markedly different at the Denali monitoring site as shown in Figure 5-7. The seasonal pattern of observed ozone is characterized by a peak in April – May, and a minimum in July – August. Maximum hourly ozone values approach 60 ppb at this location. The most substantial difference between this site and the North Slope sites is the absence of episodes of zero or near-zero ozone during the spring and a less pronounced mid-summer ozone minimum. Modeled ozone reproduces the observed seasonal pattern reasonably well although there is a tendency towards under prediction in the spring and over prediction in the fall.

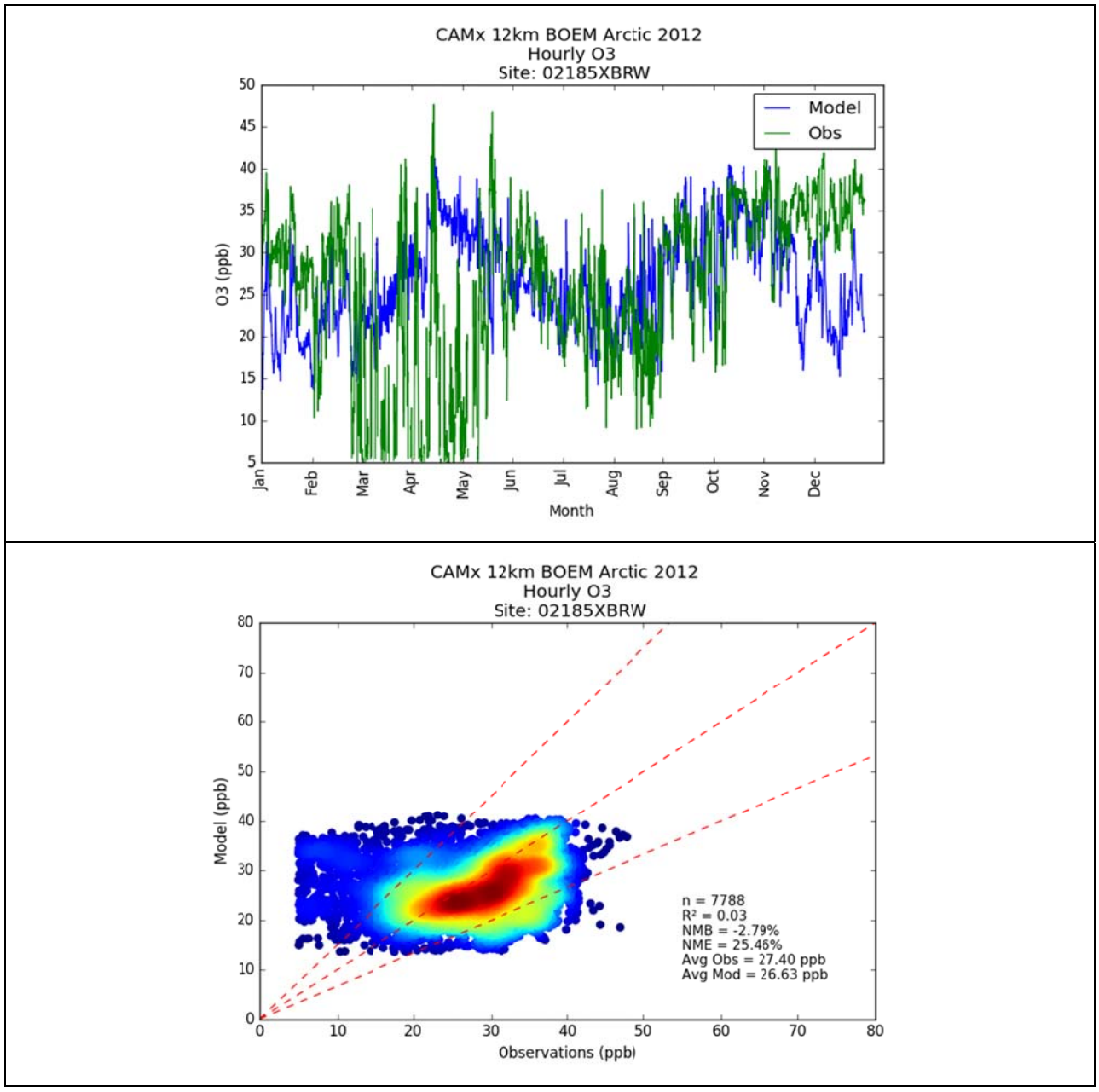

Figure 5-6. Hourly ozone model performance results at Barrow (BRW): hourly time series (top) and scatter density plot with hotter colors indicating greater density of data points (bottom).

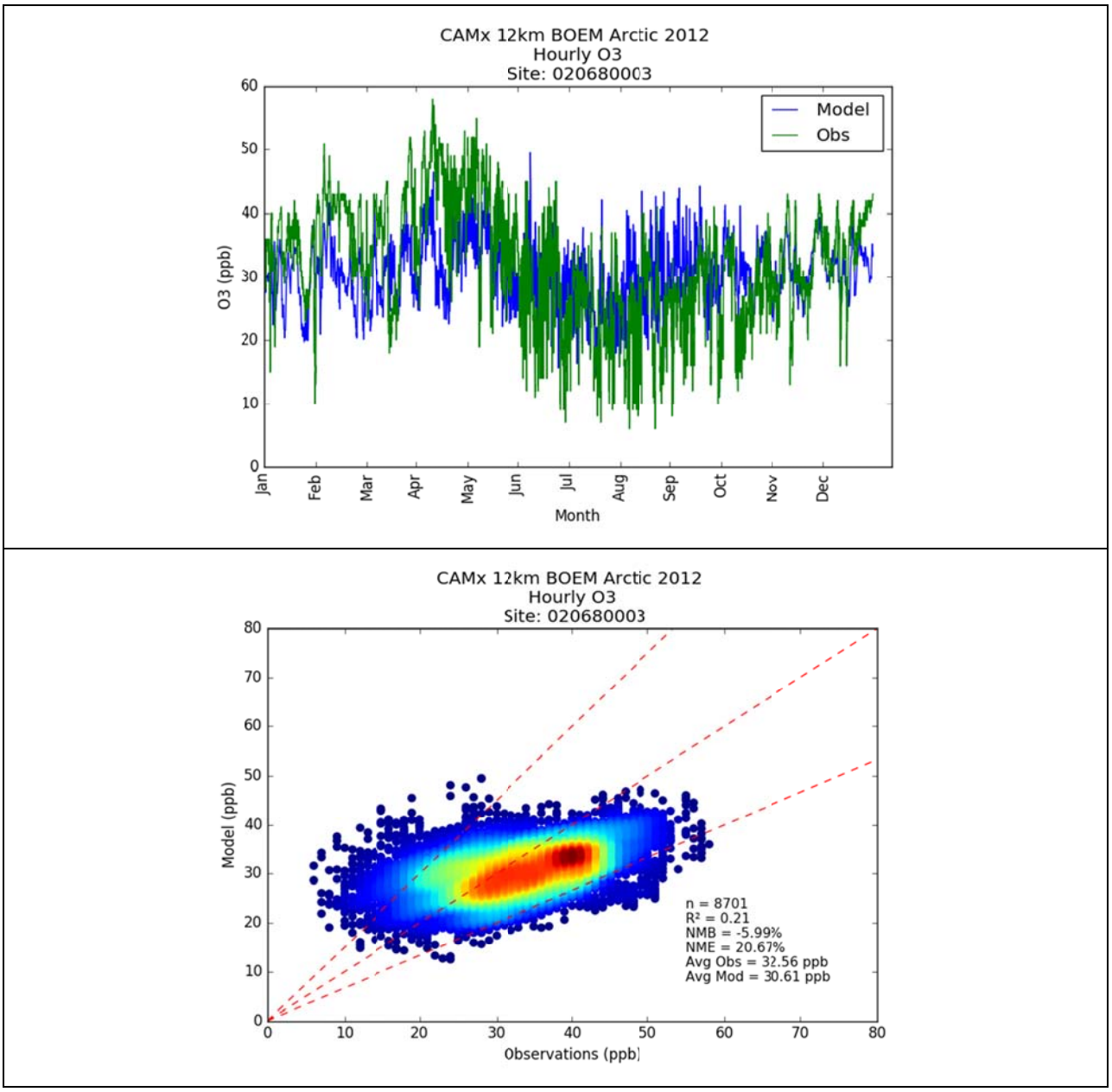

Figure 5-7. Hourly ozone model performance results at Denali: hourly time series (top) and scatter density plot with hotter colors indicating greater density of data points (bottom).

Model performance results for daily maximum 8-hour average (MDA8) ozone at sites in the NSB are summarized in Figure 5-8. Results are similar at all four sites: maximum observed and predicted 8-hour ozone is less than 50 ppb and normalized mean bias (NMB) is less than 10%; most predicted values are within ±50% of observed. However, R-square values are low and normalized mean errors (NME) range from 18 to 21%.

As suggested by the hourly ozone time series in Figure 5-6 above, model performance for MDA8 ozone at sites in the NSB varies by season with very good performance in July – September (Q3)

as compared to other times of the year as illustrated for Barrow in Figure 5-9. Results for APAD and CCP are similar (quarterly data for DS1F was not analyzed as data at this site are missing for Q1and Q2).

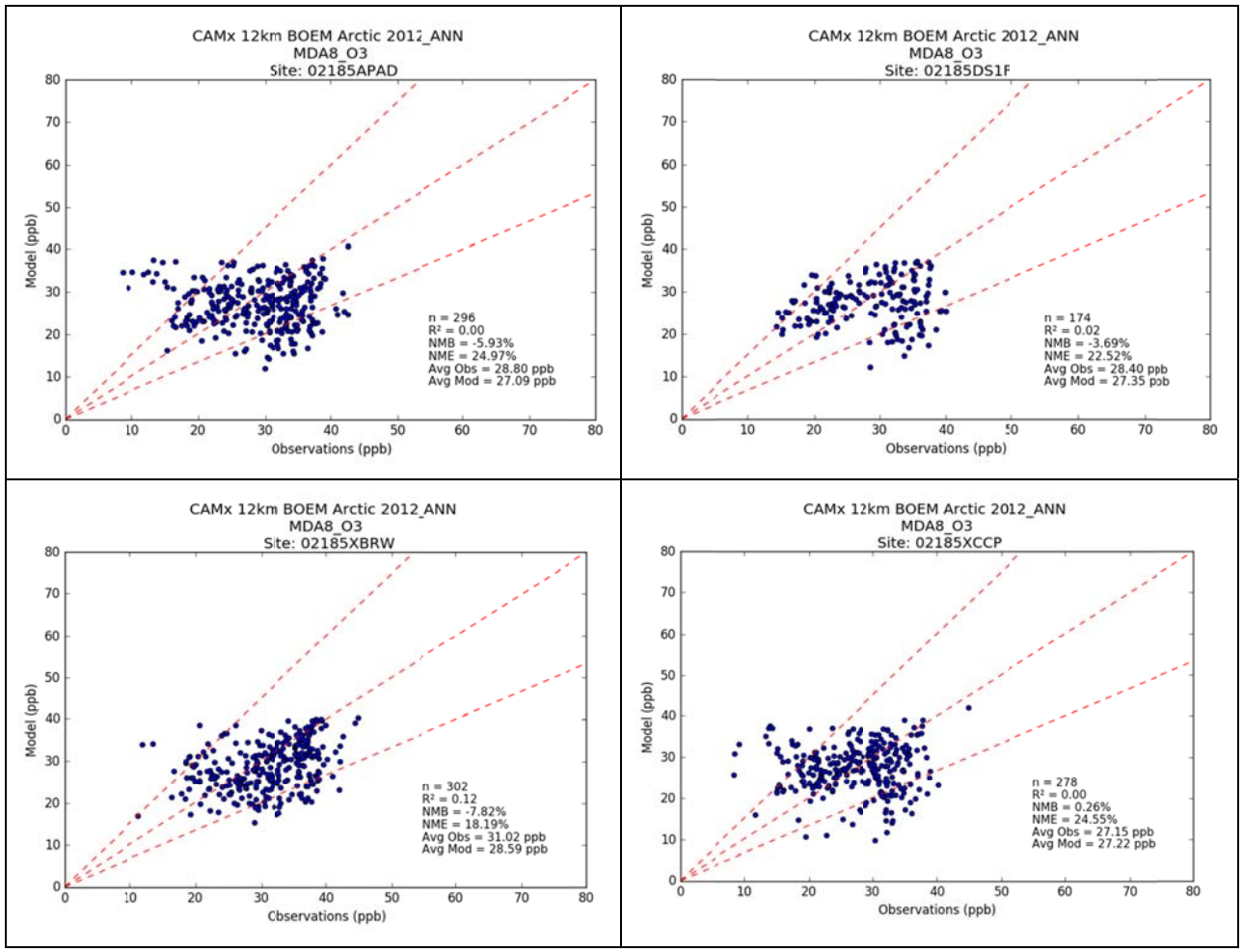

Figure 5-8. Comparisons of observed and predicted daily maximum 8-hour average ozone at APAD (top left), DS1F (top right), BRW (bottom left), and CCP (bottom right).

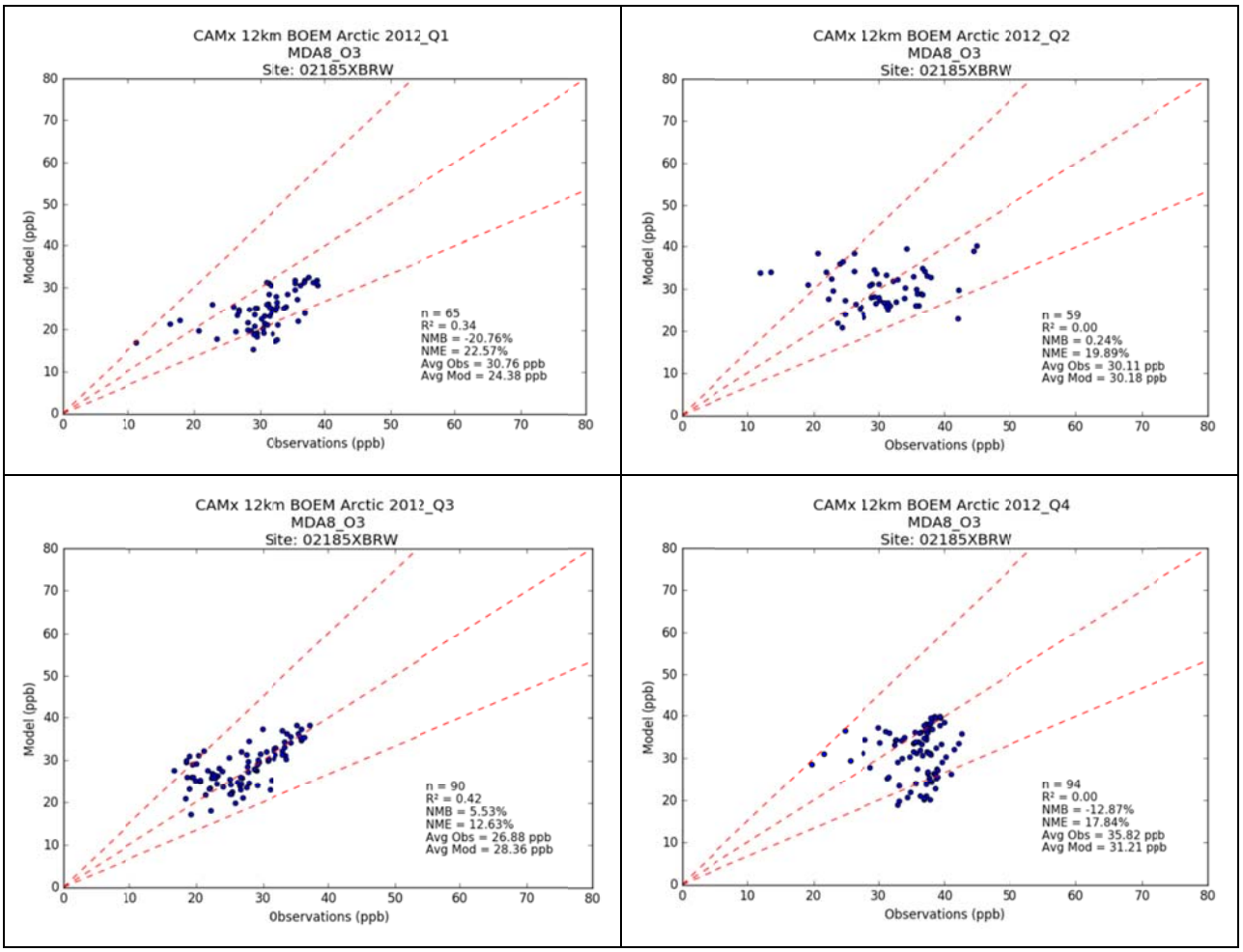

Figure 5-9. Comparisons of observed and predicted daily maximum 8-hour average ozone (MDA8) by calendar quarter at Barrow: January-March (top left), April-June (top right), July-September (bottom left), and October – November (bottom right).

5.2.2 *NO_2*

Hourly NO_2 observations for 2012 are available at the APAD, DS1F, and CCP monitoring sites although there are numerous missing values. Comparisons of predicted with observed hourly NO_2 show considerable under-prediction biases at these sites with NMB ranging from -43% to -73%. Examination of hourly time series shows that this bias is a result of frequent NO_2 spikes in the observations that are not captured in the 9-grid cell average CAMx predictions (see for example results for the CCP site in Figure 5-10). The observed NO_2 spikes occur because the monitoring site is located in close proximity to a large NO_x source. Gridded 4 km model results are not adequate to resolve these fine scale source impacts.

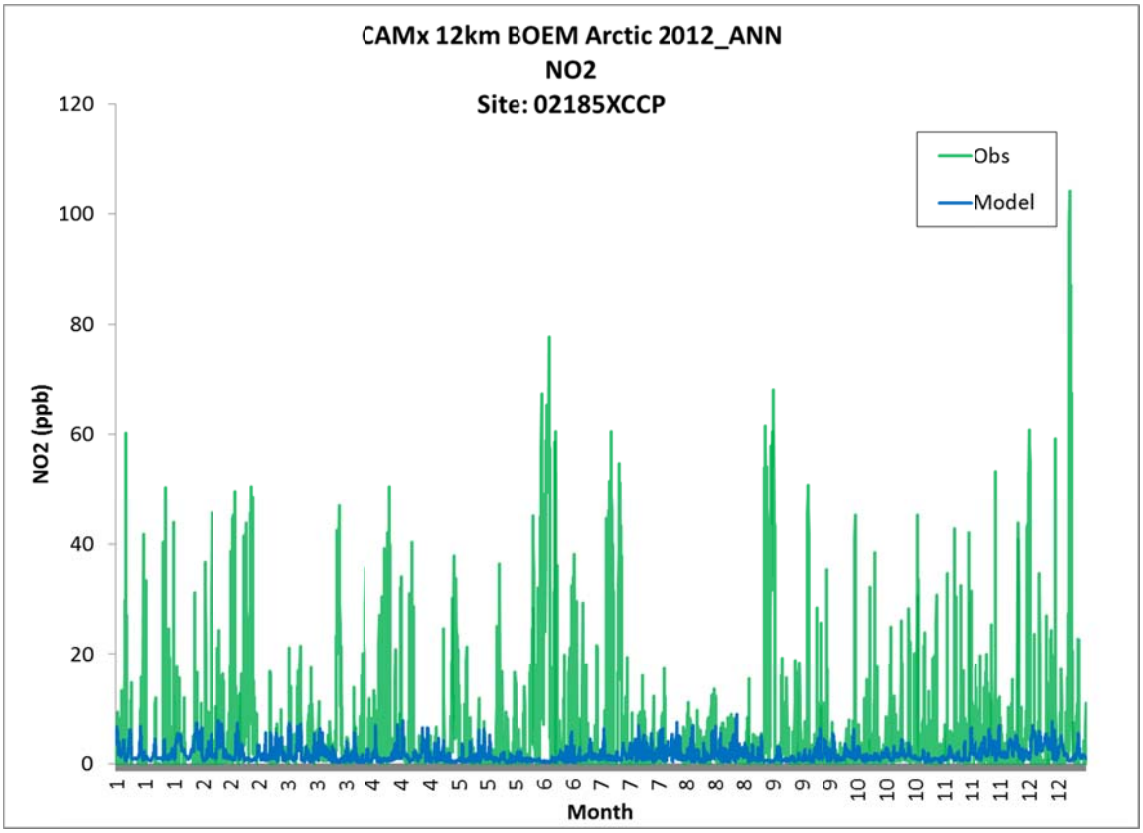

Figure 5-10. Hourly observed and predicted NO_2 concentrations during 2012 at the CCP monitoring site.

5.2.3 *$PM_{2.5}$*

Total $PM_{2.5}$ mass measurements were made during 2012 at the CCP, BTT, and Denali monitoring sites. Measurements at the CCP site were made using a Beta Attenuation Monitor (BAM) with results reported as hourly averages. Data at the BTT site and at the Denali IMPROVE network site are based on gravimetric analysis of filter samples collected every third day.

Scatter plots of observed versus predicted 24-hour average total $PM_{2.5}$ mass concentrations are shown in Figure 5-11. Since modeled emissions of sea salt are highly uncertain and no speciated ambient PM data are available with which to evaluate the sea salt emissions, results are presented here both with and without sea salt included in the model predictions. The "no sea salt" model predictions were obtained by subtracting the total predicted sodium (model species NA) and particulate chloride (model species PCL) from the sum of all $PM_{2.5}$ species output by the model. This procedure thus assumes all Na and particle bound Cl in the model originate from sea salt. However, total $PM_{2.5}$ mass may still be biased high in the "no sea salt" case to the extent that over estimation of sea salt emissions results in excess particulate nitrate via chloride substitution.

The influence of modeled sea salt on high predicted $PM_{2.5}$ days at CCP is evident: the average predicted $PM_{2.5}$ concentrations decreased by 3.3 $\mu g/m^3$ (62%) when sea salt is removed. On days during which little or no sea salt was present, the model under predicted by a wide margin. These

results are consistent with poor predictions of the timing of sea salt impacts coupled with over prediction of sea salt emissions, but it is not possible to rule out other potential sources of error given the absence of any speciated PM measurements.

Observed and modeled $PM_{2.5}$ concentrations are lower at the more remote BTT and Denali sites. Removing sea salt from the predicted values has some influence on the performance statistics at both sites, driving the bias from over prediction to under prediction but slightly reducing the NME. Predicted $PM_{2.5}$ at these sites is roughly in the same range as observed, and the NME ranges from 46 to 57%, which is more or less at the upper edge of the performance goal (50%).

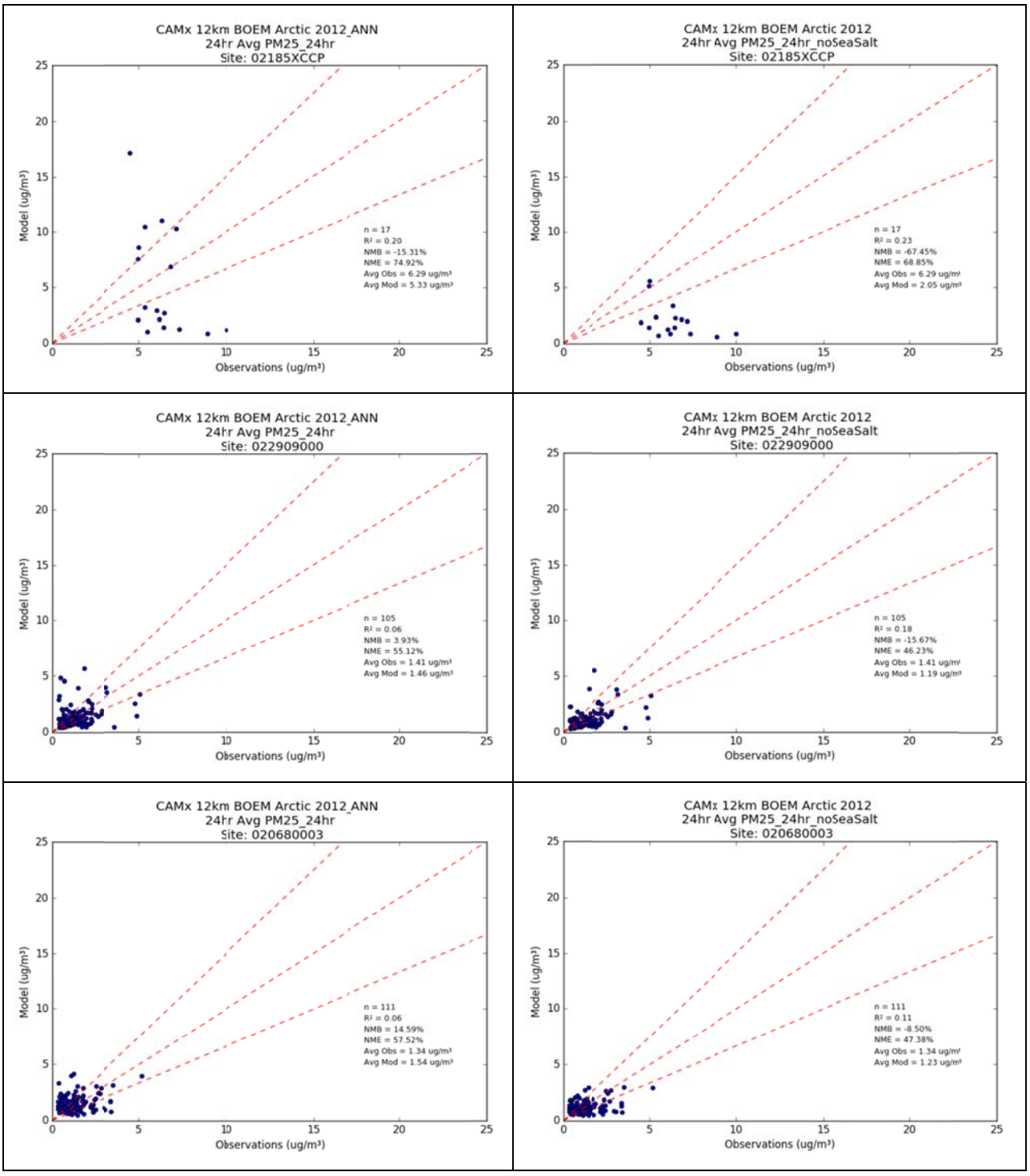

Figure 5-11. Comparisons of observed and predicted 24-hour average $PM_{2.5}$ at CCP (top), BTT (middle), and Denali (bottom) with sea salt included in the predicted values (left column) and sea salt removed from the predicted values (right column).

5.2.4 *PM_{10}*

PM_{10} measurements for 2012 are only available at the BTT and Denali monitoring sites. Measurements at both of these sites are based on gravimetric analysis of 24-hour filter samples collected every third day. Comparisons of observed and predicted PM_{10} are presented in Figure 5-12. Maximum observed concentrations are less than 10 $\mu g/m^3$ at both of these remote sites and correlations are low. The model has a tendency to under predict at both locations.

Although speciated PM data are available at the Denali IMPROVE site, this site is 757 km (470 miles) south of the coastal portions of the NSB and sits at an elevation of 658 m (2,159 ft). Speciation data from this site are therefore not likely to be representative of conditions in the NSB.

5.2.5 *Summary of Model Performance Evaluation*

In keeping with the objectives of this study, the model performance evaluation focused on the assessment of model performance over the North Slope and adjacent areas where impacts from potential new offshore energy development (as depicted in the full built-out scenario) are likely to be most pronounced. Unfortunately, contemporaneous air quality observations were very limited for this area: with ozone, NO_x and $PM_{2.5}$ data available at just a few sites. Most importantly, no speciated PM data were available within the North Slope, making it impossible to evaluate model performance with respect to PM composition.

Given the limited observations and overall small quantity of air emissions from local sources in the NSB, it is difficult to gauge how accurately the model simulates ozone production due to emissions from local sources. Nevertheless, ozone model performance fell within the bias (NMB) and error (NME) bounds considered acceptable under U.S. EPA guidance and both predicted and observed peak ozone levels are well below the NAAQS (70 ppb).

Evaluation of model performance for PM was hampered by the lack of any contemporaneous speciated PM data. Nevertheless, the strong contributions to incidences of $PM_{2.5}$ over prediction by predicted sodium (NA) and particulate chloride (PCL) supports the hypothesis that sea salt emissions are overstated in the emission inventory. Furthermore, comparisons of mean predicted NA with historical measurements of Na^+ ion mass from filter samples collected in Barrow (presented in Section 8 below) provide further evidence that sea salt emissions are over estimated. Over estimation of sea salt emissions has the potential to result in over prediction of sodium nitrate and thus over estimation of the contributions of NO_x sources to $PM_{2.5}$ and visibility impairment. The impact of sea salt over prediction on model results was evaluated via a sensitivity analysis which is described in Section 8. $PM_{2.5}$ performance at inland sites, where sea salt influences are minimized, show only weak correlations with observations but bias (NMB) and error (NME) are approximately within generally acceptable bounds.

In conclusion, aside from effects arising from the over prediction of sea salt emissions (see Section 8), there are no obvious deficiencies in the base case simulation that can be inferred on the basis of the limited observational data set.

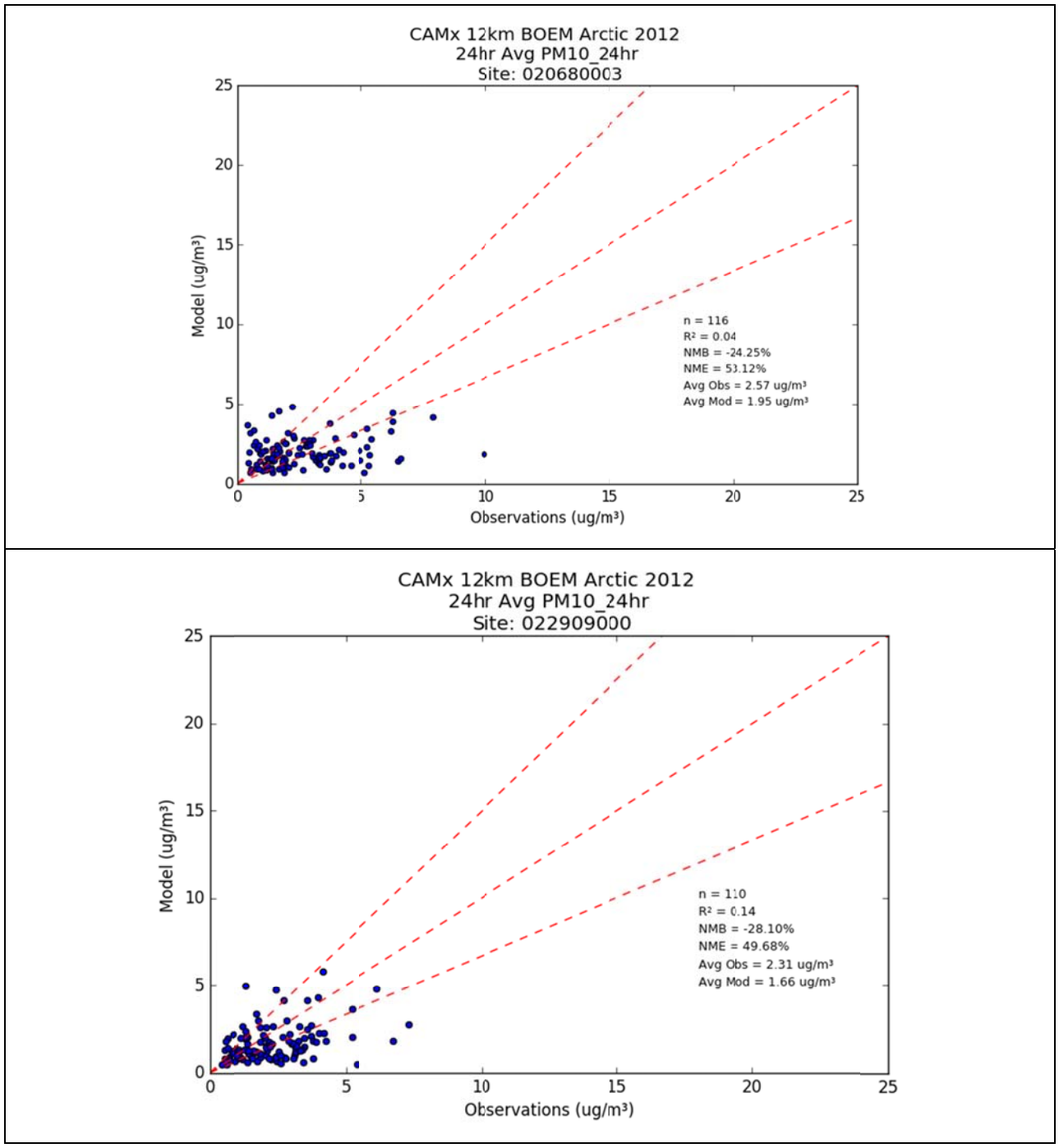

Figure 5-12. Scatter plots of observed and predicted 24-hour average PM_{10} at Denali (top) and BTT (bottom) monitoring sites.

6.0 AIR RESOURCE ASSESSMENT APPROACH

6.1 Future Year Modeling

CAMx was run with the Future Year scenario emissions inventory which includes emissions from the potential new oil & gas (O&G) sources described in Section 3. Model results were post processed for analysis of air quality impacts with respect to the NAAQS and AQRVs; PSD increments were also calculated for information purposes. Source apportionment technology was used to provide estimates of source group impacts, including impacts of potential new O&G sources. Details of the source apportionment and post processing procedures are presented in this section.

6.1.1 *Source Apportionment Design*

The CAMx Ozone Source Apportionment Technology (OSAT) and Particulate Source Apportionment Technology (PSAT) tools were used to obtain the separate air quality, deposition and visibility impacts associated with existing and new offshore O&G development in Federal waters of the Beaufort and Chukchi seas, as well as from other emission sources within the modeling domain. The CAMx OSAT and PSAT source apportionment tools use reactive tracers that operate in parallel to the host PGM to provide air quality and deposition contributions due to user-selected source groups. CAMx determines the contributions of emissions from each source group to the total CAMx model concentrations and depositions during the course of the simulation. A detailed description of the CAMx source apportionment tools is available in the CAMx user's guide (ENVIRON, 2014).

The Anthropogenic Precursor Culpability Assessment (APCA) version of OSAT was used in the future year scenario modeling. APCA differs from OSAT in that it distinguishes between natural and anthropogenic emissions; when ozone is formed due to the interaction of biogenic VOC and anthropogenic NO_x under VOC-limited conditions, a case OSAT would assign the ozone formed to the biogenic VOC, APCA recognizes that biogenic VOC is uncontrollable and re-directs the ozone formed to the anthropogenic NO_x. Thus APCA assigns ozone formed to natural emissions only when it is due to natural VOC interacting with natural NO_x emissions. Like OSAT, APCA uses four reactive tracers to track the ozone contributions of each source group: NO_x emissions (N_i), VOC emissions (V_i) and ozone formed under VOC-limited ($O3V_i$) and NO_x -limited ($O3N_i$) conditions.

For PM, three families of PSAT source apportionment tracers were used to track contributions of SO_4, NO_3/NH_4 and primary PM that require, respectively, 2, 7 and 6 reactive tracers for each family. Thus, combined APCA/PSAT source apportionment uses 19 reactive tracers to track the contribution of each source group. The Secondary Organic Aerosol (SOA) family of PSAT tracers was not used in the future year scenario source apportionment modeling because including SOA in the PSAT calculations would more than double the number of required reactive tracers resulting in doubling of the CAMx source apportionment model run time. This is because the chemistry of SOA is quite complex involving numerous gaseous, semi-volatile and particulate species so that PSAT requires 21 tracers to track the SOA contributions of each source group. In any case, only a few specific kinds of VOC species form SOA (i.e., isoprene, terpenes, sesquiterpenes, and aromatics) and these VOCs are mainly emitted by biogenic sources. Although some aromatic species such as toluene and xylene are emitted by anthropogenic sources including gasoline combustion, emissions from O&G exploration and production contain only small levels of aromatic VOC emissions overall.

6.1.2 *Future Year Source Apportionment Simulation*

The CAMx Future Year simulation was first conducted for a full calendar year over the 36 km modeling domain shown in Figure 2-1. The BCs defining inflow concentrations around the lateral boundaries of the 12 km domain were obtained from this simulation. After preparing the BCs, 12/4 km CAMx Future Year PSAT/APCA source apportionment simulation was commenced. Both the 36 km and 12/4 km simulations made use of the same 2012 WRF meteorology and model configuration used in the base case simulation.

6.2 Post-Processing of Future Year Source Apportionment Modeling Results

6.2.1 *Overview*

The CAMx future year scenario ozone and PM source apportionment modeling outputs were post-processed for comparison against the NAAQS and PSD concentration increments listed in Table 6-1, and other thresholds of concern (TOC) as discussed below. For analyzing NAAQS and AQRV impacts at Class I and specified Class II areas, the TOCs used were defined by the Federal Land Manager (FLM) that manages each Class I/II area as prescribed in the June 23, 2011 Memorandum of Understanding (MOU) for evaluating on-shore O&G AQ/AQRV impacts (USDA et al., 2011).

CAMx source apportionment results for individual source categories were used to evaluate the impacts of each source group as defined in Table 6-2. Note that, with the exception of Source Group E, source groups defined for anthropogenic emission sources (i.e., groups B, C, D, G, and H) all refer to emissions included in the Arctic AQ Study emissions inventory (i.e., emissions from sources within the NSB and adjacent State and Federal waters of the Chukchi and Beaufort seas). Source Group E represents anthropogenic emissions from sources outside the NSB, including sources in other parts of Alaska and northwestern Canada which fall within the 4/12 km modeling domain (see Figure 4-1). All new O&G sources in the Future Year scenario are represented by Source Group D. Existing O&G sources (i.e., O&G sources included in the Base Year scenario that are also included in the Future Year scenario), are represented by Source Group B. All other anthropogenic sources in the Arctic AQ Study emission inventory are represented by Source Group C. Source groups BY and FY do not represent source apportionment results but are instead used here to represent results from the "host" model runs for the Base Year and Future Year, respectively. These results represent the combined impact of emissions from all sources included in the modeling domain, including contributions from the BCs specified at the outer boundaries of the 12 km domain.

Note that individual sources in Source Groups B and C are all included in both the Base Year and the Future Year scenarios, although some of these sources are projected to have different levels of emissions in the Future Year as compared to the Base Year as shown in Table 6-3. Notwithstanding these changes, by far the most noteworthy differences between the Base Year and Future Year scenarios are the inclusion of new O&G sources in the Future Year scenario; changes in emissions from existing sources (Source Groups B and C) are minor compared to emissions from the new O&G sources. The 38% reduction in SO_2 emissions from existing sources is due to the switch to Ultra Low Sulfur Diesel (ULSD) in power plants and home heating equipment as described in Fields Simms et al. (2014).

Table 6-1. NAAQS and PSD increments.

Pollutant	Pollutant/Averaging Time	NAAQS	PSD Class I Increment[a]	PSD Class II Increment[a]
CO	1-hour[b]	**35 ppm** 40,000 µg/m^3	--	--
CO	8-hour[b]	**9 ppm** 10,000 µg/m^3	--	--
NO_2	1-hour[c]	**100 ppb** 188 µg/m^3	--	--
NO_2	Annual[d]	**53 ppb** 100 µg/m^3	2.5 µg/m^3	25 µg/m^3
O_3	8-hour[e]	**0.070 ppm** 137 µg/m^3	--	--
PM_{10}	24-hour[f]	**150 µg/m^3**	8 µg/m^3	30 µg/m^3
PM_{10}	Annual[g]	--	4 µg/m^3	17 µg/m^3
$PM_{2.5}$	24-hour[h]	**35 µg/m^3**	2 µg/m^3	9 µg/m^3
$PM_{2.5}$	Annual[i]	**12 µg/m^3**	1 µg/m^3	4 µg/m^3
SO_2	1-hour[j]	**75 ppb** 196 µg/m^3		
SO_2	3-hour[k]	**0.5 ppm** 1,300 µg/m^3	25 µg/m^3	512 µg/m^3
SO_2	24-hour	--	5 µg/m^3	91 µg/m^3
SO_2	Annual[d]	--	2 µg/m^3	20 µg/m^3

[a] The PSD demonstrations serve information purposes only and do not constitute a regulatory PSD increment consumption analysis

[b] No more than one exceedance per calendar year

[c] 98th percentile, averaged over 3 years

[d] Annual mean not to be exceeded

[e] Fourth-highest daily maximum 8-hour ozone concentrations in a year, averaged over 3 years, NAAQS promulgated December 28, 2015

[f] Not to be exceeded more than once per calendar year on average over 3 years.

[g] 3-year average of the arithmetic means over a calendar year

[h] 98th percentile, averaged over 3 years

[i] Annual mean, averaged over 3 years, NAAQS promulgated December 14, 2012

[j] 99th percentile of daily maximum 1-hour concentrations in a year, averaged over 3 years

[k] No more than one exceedance per calendar year (secondary NAAQS)

Table 6-2. Source groups for CAMx source apportionment.[a]

Source Group	Name	Source Categories
A	Natural[b]	Biogenic, Lightning NO_x
B	Baseline O&G	Existing O&G sources included in Base Year scenario of the Arctic AQ Study Emissions Inventory
C	Baseline Other Anthropogenic	Existing anthropogenic sources other than O&G included in Base Year scenario of the Arctic AQ Study Emissions Inventory
D	New O&G	New O&G sources included in the Future Year scenario
E	Outside of NSB Anthropogenic	Anthropogenic sources outside of the NSB and adjacent State and Federal waters
F	Fires	All wildfires and prescribed burns
G	Baseline All	Source Groups B and C
H	NSB All	Source Groups B, C and D
FY	Future Year	All sources in Future Year scenario
BY	2012 Base Year	2012 Base Year run results

[a] Results for groups A – H are from the Future Year scenario source apportionment outputs; results for group FY are from the Future Year scenario "host model" (all sources combined) outputs; results for group BY are from the "host model" (all sources combined) outputs from the Base Year scenario outputs.

[b] Although sea salt represents a "natural" source of emissions, a tracer for sea salt is not included in PSAT so sea salt contributions are not included in Source Group A.

Table 6-3. Emission totals by source group in the Arctic AQ Study emissions inventory (tons per year).

	Species	Baseline Other Anthropogenic	Baseline O&G	New O&G	Biogenic[a]	Fire[a]
Base Year (BY)	NO_x	2,221	45,509	-	1,782	482
	$PM_{2.5}$	3,599	1,203	-	-	1,207
	SO_2	165	1,119	-	-	88
	VOC	818	2,241	-	150,967	392
Future Year (FY)	NO_x	2,368	45,627	30,751	1,782	482
	$PM_{2.5}$	3,600	1,220	1,433	-	1,207
	SO_2	103	1,130	1,955	-	88
	VOC	826	2,302	1,769	150,967	392
FY - BY	NO_x	146	117	30,751	-	-
	$PM_{2.5}$	1	17	1,433	-	-
	SO_2	-63	12	1,955	-	-
	VOC	8	61	1,769	-	-
% Change	NO_x	6.6%	0.3%	N/A	-	-
	$PM_{2.5}$	0.0%	1.4%	N/A	-	-
	SO_2	-37.9%	1.0%	N/A	-	-
	VOC	0.9%	2.7%	N/A	-	-

[a] Biogenic and fire emission totals are for the full 4 km domain (see Fig. 4-1).

6.2.2 *Comparison against NAAQS*

CAMx Future Year scenario predicted total concentrations from all emission sources were post-processed for comparison to the applicable NAAQS listed in Table 6-1 above. In many photochemical modeling studies, comparisons to the ozone and $PM_{2.5}$ NAAQS are performed in two different ways. Firstly, the CAMx predictions are compared directly against each NAAQS. This is referred to as the "absolute" prediction comparison. These absolute prediction comparisons may be misleading in cases in which the model exhibits substantial prediction bias. In recognition of this, U.S. EPA modeling guidance (U.S. EPA, 2007; 2014) recommends using the model in a relative sense when projecting future year ozone, $PM_{2.5}$ and regional haze levels, and the U.S. EPA has developed the Modeled Attainment Test Software (MATS; Abt. 2014) for making such future year projections. This second approach uses the ratio of future year to current year modeling results to develop Relative Response Factors (RRFs) that are applied to

observed current year Design Values (abbreviated as either DVC or DVB) to make future year Design Value (DVF) projections (i.e., DVF = DVC x RRF). While this approach avoids issues associated with possible model bias, it requires a robust set of air quality observations suitable for calculating the current year design values. Given the extremely limited availability of observations in the NSB, the MATS approach was not applied in this study.

6.2.3 *Impacts at Class I and specified Class II areas designated as national parks, national preserves, and national wildlife refuges*

Incremental AQ/AQRV contributions associated with emissions from each source group listed in Table 6-2 were calculated at the Class I and specified Class II areas shown in Figure 1-3 and listed in Table 1-2. Receptors for each Class I and specified Class II area were defined based on the spatial extent of the Class I/II area defined using shapefiles obtained from the applicable Federal Land Management agency. A GIS was used to determine the set of grid cells consisting of all cells with a minimum Class I/II area overlap of 5%. Model results for the identified grid cells were then used to represent predicted ambient concentrations and deposition in each area.

6.2.3.1 Incremental Visibility Impacts

Visibility impacts were calculated for each source group using incremental concentrations as quantified by the CAMx PSAT/APCA tool. Changes in light extinction from CAMx model concentration increments due to emissions from each source group were calculated for each day at grid cells representing each Class I and specified Class II area. The FLAG (2010) procedures were used in the incremental visibility assessment analysis.

The visibility evaluation metric used in this analysis is based on the Haze Index (HI) which is measured in deciview (dv) units and is defined as follows:

$$HI = 10 \times \ln[b_{ext}/10]$$

Where b_{ext} is the atmospheric light extinction measured in inverse megameters (Mm^{-1}) and is calculated primarily from atmospheric concentrations of particulates. A more intuitive measure of haze is visual range (VR), which is defined as the distance at which a large black object just disappears from view, and is measured in kilometers. Visual range is related to b_{ext} by the formula $VR = 3912 / b_{ext}$. The advantage of using the HI rather than VR is that a given change in HI is approximately associated with the same degree of perceived change in visibility regardless of the baseline conditions, whereas small changes in VR are much more noticeable under clean conditions as compared to hazy conditions.

The incremental concentrations due to each source group were added to natural background extinction in the extinction equation (b_{ext}) and the difference between the Haze Index with the source group concentrations included and the Haze Index based solely on natural background concentrations is calculated. This quantity is the change in Haze Index, which is referred to as "delta deciview" (Δdv):

$$\Delta dv = 10 \times \ln[b_{ext(SC+background)}/10] - 10 \times \ln[b_{ext(background)}/10]$$

$$\Delta dv = 10 \times \ln[b_{ext(SC+background)}/b_{ext(background)}]$$

Here $b_{ext(SC+background)}$ refers to atmospheric light extinction due to impacts from the source category plus background concentrations, and $b_{ext(background)}$ refers to atmospheric light extinction due to natural background concentrations only.

For each source group, the estimated visibility degradation at the Class I areas and specified Class II areas due to the source group is calculated in terms of the number of days that exceed a threshold change in deciview (Δdv) relative to background conditions. The number of days with a Δdv greater than 0.5 and 1.0 are reported.

IMPROVE Reconstructed Mass Extinction Equations

The FLAG (2010) procedures for evaluating visibility impacts at Class I areas use the revised IMPROVE reconstructed mass extinction equation to convert PM species in μg/m^3 to light extinction (b_{ext}) in inverse megameters (Mm^{-1}) as follows:

$$b_{ext} = b_{SO4} + b_{NO3} + b_{EC} + b_{OCM} + b_{Soil} + b_{PMC} + b_{SeaSalt} + b_{Rayleigh} + b_{NO2}$$

where

$$b_{SO4} = 2.2 \times f_S(RH) \times [\text{Small Sulfate}] + 4.8 \times f_L(RH) \times [\text{Large Sulfate}]$$

$$b_{NO3} = 2.4 \times f_S(RH) \times [\text{Small Nitrate}] + 5.1 \times f_L(RH) \times [\text{Large Nitrate}]$$

$$b_{OCM} = 2.8 \times [\text{Small Organic Mass}] + 6.1 \times [\text{Large Organic Mass}]$$

$$b_{EC} = 10 \times [\text{Elemental Carbon}]$$

$$b_{Soil} = 1 \times [\text{Fine Soil}]$$

$$b_{CM} = 0.6 \times [\text{Coarse Mass}]$$

$$b_{SeaSalt} = 1.7 \times f_{SS}(RH) \times [\text{Sea Salt}]$$

$$b_{Rayleigh} = \text{Rayleigh Scattering (Site-specific)}$$

$$b_{NO2} = 0.33 \times [NO_2 \text{ (ppb)}] \text{ {or as: } } 0.1755 \times [NO_2 \text{ (μg/m}^3\text{)}]\}.$$

f(RH) are relative humidity adjustment factors that account for the fact that sulfate, nitrate and sea salt aerosols are hygroscopic and are more effective at scattering solar radiation at higher relative humidity. FLAG (2010) recommends using monthly average f(RH) values rather than the hourly averages recommended in the previous FLAG (2000) guidance document in order to moderate the effects of extreme weather events on the visibility results.

The revised IMPROVE equation treats "large sulfate" and "small sulfate" separately because large and small aerosols affect an incoming beam of light differently. However, the IMPROVE measurements do not separately measure large and small sulfate; they measure only the total $PM_{2.5}$ sulfate. Similarly, CAMx calculates a single concentration of particulate sulfate for each grid cell. Part of the definition of the new IMPROVE equation is a procedure for calculating the large and small sulfate contributions based on the magnitude of the model output sulfate concentrations; the procedure is documented in FLAG (2010). The sulfate concentration magnitude is used as a surrogate for distinguishing between large and small sulfate concentrations. For a given grid cell, the large and small sulfate contributions are calculated from the model output sulfate (which is the "Total Sulfate" referred to in the FLAG (2010) guidance) as:

For Total Sulfate < 20 μg/m^3:

$$[\text{Large Sulfate}] = ([\text{Total Sulfate}] / 20\ \mu g/m^3) \times [\text{Total Sulfate}]$$

For Total Sulfate ≥ 20 μg/m^3:

$$[\text{Large Sulfate}] = [\text{Total Sulfate}]$$

For all values of Total Sulfate:

$$[\text{Small Sulfate}] = [\text{Total Sulfate}] - [\text{Large Sulfate}]$$

The procedure is identical for nitrate and organic mass.

For calculating light extinction by NO_2 for each source group, the NO_x concentration assigned to the source group by the CAMx source apportionment methodology was assumed to be 100% NO_2 since PSAT does not directly track the NO_2 contribution from a source group. This differs from the procedure used for other post-processing calculations such as for analysis of NAAQS and PSD impacts for which the PSAT RGN tracer was used as the basis for obtaining source contributions for NO_2.[9] The use of NO_x to represent visibility impacts of NO_2 was used here to simplify the visibility calculations.

Although sodium and particulate chloride are treated in the CAMx core model, these species are not carried in the CAMx PSAT tool. This does not affect the calculations of visibility impacts from individual anthropogenic source groups as anthropogenic sources generally do not emit sodium or particulate chloride.

Predicted daily average modeled concentrations apportioned to each source group for receptor grid cells containing Class I and specified Class II areas were processed using the revised IMPROVE reconstructed mass extinction equation to obtain $b_{ext(SC+background)}$ and $b_{ext(background)}$ at each specified receptor area, from which Δdv was calculated as described above.

Annual average natural conditions for each Class I area were obtained from Table 6 in FLAG (2010) and monthly relative humidity factors for each Class I area were obtained from Tables 7-9 in FLAG (2010). As Denali National Park and Preserve is the only Alaska area included in these tables, the values listed for Denali were used to represent all of the Class I/II areas analyzed in this study. The Δdv was calculated for each day of the annual CAMx run for each grid cell that overlaps a Class I/II area by 5% or more. The highest Δdv across all grid cells overlapping a Class I/II area was selected to represent the daily value at that Class I/II area. The number of days with visibility impacts due to emissions from each source group exceeding the 0.5 and 1.0 Δdv thresholds is reported.

6.2.3.2 Sulfur and Nitrogen Deposition

CAMx-predicted wet and dry fluxes of sulfur- and nitrogen-containing species were processed to estimate total annual sulfur (S) and nitrogen (N) deposition values at each Class I and specified

[9] For these other post-processing calculations, source apportionment of NO_2 is based on source apportionment of total reactive nitrogen (RGN) which consists of NO, NO_2 and other reactive nitrogen compounds (e.g., N_2O_5, HONO, etc.). For each hour and grid cell, a source group's incremental PSAT RGN contribution is converted to NO_2 by multiplying by the total (all sources) NO_2/RGN concentration ratio.

Class II area. The Maximum annual S and N deposition values from any grid cell that intersects a Class I or a specified Class II receptor area was used to represent deposition for that area, in addition to the average annual deposition values of all grid cells that represent a Class I or a specified Class II receptor area. Although the convention in the past has been to report just the maximum deposition in any receptor in a Class I/II area, since deposition relates to the total amount deposited across an entire watershed, the average metric may be considered a more relevant parameter for evaluating potential environmental effects in some cases. Maximum and average predicted S and N deposition impacts are reported separately for each source group.

Nitrogen deposition impacts were calculated by taking the sum of the nitrogen contained in the fluxes of all nitrogen species modeled by CAMx PSAT source apportionment tool. CAMx species used in the nitrogen deposition flux calculation are: reactive gaseous nitrate species (RGN: NO, NO_2, NO_3 radical, HONO, N_2O_5), total peroxy nitrate (TPN: gaseous peroxyl acetyl nitrate plus peroxy nitric acid), organic nitrates (NTR), particulate nitrate formed from primary emissions plus secondarily formed particulate nitrate (NO_3), gaseous nitric acid (HNO_3), gaseous ammonia (NH_3) and particulate ammonium (NH_4). CAMx species used in the sulfur deposition calculation are primarily sulfur dioxide emissions (SO_2) and particulate sulfate ion from primary emissions plus secondarily formed sulfate (SO_4).

FLAG (2010) recommends that applicable sources assess impacts of nitrogen and sulfur deposition at Class I areas. This guidance recognizes the importance of establishing critical deposition loading values ("Critical Loads") for each specific Class I area as these Critical Loads are completely dependent on local atmospheric, aquatic and terrestrial conditions and chemistry. Critical Load thresholds are essentially a level of atmospheric pollutant deposition below which negative ecosystem effects are not likely to occur. FLAG (2010) does not include any Critical Load levels for specific Class I areas and refers to site-specific critical load information on FLM websites for each area of concern. Critical Load values have not been established for areas in Alaska. The FLAG 2010 guidance does, however recommend the use of deposition analysis thresholds (DATs[10]) developed by the National Park Service and the USFWS. The DATs represent screening level values for nitrogen and sulfur deposition for individual projects with deposition impacts below the DATS considered negligible. For the Lower 48 states, a DAT of 0.005 kilograms per hectare per year (kg/ha/yr) for both nitrogen and sulfur deposition has been established for both nitrogen and sulfur deposition and in Class I areas west of the Mississippi and a DAT of 0.01 kg/ha/yr has been established for both N and S deposition for areas east of the Mississippi. DATs have not specifically been established for Alaska. As a screening analysis, results for Source Group D (new O&G sources) were compared to the DATs. However, deposition in excess of the DATs does not necessarily represent an adverse impact as the cumulative deposition from all sources may still be below the Critical Load. Comparison of deposition impacts from cumulative sources to the DAT is not appropriate.

6.2.3.3 PSD Increments

The maximum contribution of new O&G emissions were reported for each Class I and specified Class II area and compared against the PSD increments given in Table 6-1. Under the CAA, a PSD increment consumption analysis requires major stationary sources subject to PSD review to

[10] http://www.nature.nps.gov/air/Pubs/pdf/flag/nsDATGuidance.pdf

demonstrate that emission increases from the proposed source in conjunction with all other emissions increases or reductions in the impacted area (typically within 50 kilometers) will not cause or contribute to concentrations of air pollutants that exceed PSD increments. PSD increments have been established for NO_x, SO_2 and PM in Class I and Class II areas. Actions to be authorized by BOEM do not typically constitute major stationary sources and do not typically trigger PSD permits or review. However, a comparison of ambient concentrations from an accumulation of new O&G sources within the entire study area to PSD increments at specific Class I and Class II areas is included in this analysis for information purposes. This information is presented to aid state agencies in tracking potential minor source increment consumption and to aid Federal Land Managers responsible for protecting air resources in Class I and in Class II areas designated as national parks, national preserves, and national wildlife refuges.

7.0 AIR RESOURCE ASSESSMENT RESULTS

7.1 NAAQS Impacts

Future year CAMx modeling results were used to examine future air quality relative to the 2012 base year conditions and relative to the NAAQS for O_3, $PM_{2.5}$, PM_{10}, NO_2, SO_2, and CO. Results are also presented in terms of the impacts of individual source group contributions.

7.1.1 *Ozone*

The ozone NAAQS is defined as the three-year average of the 4th highest maximum daily average 8-hour (MDA8) ozone concentration. Since only one calendar year of modeling results is available for the base year and future year scenarios, the future year 4th highest MDA8 ozone concentration is used as a pseudo-NAAQS comparison metric.

Modeled 4th highest MDA8 values in each model grid cell for the base and future year scenarios and the corresponding differences are shown in Figure 7-1. Modeled 4th highest MDA8 values are all well below the 70 ppb NAAQS with values over the lower elevations of the North Slope in the upper 30s to lower 40s ppb. Highest ozone values are predicted to occur over the higher elevations of the Brooks Range. Differences between the base and future year scenarios include increases of generally less than 1 ppb mostly over portions of the coastal plain with a maximum increase of 1.2 ppb in the coastal portion of the ANWR and decreases of up to 12.9 ppb with most decreases occurring over the Chukchi and Beaufort seas. Comparison of the spatial distributions of the decreases with the distribution of increased NO_x emissions (Figure 3-3) suggests that the predicted ozone reductions are associated with VOC limited ozone formation conditions near these new NO_x sources.

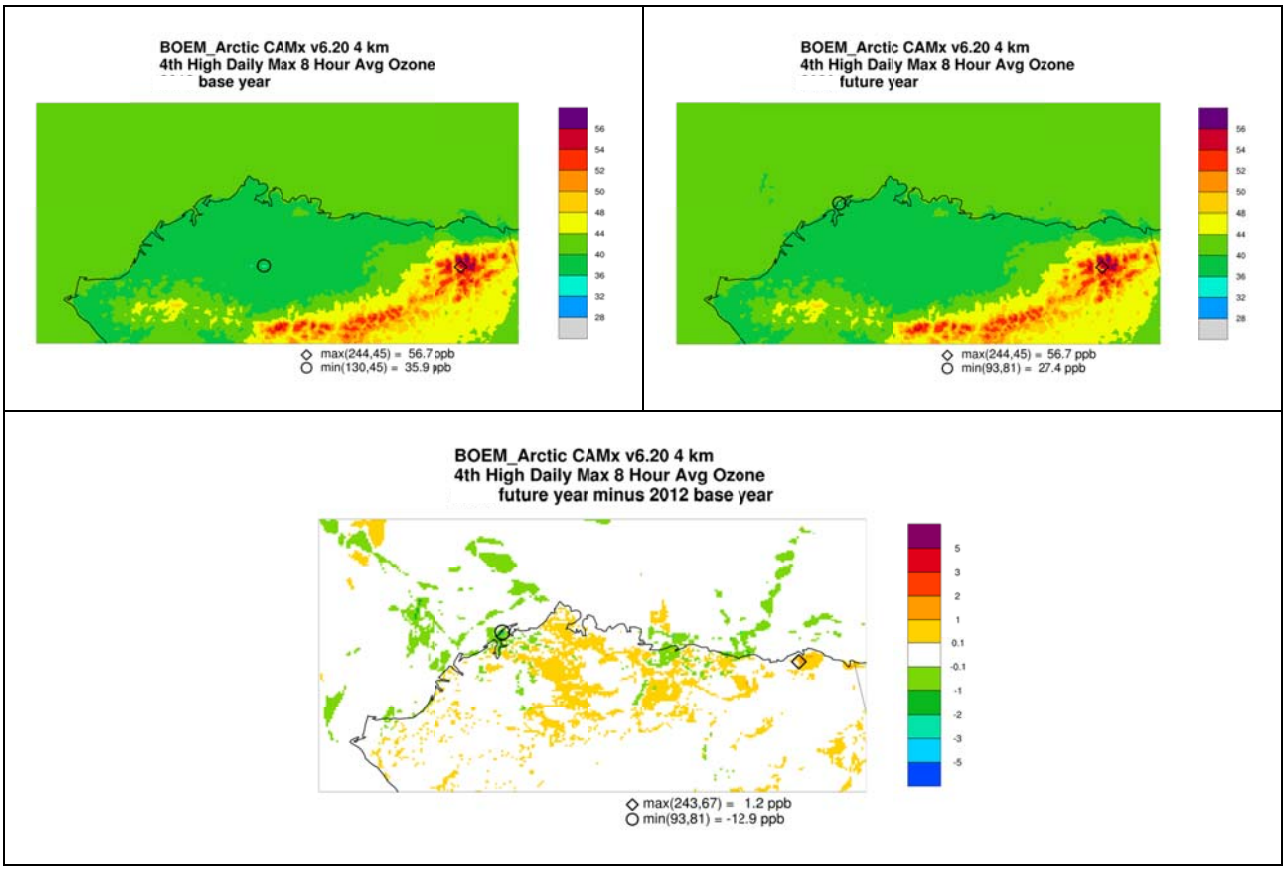

Figure 7-1. Modeled 4th highest MDA8 ozone for the base year (upper left) and future year (upper right) scenarios and their differences (bottom center).

Source group contributions to ozone under the future year scenario are shown in Figure 7-2. Boundary conditions along the outer edges of the 12 km domain (see Figure 4-1) account for most of the modeled 4th highest MDA8 from all sources outside the 4 km domain. Natural sources (biogenics and lightning NO_x) and fires contribute a few ppb. Anthropogenic sources (Source Group H) contribute up to 11.4 ppb with nearly all of this accounted for by baseline sources (Source Group G). Source contributions from O&G sources are compared with contributions from all anthropogenic sources in Figure 7-3. Non-oil and gas anthropogenic source contributions are small (less than 0.5 ppb). New O&G sources (Source Group D) contribute a maximum of 3.3 ppb to the maximum future year contribution of all anthropogenic sources (11.4 ppb).

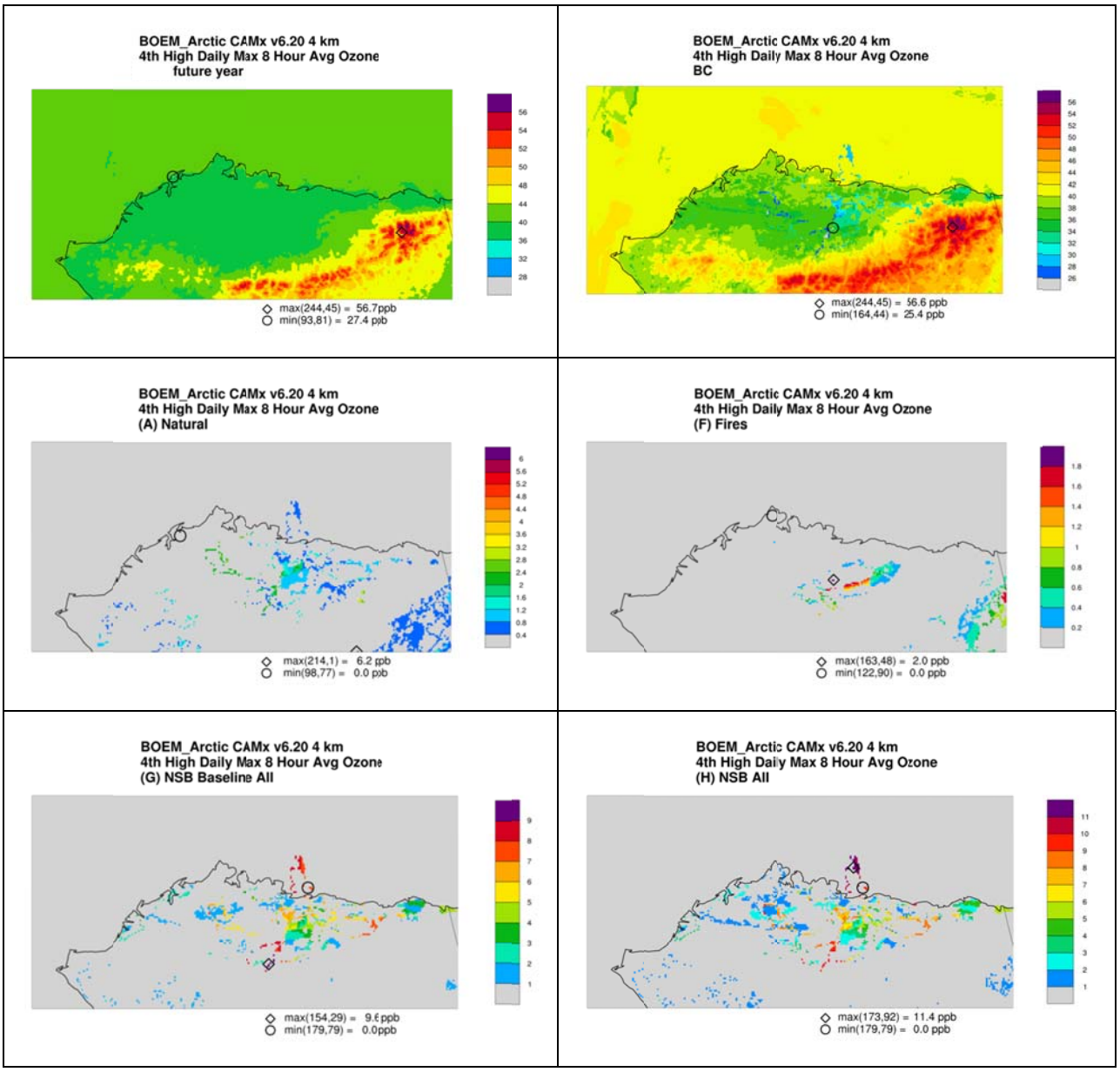

Figure 7-2. Source group contributions to 4th highest DMA8 ozone concentrations under the future year scenario: all sources (top left), boundary conditions (top right), natural sources (middle left), fires (middle right), all baseline anthropogenic sources (bottom left), and all future scenario anthropogenic sources (bottom right); note different color scales used in each panel.

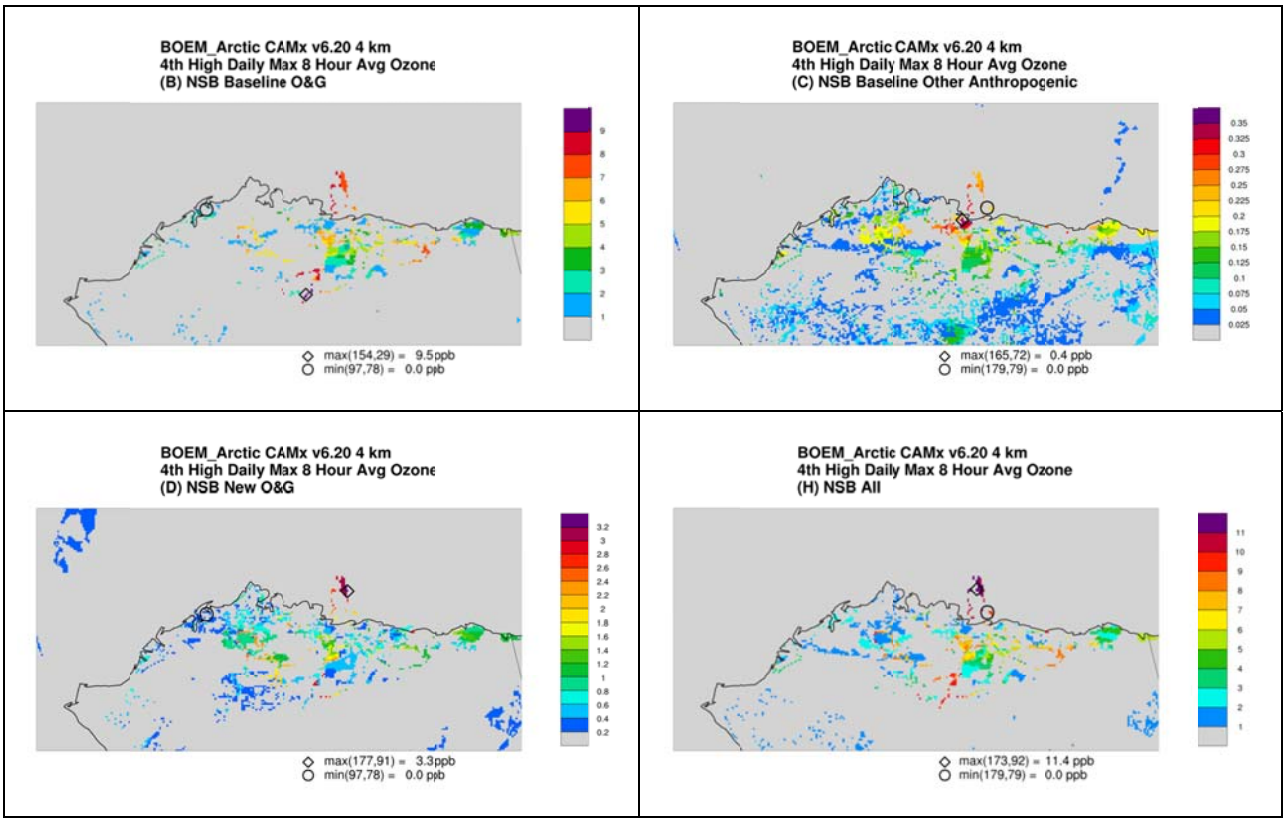

Figure 7-3. Source group contributions to 4th highest DMA8 ozone concentrations under the future year scenario: all baseline O&G sources (top left), other baseline anthropogenic sources (top right), new O&G sources (bottom left), and all anthropogenic sources (bottom right); note different color scales used in each panel.

7.1.2 *$PM_{2.5}$*

CAMx source apportionment absolute modeling results from the Future Year scenario are analyzed and compared with the $PM_{2.5}$ 24-hour and annual NAAQS in this section. There are two $PM_{2.5}$ NAAQS, one for 24-hour averaging time that is expressed as a three-year average of the annual 98th percentile in a year with a threshold of 35 µg/m^3 and an annual average over three-years with a threshold of 12 µg/m^3. With one year of complete everyday modeling, the annual 98th percentile will correspond to the 8th highest 24-hour $PM_{2.5}$ concentration in a year.

7.1.2.1 24-Hour $PM_{2.5}$

As noted above, the 24-hour $PM_{2.5}$ NAAQS is defined as the three-year average of the annual 98th percentile daily average which corresponds to the 8th highest daily average in each year assuming complete data. Since only one calendar year of modeling results are available for the base year and future year scenarios, the future year 8th highest daily average $PM_{2.5}$ concentration was selected for comparison with the NAAQS.

Modeled 8th highest daily $PM_{2.5}$ concentrations in each model grid cell for the base and future year scenarios and the corresponding differences are shown in Figure 7-4. Since the base and

future year predicted 8th highest values are strongly impacted by highly uncertain sea salt emissions as discussed in Section 5.2.3, results are presented here both with and without the contribution of sea salt emissions included. Modeled sea salt concentrations in the coastal areas are generally in the 10 – 20 μg/m^3 range. Although sea salt emissions are the same in both the base and future year scenarios, the $PM_{2.5}$ differences shown in the bottom row of Figure 7-4 are larger under the "no sea salt" case mostly because the additional emissions from new sources in the future year scenario have a stronger influence on which day the 8th highest $PM_{2.5}$ value occurs when sea salt is not included in the total $PM_{2.5}$ mass.[11] $PM_{2.5}$ concentrations are below about 10 μg/m^3 nearly everywhere throughout the domain except for a few grid cells in Barrow where concentrations are modeled to exceed the 35 μg/m^3 NAAQS even with sea salt removed. Further investigation of these high values showed that the major contributor is unpaved road dust. Such dusty conditions along unpaved roads are known to occur in populated areas in Alaska during the summer (ADEC, 2011b), however estimates of the magnitude of road dust emissions are highly uncertain in the Arctic AQ Study emissions inventory due mainly to the necessary use of non-local data for estimating emissions (Fields Simms et al., 2014). As with sea salt, unpaved road dust emissions are unchanged between the base and future year scenarios and therefore do not impact the future minus base year differences.

Future minus base year scenario maximum differences are generally less than 5 μg/m^3 except for a location near Wainwright where increased support vessel activity and a new petroleum processing facility with an assumed 200 MMbbl/yr throughput under the full build-out scenario results in a projected increase of 13.8 μg/m^3 which is 40% of the 35 μg/m^3 NAAQS.

[11] Comparison of the future year minus base year differences for annual averages shows only negligible differences between the with and without sea salt cases – see Figure 7-7.

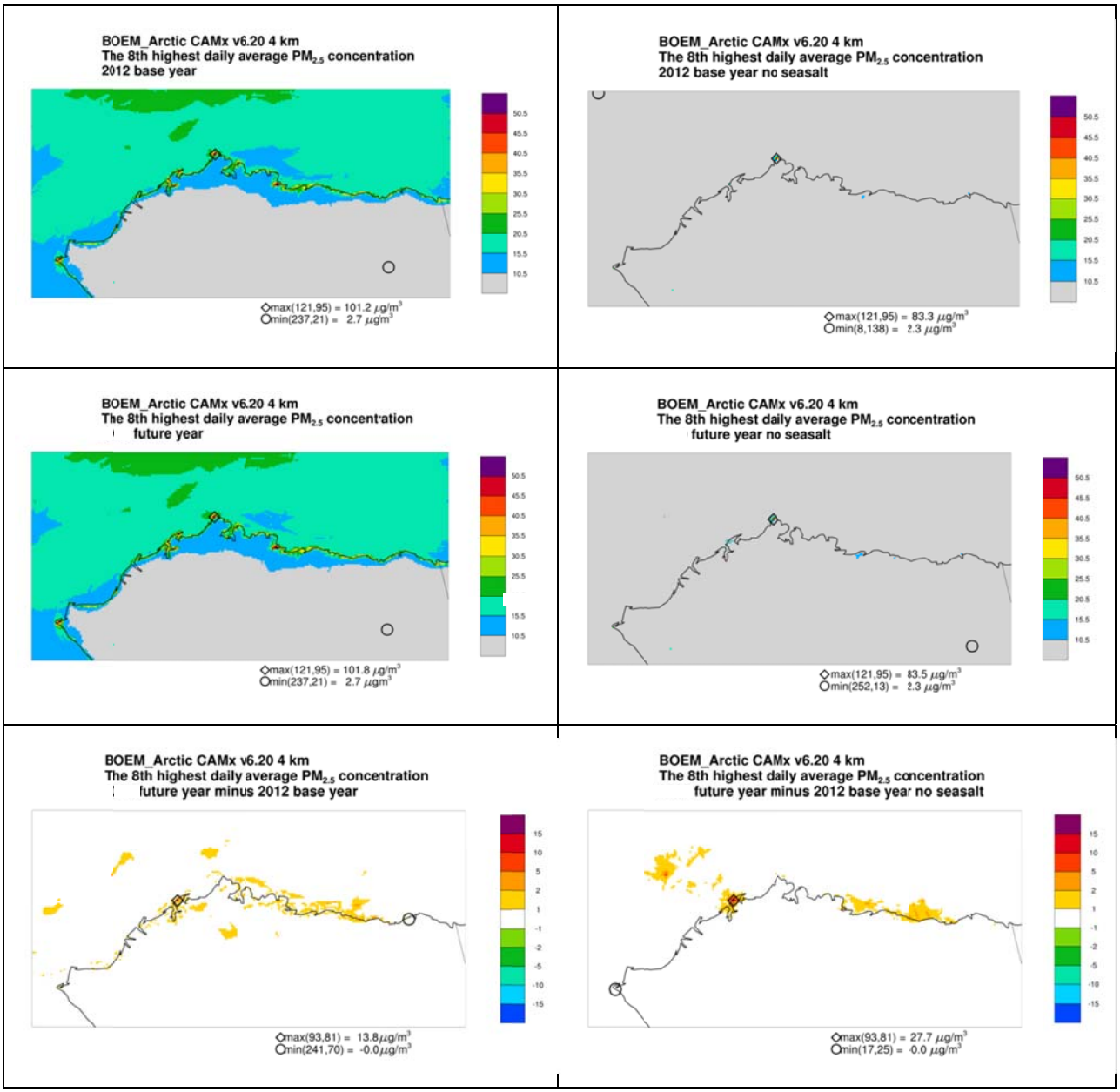

Figure 7-4. Modeled 8th highest daily average $PM_{2.5}$ concentrations for the base year (upper left) and future year (upper right) scenarios, the base year and future year scenarios with sea salt removed (middle row), and their differences (bottom center).

Source group contributions to the modeled 8th highest daily average $PM_{2.5}$ concentrations are shown in Figures 7-5 and 7-6. Source group contributions to these peak PM days exhibit considerable spatial variability as the peak PM events are typically driven by emissions from local sources. Boundary conditions, natural sources and fires are the primary contributors to $PM_{2.5}$ in most interior portions of the NSB but represent only minor contributors to the peak PM days in inhabited coastal areas and areas where mobile sources and oil and gas activities occur.

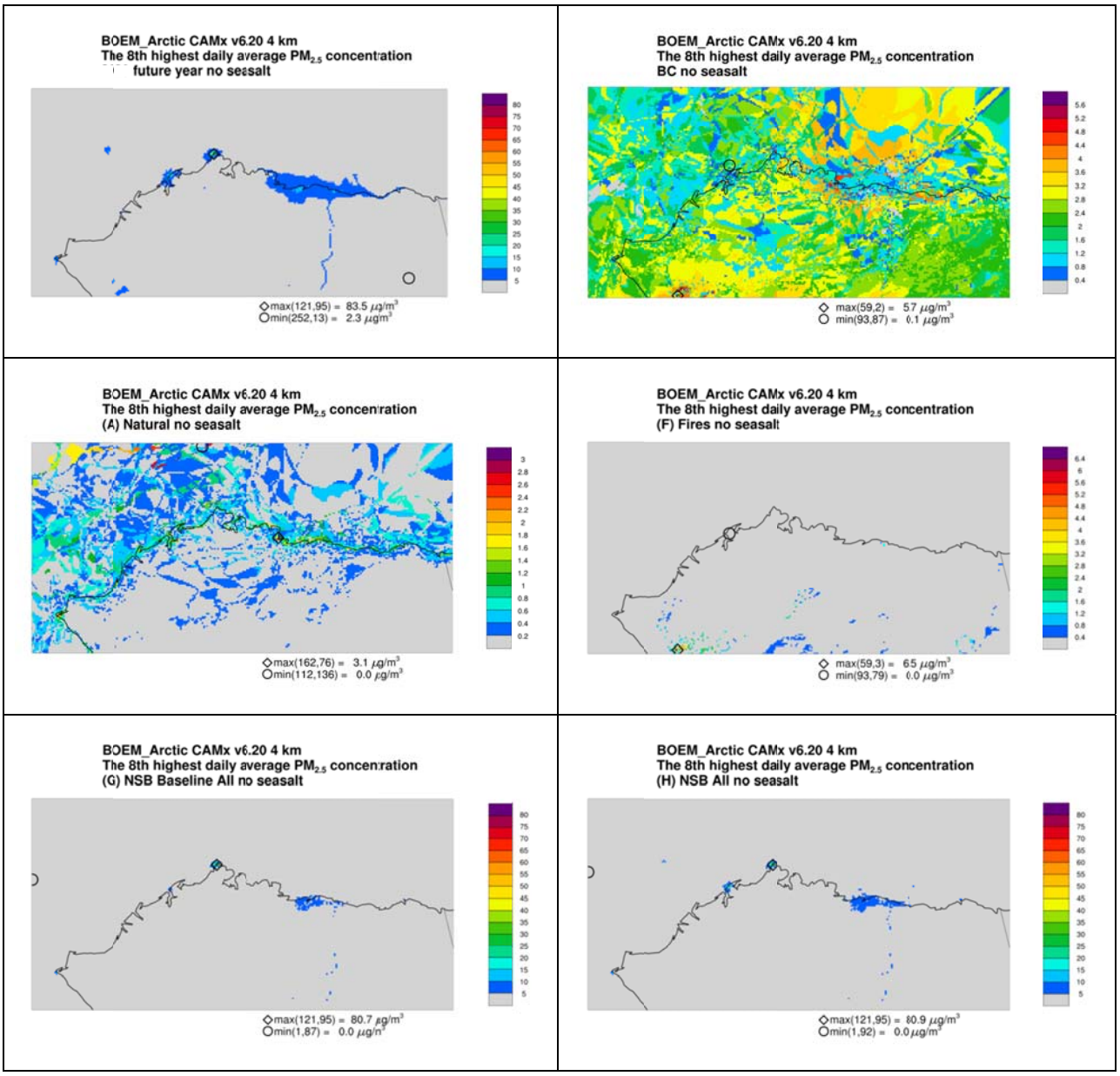

Figure 7-5. Source group contributions to 8th highest daily average $PM_{2.5}$ concentrations under the future year, no sea salt scenario: all sources (top left), boundary conditions (top right), natural sources (middle left), fires (middle right), all baseline anthropogenic sources (bottom left), and all future scenario anthropogenic sources (bottom right); note different color scales used in each panel.

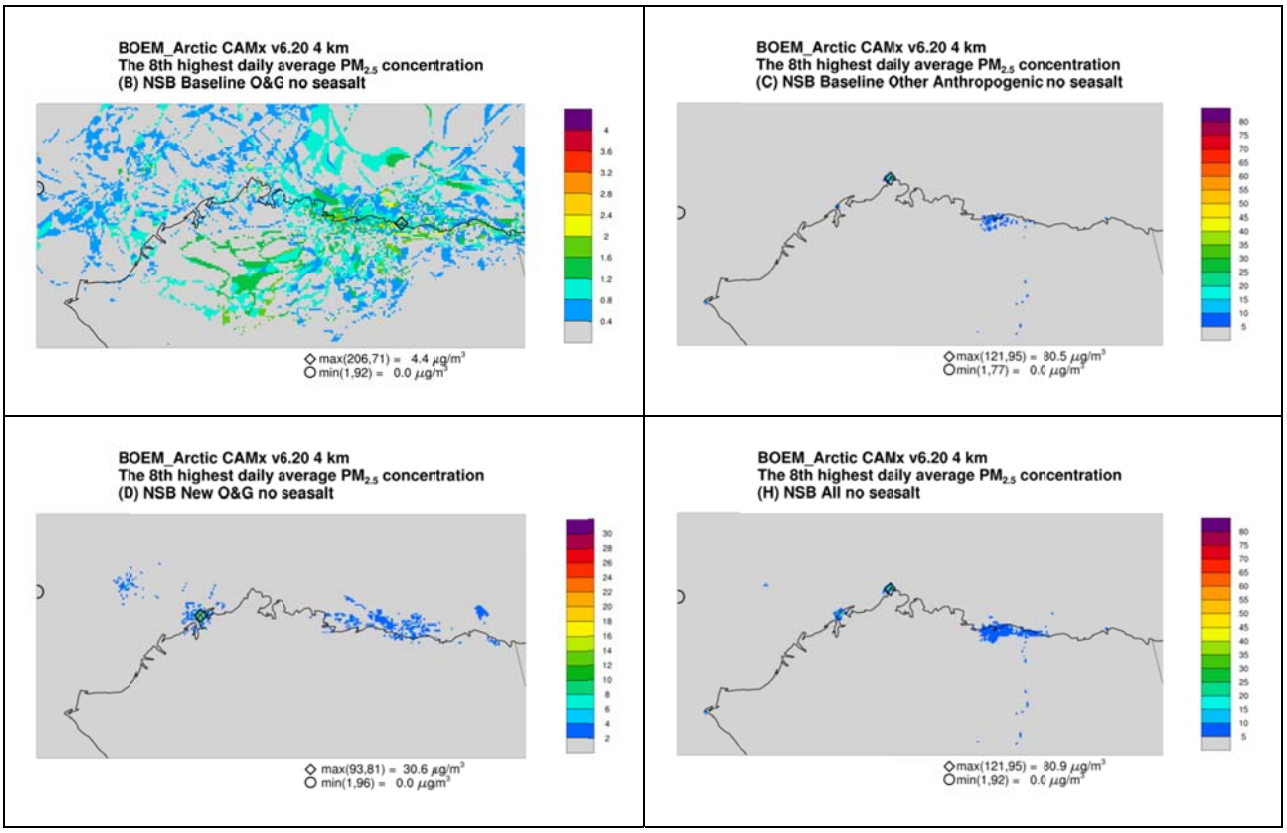

Figure 7-6. Source group contributions to 8th highest daily average $PM_{2.5}$ concentrations under the future year, no sea salt scenario: all baseline oil and gas sources (top left), other baseline anthropogenic sources (top right), new NSB oil and gas sources bottom left), and all anthropogenic sources (bottom right); note different color scales used in each panel.

7.1.2.2 Annual $PM_{2.5}$

Annual average $PM_{2.5}$ model results for the base and future years and the future minus base difference are presented in Figure 7-7. As for the daily $PM_{2.5}$ results described above, results are presented both with and without the highly uncertain sea salt emissions included. Aside from sea salt impacts, pockets of slightly elevated $PM_{2.5}$ occur along the coast in communities or near oil and gas sources. The highest annual average is predicted in Barrow and is associated with unpaved road dust as described in the previous section. The predicted annual average in Barrow exceeds the 12 µg/m^3 NAAQS, even after excluding sea salt. The maximum difference between the future and base year scenarios (8.5 µg/m^3) is predicted to occur near Wainwright.

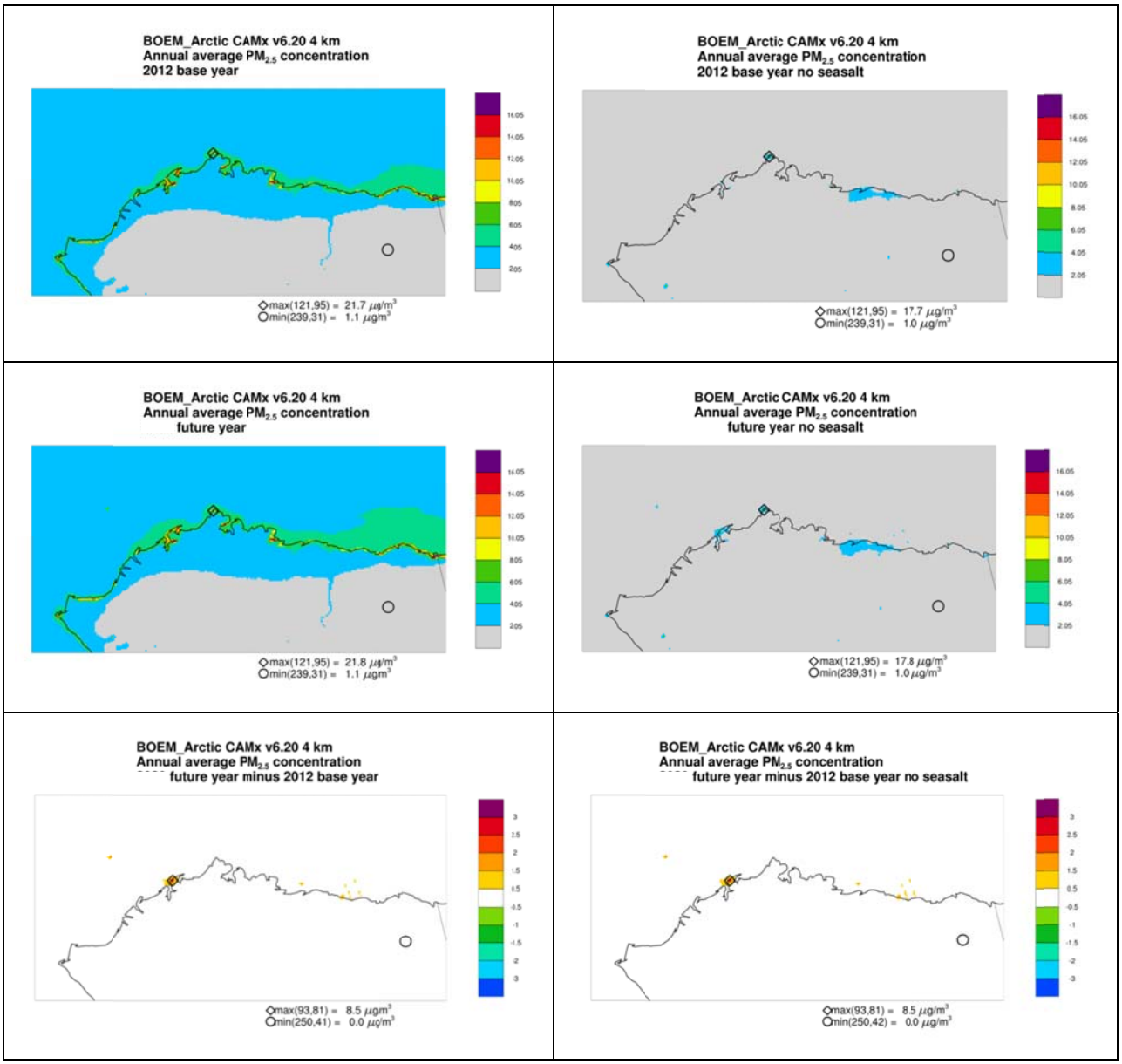

Figure 7-7. Modeled annual average $PM_{2.5}$ concentrations for the base year (upper left) and future year (upper right) scenarios, the base year and future year scenarios with sea salt removed (middle row), and their differences (bottom center).

Source group contributions to annual average $PM_{2.5}$ are shown in Figures 7-8 and 7-9. Most noteworthy features of these results are similar to those described above for the 24-hour $PM_{2.5}$ contributions.

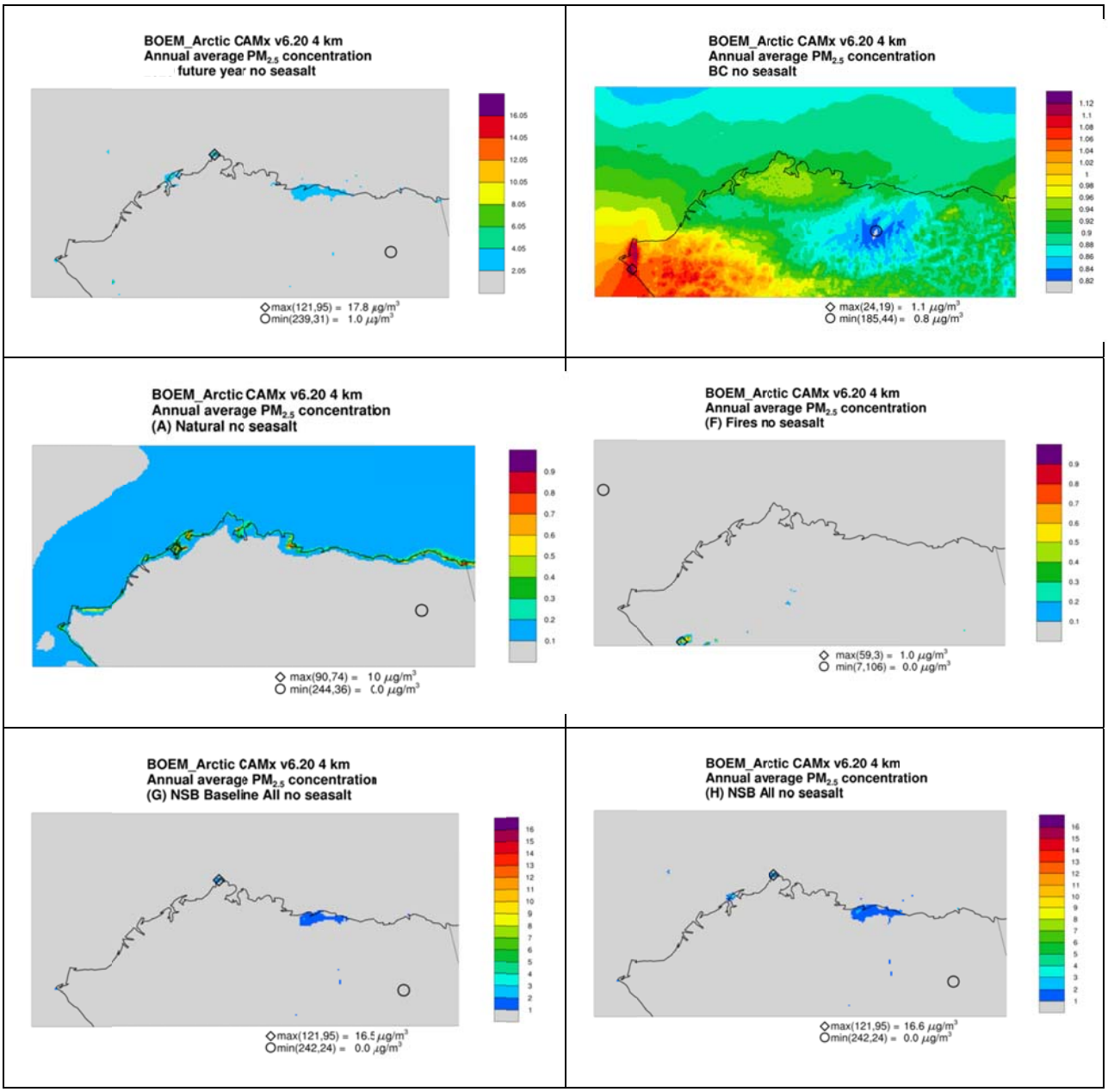

Figure 7-8. Source group contributions to annual average $PM_{2.5}$ concentrations under the future year, no sea salt scenario: all sources (top left), boundary conditions (top right), natural sources (middle left), fires (middle right), all baseline anthropogenic sources (bottom left), and all future scenario anthropogenic sources (bottom right); note different color scales used in each panel.

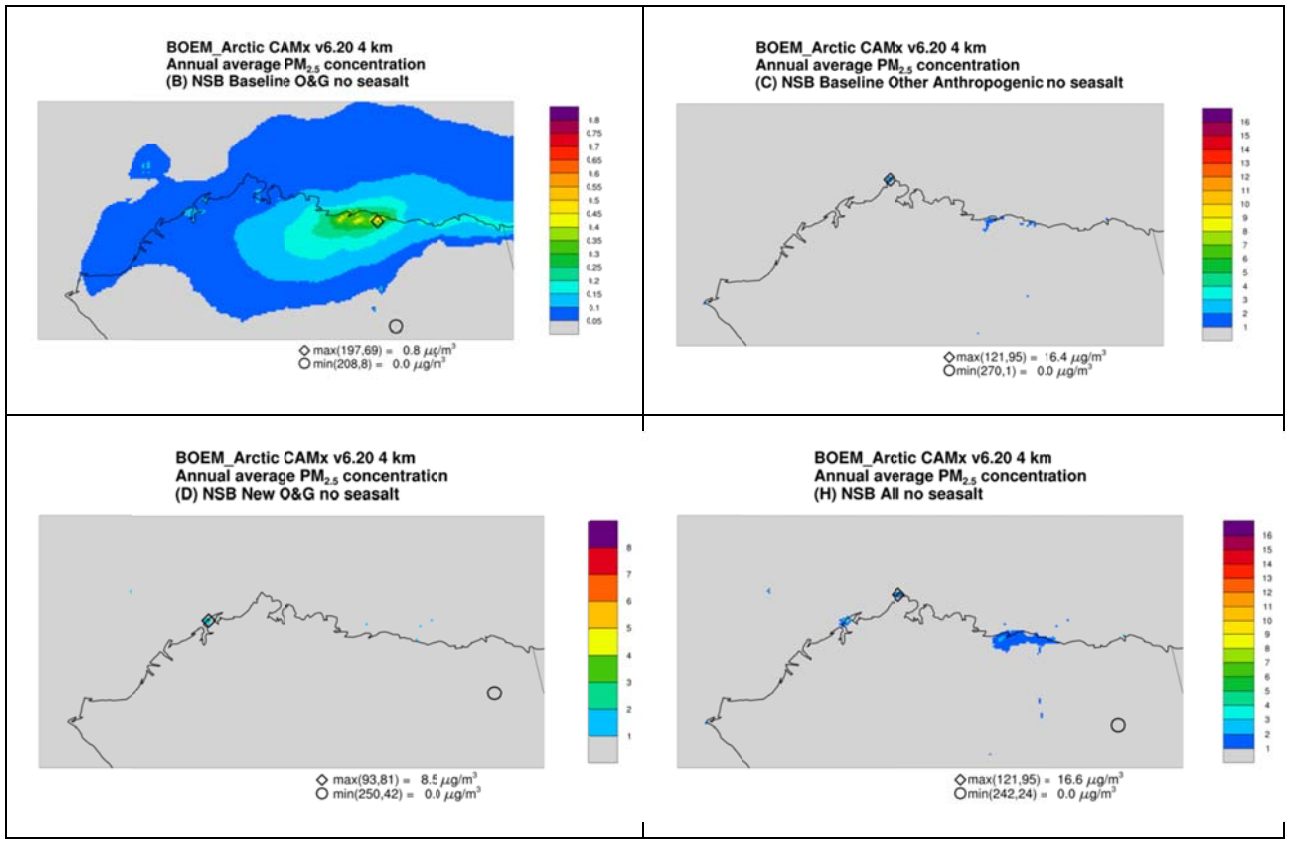

Figure 7-9. Source group contributions to annual average $PM_{2.5}$ concentrations under the future year, no sea salt scenario: all baseline oil and gas sources (top left), other baseline anthropogenic sources (top right), new oil and gas sources (bottom left), and all anthropogenic sources (bottom right); note different color scales used in each panel.

7.1.3 *PM_{10}*

The daily average PM_{10} NAAQS (150 µg/m^3) is not to be exceeded more than once per year on average over 3 years. Based on this formulation, model results are shown in Figure 7-10 in terms of the second highest daily average PM_{10} concentration in each model grid cell. As for $PM_{2.5}$ above, results are shown both with and without sea salt included. The main features of these results are similar to those described for $PM_{2.5}$ in the previous section. The local unpaved road dust peak in Barrow exceeds the NAAQS; concentrations elsewhere are below the NAAQS. The maximum difference between the base and future year scenarios is an increase of 18 µg/m^3 near Wainwright where increased support vessel activity and a new petroleum processing facility with an assumed 200 MMbbl/yr throughput is located under the full build-out scenario .

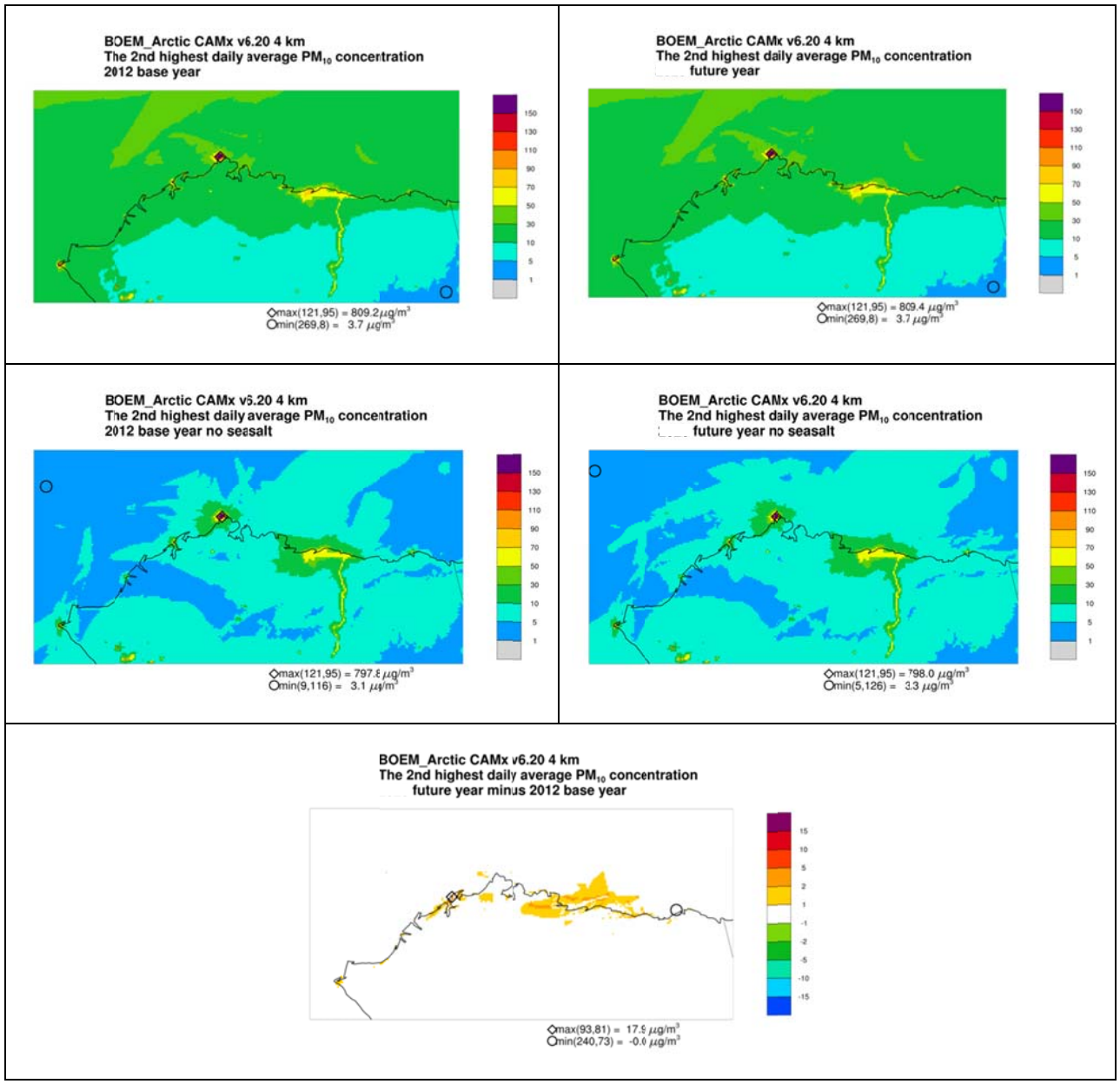

Figure 7-10. Modeled annual average PM_{10} concentrations for the base year (upper left) and future year (upper right) scenarios, the base year and future year scenarios with sea salt removed (middle row), and their differences (bottom center).

7.1.4 *NO_2*

Results are presented here for both the 1-hour average NO_2 NAAQS (100 ppb) and the annual average NO_2 NAAQS (53 ppb). Figures 7-11 and 7-12 display modeled 1-hour average NO_2 design values (based on the 8th highest daily 1-hour maximum) and modeled annual average NO_2 concentrations, respectively, for the base and future year scenarios. All modeled 8th highest 1-hour NO_2 concentrations are below the 100 ppb NAAQS. The NO_2 impacts associated with new oil and gas sources under the future year scenario result in a maximum increase in the 1-hour

design value of 72 ppb in the immediate vicinity of the new sources. Modeled annual average NO_2 concentrations are below the NAAQS; annual average NO_2 concentrations increase by a maximum of 23 ppb in the future year scenario relative to the base year.

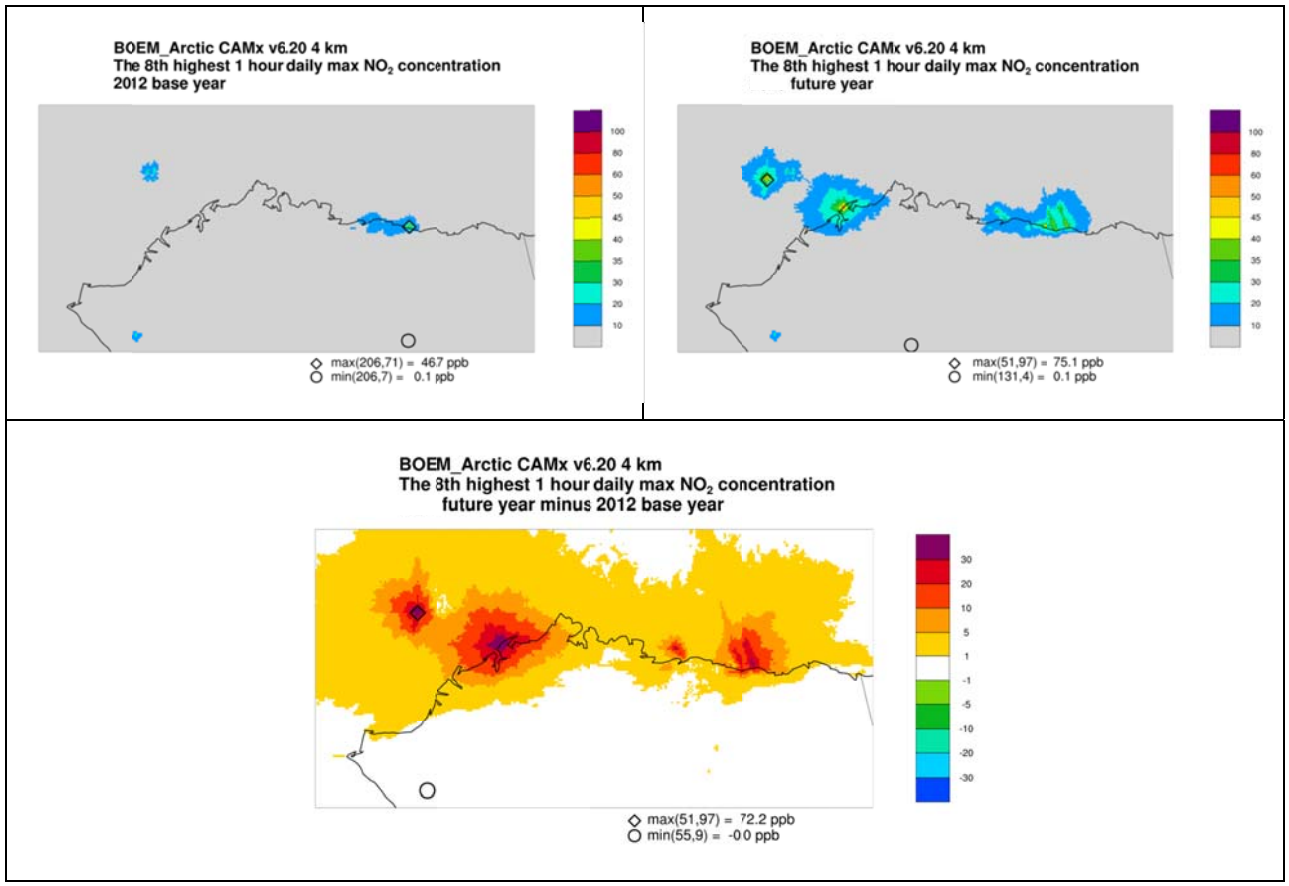

Figure 7-11. Modeled 8th highest 1-hour daily maximum NO_2 concentrations for the base year (upper left), future year (upper right) and future minus base year (bottom center).

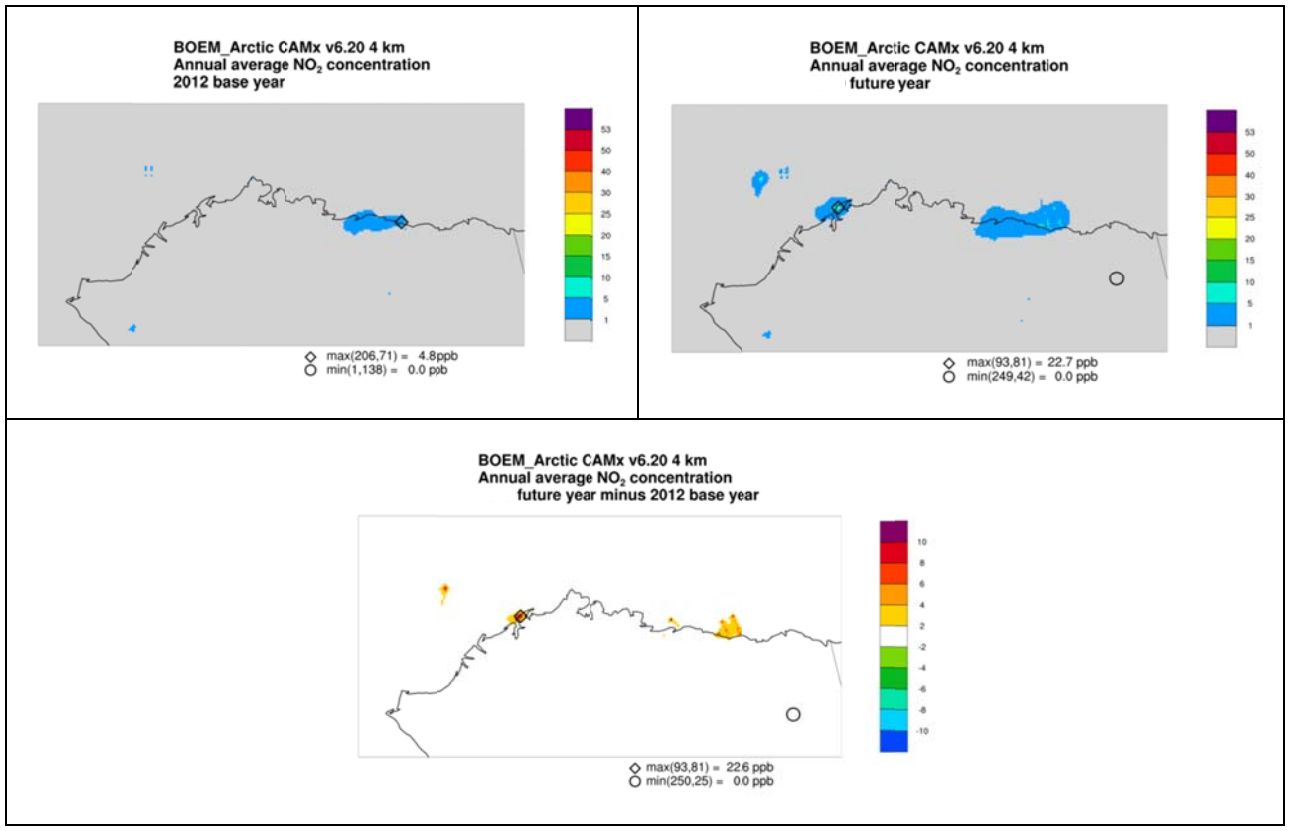

Figure 7-12. Modeled annual average NO_2 concentrations for the base year (upper left), future year (upper right) and future minus base year (bottom center).

Source group contributions to the future year 8th highest daily maximum 1-hour NO_2 concentrations (i.e., the modeled 1-hour NO_2 design values) are shown in Figure 7-13. Oil and gas sources are the dominant contributor to the 1-hour NO_2 design values. Local peak impacts from the new oil and gas sources included in the future year scenario are predicted to be higher than peak impacts from baseline sources.

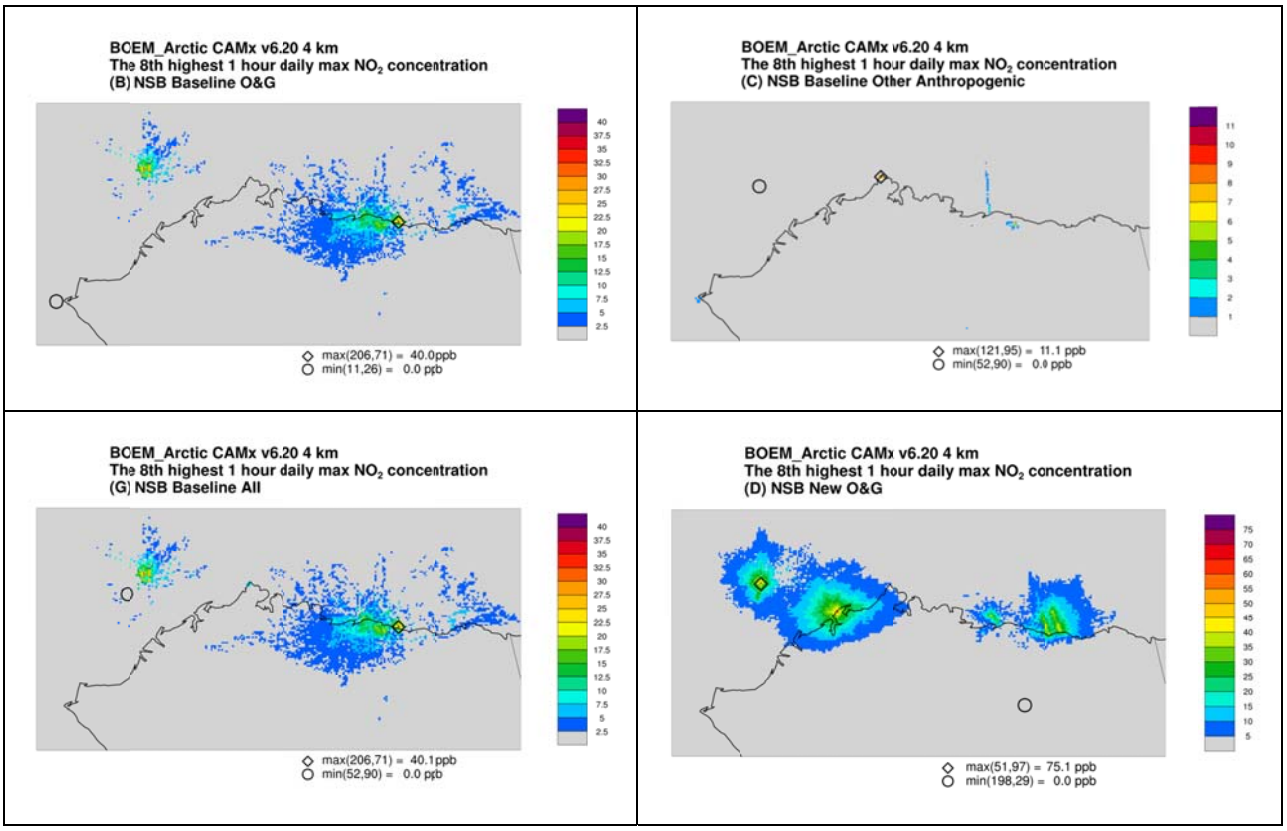

Figure 7-13. Source group contributions to the 8th highest daily maximum 1-hour NO_2 concentrations under the future year scenario for baseline oil and gas sources (top left), baseline other anthropogenic sources (top right), all baseline anthropogenic sources (bottom left), and new oil and gas sources (bottom right).

7.1.5 *SO_2*

The SO_2 NAAQS (75 ppb) is based on a design value defined as the 4th highest daily maximum 1-hour SO_2 concentration averaged over three years. Modeled 4th highest daily maximum 1-hour SO_2 concentrations were therefore used to represent the SO_2 design values as shown for the base and future year scenarios along with the future – base year differences in Figure 7-14. All predicted values are less than the NAAQS. While existing sources are modeled to have design values below 1 ppb, new O&G sources included in the future year scenario are anticipated to have higher SO_2 emissions, resulting in a maximum SO_2 design value of 57 ppb near the offshore platform in the Chukchi Sea.

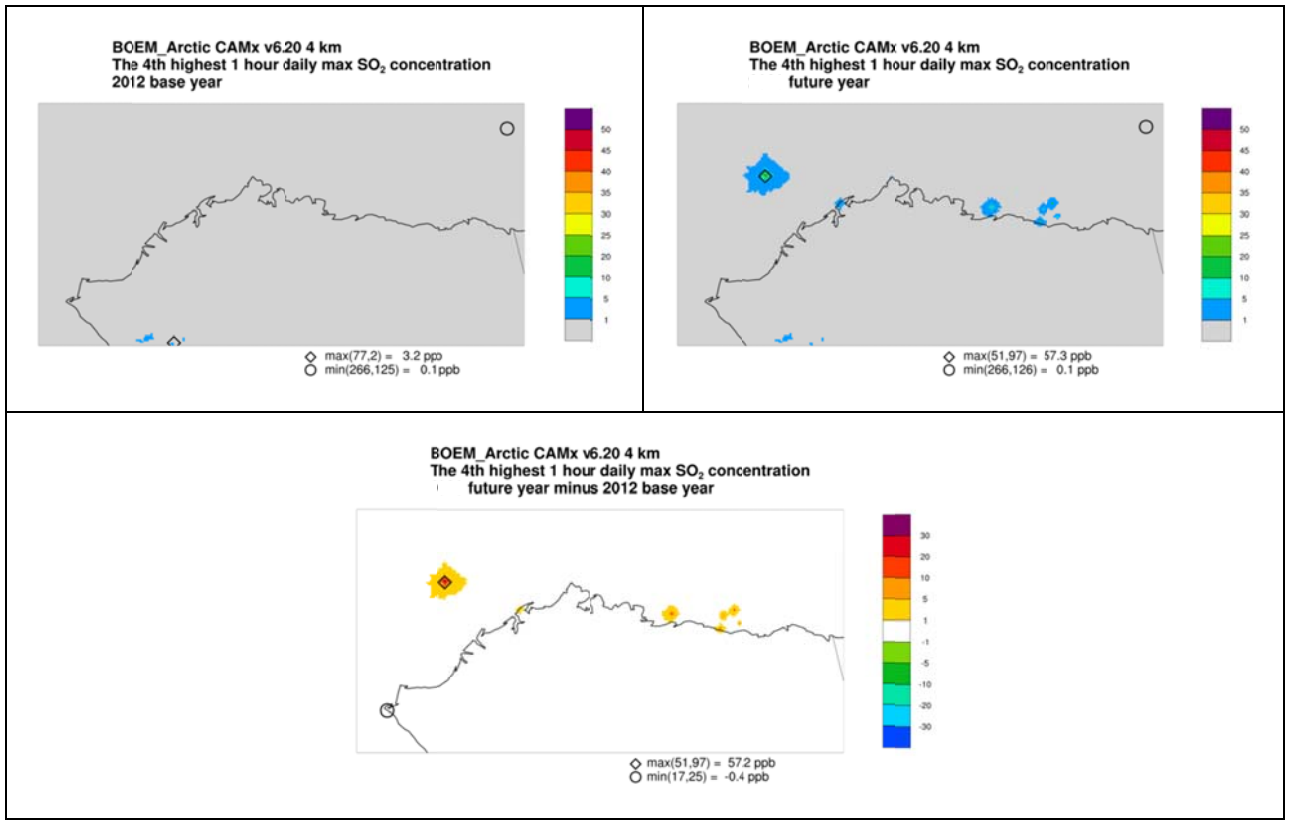

Figure 7-14. Modeled fourth highest daily maximum 1-hour SO_2 concentrations for the base year (top left), future year (top right), and future minus base year (bottom center).

7.1.6 *CO*

There are two CO NAAQS: a 1-hour (35 ppm) and an 8-hour (9 ppm); both NAAQS are formulated as values "not to be exceeded more than once per year". In nearly all cases, the 8-hour standard is the more stringent of the two. Modeled second highest 8-hour CO concentrations for the base and future year scenarios and the future minus base year differences are shown in Figure 7-15. All modeled values are well below the NAAQS; the most substantial impacts are from wildfire emissions in the southwestern portion of the domain. Oil and gas sources are not major CO emitters and the CO increases in the future year scenario are all below 0.2 ppm.

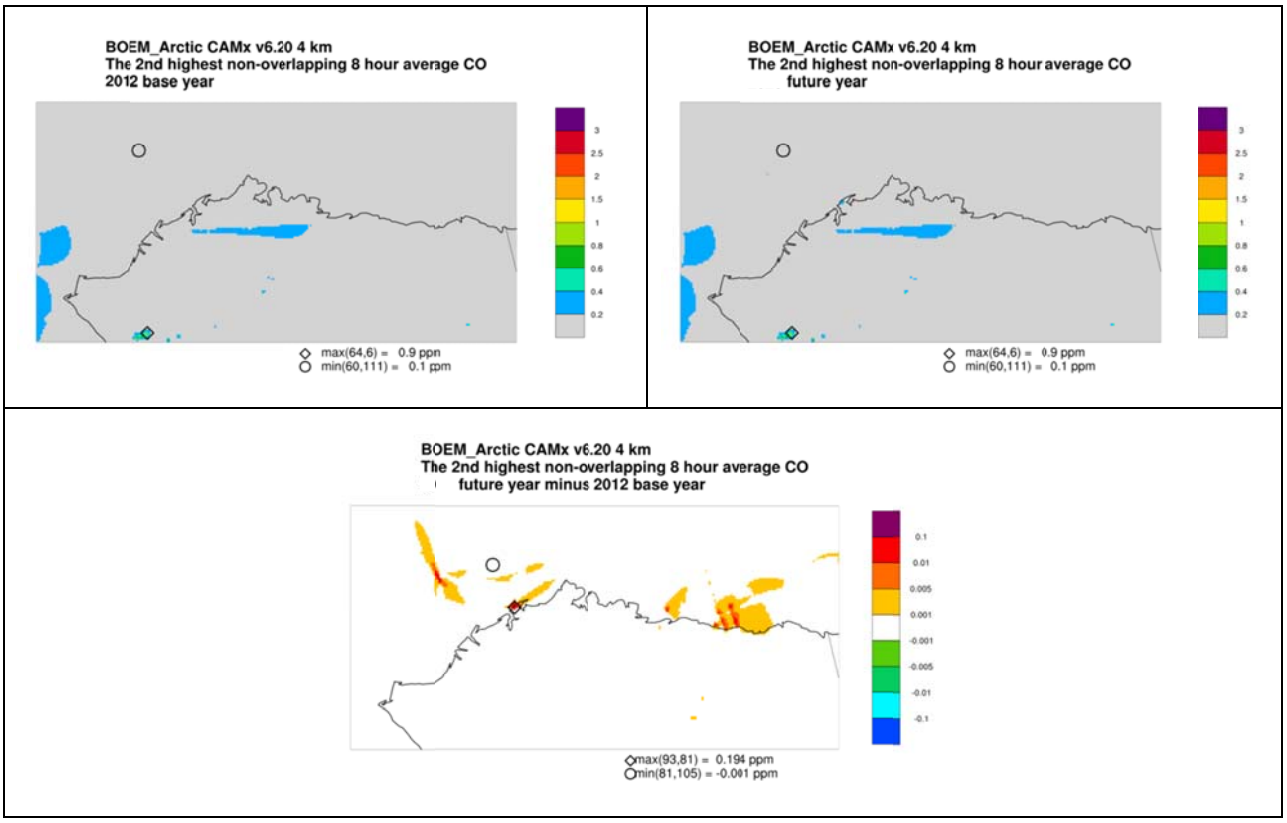

Figure 7-15. Modeled 2nd highest non-overlapping 8-hour average CO concentrations in the base year (top left), future year (top right), and the future minus base difference (bottom center).

7.2 PSD Impacts

Incremental impacts of each source group at Class I and specified Class II areas were calculated for all pollutants for which PSD increments have been set (NO_2, SO_2, PM_{10}, $PM_{2.5}$). Increment consumption is based on the source group contribution calculated from the CAMx source contribution results. Increment consumption for all 24-hour average increments and the 3-hour average SO_2 increment are based on the annual second highest values. Increments are based on the maximum value over grid cells which overlap with the designated Class I/II area.

Comparisons of impacts from the proposed action with maximum allowed PSD increments are presented here as an evaluation of a "threshold of concern" for potentially significant adverse impacts but do not represent a regulatory PSD increment consumption analysis.

Results of the PSD increments analysis for all new O&G sources (Source Group D) are summarized in Table 7-1 for areas overlapping with the 4 km modeling domain and in Table 7-2 for areas overlapping with the 12 km modeling domain. Note that areas lying wholly or partially within the 4 km domain appear in both tables; results in Table 7-1 are based on the 4 km grid output and results in Table 7-2 are based on the 12 km grid output.

For the specified Class II areas, maximum impacts are predicted to occur in ANWR Area 1002 and these impacts are all well below the applicable allowable Class II PSD increment. As a

percentage of the allowed increment, the 24-hour $PM_{2.5}$ impact in ANWR Area 1002 (2.761 $\mu g/m^3$) is the largest, representing 31% of the allowed Class II increment of 9 $\mu g/m^3$. Within the Class I areas, the 24-hour $PM_{2.5}$ impact at (0.059 $\mu g/m^3$ at Denali National Preserve) is 3% of the allowed Class I increment of 2 $\mu g/m^3$.

Table 7-1. Contributions of new O&G sources to PSD increment consumption in Class I/II areas within the 4 km modeling domain (maximum grid cell contributions).

Pollutant	NO_2 (µg/m^3)	PM_{10} (µg/m^3)		$PM_{2.5}$ (µg/m^3)		SO_2 (µg/m^3)		
Averaging Time	**Annual[3]**	**24-hour[2]**	**Annual[3]**	**24-hour[4]**	**Annual[3]**	**3-hour[2]**	**24-hour[2]**	**Annual[3]**
Class II	**PSD Class II Increment[1]**							
	25	30	17	9	4	512	91	20
Alaska Maritime National Wildlife Refuge	0.469	1.452	0.194	1.434	0.188	0.113	0.032	0.004
ANWR 1980 Additions	0.022	0.767	0.042	0.766	0.041	0.019	0.012	0.001
ANWR Area 1002	0.583	2.823	0.239	2.761	0.235	0.172	0.059	0.006
ANWR Wilderness	0.044	2.057	0.119	2.053	0.118	0.029	0.014	0.001
Cape Krusenstern National Monument	0.007	0.424	0.026	0.422	0.026	0.010	0.003	0.000
Gates of the Arctic National Park	0.014	0.435	0.032	0.435	0.032	0.013	0.007	0.001
Gates of the Arctic National Preserve	0.007	0.417	0.017	0.417	0.017	0.007	0.004	0.000
Kobuk Valley National Park	0.006	0.183	0.014	0.182	0.014	0.004	0.003	0.000
Noatak National Preserve	0.013	0.428	0.023	0.428	0.023	0.010	0.005	0.000
Yukon Flats National Wildlife Refuge	0.000	0.000	0.000	0.000	0.000	0.000	0.000	0.000

Table 7-2. Contributions of new O&G sources to PSD increment consumption in Class I/II areas within the 12 km modeling domain (maximum grid cell contributions).

Pollutant	NO_2 (µg/m^3)	PM_{10} (µg/m^3)		$PM_{2.5}$ (µg/m^3)		SO_2 (µg/m^3)		
Averaging Time	**Annual[3]**	**24-hour[2]**	**Annual[3]**	**24-hour[4]**	**Annual[3]**	**3-hour[2]**	**24-hour[2]**	**Annual[3]**
Class I	**PSD Class I Increment[1]**							
	2.5	8	4	2	1	25	5	2
Denali National Park	0.000	0.049	0.002	0.048	0.002	0.001	0.000	0.000
Denali National Preserve	0.000	0.059	0.003	0.059	0.003	0.001	0.001	0.000
Class II	**PSD Class II Increment[1]**							
	25	30	17	9	4	512	91	20
Alaska Maritime National Wildlife Refuge	0.062	1.249	0.108	1.224	0.106	0.053	0.022	0.001
ANWR Area 1002	0.291	2.384	0.182	2.370	0.180	0.116	0.034	0.004
ANWR 1980 Additions	0.021	0.665	0.038	0.664	0.038	0.018	0.011	0.001
ANWR Wilderness	0.047	1.984	0.115	1.980	0.114	0.031	0.016	0.001
Bering Land Bridge National Preserve	0.013	0.531	0.043	0.527	0.042	0.015	0.006	0.000
Cape Krusenstern National Monument	0.007	0.510	0.030	0.508	0.029	0.009	0.003	0.000
Gates of the Arctic National Park	0.015	0.441	0.033	0.440	0.033	0.014	0.006	0.001
Gates of the Arctic National Preserve	0.006	0.337	0.015	0.337	0.015	0.006	0.003	0.000
Innoko National Wildlife Refuge	0.002	0.114	0.008	0.114	0.008	0.003	0.001	0.000
Kanuti National Wildlife Refuge	0.002	0.193	0.005	0.193	0.005	0.002	0.001	0.000
Kobuk Valley National Park	0.006	0.169	0.014	0.168	0.014	0.005	0.003	0.000

Pollutant	NO_2 (µg/m^3)	PM_{10} (µg/m^3)		$PM_{2.5}$ (µg/m^3)		SO_2 (µg/m^3)		
Averaging Time	**Annual[3]**	**24-hour[2]**	**Annual[3]**	**24-hour[4]**	**Annual[3]**	**3-hour[2]**	**24-hour[2]**	**Annual[3]**
Koyukuk National Wildlife Refuge	0.003	0.153	0.012	0.153	0.012	0.004	0.001	0.000
Noatak National Preserve	0.012	0.425	0.022	0.425	0.021	0.010	0.005	0.000
Nowitna National Wildlife Refuge	0.001	0.106	0.005	0.106	0.005	0.002	0.001	0.000
Selawik National Wildlife Refuge	0.004	0.419	0.025	0.418	0.025	0.006	0.002	0.000
Tetlin National Wildlife Refuge	0.000	0.030	0.001	0.030	0.000	0.000	0.000	0.000
Wrangell-St. Elias National Park	0.000	0.019	0.000	0.019	0.000	0.000	0.000	0.000
Wrangell-St. Elias National Preserve	0.000	0.022	0.000	0.022	0.000	0.000	0.000	0.000
Yukon-Charley Rivers National Preserve	0.000	0.081	0.002	0.081	0.002	0.001	0.000	0.000
Yukon Delta National Wildlife Refuge	0.003	0.212	0.017	0.211	0.017	0.004	0.002	0.000
Yukon Flats National Wildlife Refuge	0.001	0.126	0.005	0.126	0.005	0.002	0.001	0.000

7.3 AQRV Impacts

7.3.1 *Visibility*

Incremental visibility impacts were calculated for each source group as well as the cumulative impact of all sources combined. The approach used the incremental concentrations as quantified by the CAMx PSAT/APCA source apportionment tool simulation of for each source group. Changes in light extinction from CAMx model concentration increments due to emissions from each source group were calculated for each day at grid cells that intersect Class I and specified Class II areas within the 12/4 km modeling domain. The calculation of incremental visibility impacts followed procedures recommended by the Federal Land Managers (FLAG, 2010) as described in Section 6.2.3.

For each source group, the estimated visibility degradation at each Class I/II area in the 12/4 km modeling domain due to emissions from the source group is presented in terms of the number of days that exceed a threshold change in deciview (Δdv) relative to background conditions. The number of days with a Δdv greater than 0.5 and 1.0 are reported. Note that some of the specified Class II areas straddle the boundary of the 4 km domain which means that model results are available at 4 km resolution for a portion of the area and at 12 km resolution for the entire area. For this reason, two sets of results are reported, one based on the high resolution model results on the 4 km domain and one based on model results on the 12 km domain. The only Class I areas (Denali National Park and Preserve) are located entirely outside of the 4 km domain so results for this area appear only in 12 km results.

Results of the incremental visibility impact assessment for Source Group D (new O&G sources) are presented in Table 7-3 for the 4 km model output and Table 7-4 for the 12 km model output. Maximum Δdv exceeds 1.0 at all areas in the 4 km domain except for Yukon Flats; the 8th highest Δdv also exceed 1.0 at all areas except for Yukon Flats and Kobuk Valley. Several additional areas located entirely within the 12 km domain are also calculated to have Δdv greater than 1.0. However, the only Class I area (Denali National Park) is calculated to experience a maximum Δdv of less than 1.0 and an 8th highest Δdv of less than 0.5 with only one day exceeding 0.5.

Table 7-3. Incremental visibility impacts relative to natural background conditions from Source Group D based on 4 km domain model results.

Area	Max Δdv	8th High Δdv	No. Days	
			>1.0	>0.5
Class II Areas				
Alaska Maritime National Wildlife Refuge	7.40	6.01	160	224
ANWR 1980 Additions	4.95	2.30	39	66
ANWR Area 1002	11.52	10.28	146	193
ANWR Wilderness	10.57	5.72	95	158
Cape Krusenstern National Monument	3.06	1.38	13	37

Area	Max Δdv	8th High Δdv	No. Days	
			>1.0	>0.5
Gates of the Arctic National Park	3.03	2.23	24	48
Gates of the Arctic National Preserve	2.49	1.45	13	26
Kobuk Valley National Park	1.97	0.78	4	21
Noatak National Preserve	2.93	1.78	24	55
Yukon Flats National Wildlife Refuge	<0.005	<0.005	0	0

Table 7-4. Incremental visibility impacts relative to natural background conditions from Source Group D based on 12 km domain model results.

Area	Max Δdv	8th High Δdv	No. Days	
			>1.0	>0.5
Class I Areas				
Denali National Park	0.52	0.22	0	1
Denali National Preserve	0.48	0.32	0	0
Class II Areas				
Alaska Maritime National Wildlife Refuge	6.90	4.18	87	141
ANWR Area 1002	10.68	9.56	131	186
ANWR 1980 Additions	4.68	2.14	35	69
ANWR Wilderness	9.95	5.60	95	158
Bering Land Bridge National Preserve	3.72	2.52	36	80
Cape Krusenstern National Monument	3.50	1.78	16	39
Gates of the Arctic National Park	2.84	1.96	25	48
Gates of the Arctic National Preserve	2.26	1.33	13	25
Innoko National Wildlife Refuge	1.34	0.68	1	13
Kanuti National Wildlife Refuge	1.48	0.62	4	8

Area	Max Δdv	8th High Δdv	No. Days	
			>1.0	>0.5
Kobuk Valley National Park	1.95	1.11	9	32
Koyukuk National Wildlife Refuge	1.12	0.82	3	23
Noatak National Preserve	3.06	1.80	26	54
Nowitna National Wildlife Refuge	0.94	0.58	0	10
Selawik National Wildlife Refuge	2.95	1.49	16	43
Tetlin National Wildlife Refuge	0.31	0.04	0	0
Wrangell-St. Elias National Park	0.17	0.02	0	0
Wrangell-St. Elias National Preserve	0.18	0.03	0	0
Yukon-Charley Rivers National Preserve	0.64	0.24	0	2
Yukon Delta National Wildlife Refuge	1.37	0.93	5	28
Yukon Flats National Wildlife Refuge	1.03	0.62	2	12

7.3.2 *Acid Deposition*

CAMx-predicted wet and dry fluxes of sulfur- and nitrogen-containing species were processed to estimate total annual sulfur (S) and nitrogen (N) deposition values at each Class I and specified Class II area in the 12/4 km modeling domain. Total N deposition results from the 4 km and 12 km results are presented in Tables 7-5 and 7-6, respectively; total S deposition results are presented in Tables 7-7 and 7-8. As described in Section 6.2.3.2, the maximum annual S and N deposition values from any grid cell that intersects a Class I or specified Class II receptor area was used to represent deposition for that area, in addition to the average annual deposition values of all grid cells that intersect a Class I or specified Class II receptor area. Maximum and average predicted S and N deposition impacts were estimated separately for each source group and together across all source groups. Results for the Base Year, Future Year minus Base Year, and for the contributions from new O&G sources (Source Group D) are presented in the above referenced tables.

As discussed in Section 6.2.3.2, Deposition Analysis Thresholds (DATs) or Critical Loads for S and N deposition specifically applicable to Alaska are not currently available. Comparison of the maximum N and S deposition from new O&G sources (Source Group D) with western (0.005 kg/ha/yr) and eastern (0.01 kg/ha/yr) DATs developed for the Lower 48 states indicates N deposition above the 0.01 kg/ha/yr DAT in all areas within the 4 km domain and in some areas

within the 12 km domain outside of the 4 km domain. S deposition is lower but the maximum grid cell S deposition from Source Group D exceeds 0.01 kg/ha/yr in the Alaska Maritime National Wildlife Refuge and in ANWR Area 1002.

Table 7-5. Annual nitrogen deposition (kg/ha/year) from 4 km model results.

Area	BY		FY - BY		Source Group D: New O&G	
	Max	Avg	Max	Avg	Max	Avg
Alaska Maritime National Wildlife Refuge	0.7623	0.4283	0.0850	0.0403	0.0834	0.0379
ANWR 1980 Additions	0.5013	0.3042	0.1471	0.0073	0.0408	0.0059
ANWR Area 1002	0.4101	0.3022	0.1444	0.0658	0.1370	0.0608
ANWR Wilderness	0.5465	0.2987	0.0598	0.0127	0.0529	0.0111
Cape Krusenstern National Monument	0.6292	0.4469	0.0168	0.0123	0.0148	0.0115
Gates of the Arctic National Park	0.5189	0.3400	0.0320	0.0114	0.0276	0.0094
Gates of the Arctic National Preserve	0.4856	0.3372	0.0194	0.0111	0.0174	0.0088
Kobuk Valley National Park	0.4661	0.4401	0.0162	0.0142	0.0138	0.0121
Noatak National Preserve	0.9320	0.4334	0.0478	0.0144	0.0383	0.0125

Table 7-6. Annual nitrogen deposition (kg/ha/year) from 12 km model results.

Area	BY		FY – BY		Source Group D: New O&G	
	Max	Avg	Max	Avg	Max	Avg
Denali National Park	1.2846	0.4531	0.0014	0.0008	0.0009	0.0004
Denali National Preserve	0.7570	0.3237	0.0027	0.0012	0.0016	0.0007
Alaska Maritime National Wildlife Refuge	0.6497	0.3256	0.0623	0.0229	0.0595	0.0215
ANWR Area 1002	0.3997	0.2984	0.1158	0.0636	0.1144	0.0587
ANWR 1980 Additions	0.4931	0.3114	0.0442	0.0063	0.0393	0.0051
ANWR Wilderness	0.4612	0.2987	0.0625	0.0133	0.0568	0.0116
Bering Land Bridge National Preserve	0.5500	0.2303	0.0197	0.0092	0.0200	0.0089
Cape Krusenstern National Monument	0.5284	0.3961	0.0139	0.0087	0.0124	0.0081
Gates of the Arctic National Park	0.7143	0.3646	0.0254	0.0075	0.0217	0.0062
Gates of the Arctic National Preserve	0.4915	0.3242	0.0153	0.0053	0.0129	0.0043
Innoko National Wildlife Refuge	0.3538	0.2614	0.0040	0.0025	0.0029	0.0018
Kanuti National Wildlife Refuge	0.3182	0.2284	0.0032	0.0018	0.0026	0.0014
Kobuk Valley National Park	0.7464	0.4515	0.0170	0.0097	0.0145	0.0083
Koyukuk National Wildlife Refuge	0.5272	0.2345	0.0058	0.0024	0.0051	0.0021
Noatak National Preserve	0.7973	0.4388	0.0373	0.0132	0.0314	0.0115
Nowitna National Wildlife Refuge	0.8724	0.2546	0.0030	0.0017	0.0021	0.0012
Selawik National Wildlife Refuge	0.3488	0.2372	0.0086	0.0048	0.0075	0.0044
Tetlin National Wildlife Refuge	0.4126	0.3069	0.0004	0.0002	0.0001	0.0001
Wrangell-St. Elias National Park	0.4225	0.2613	0.0004	0.0002	0.0001	$<5x10^{-5}$
Wrangell-St. Elias National Preserve	0.4707	0.2777	0.0006	0.0003	0.0001	$<5x10^{-5}$

Area	BY		FY – BY		Source Group D: New O&G	
	Max	Avg	Max	Avg	Max	Avg
Yukon-Charley Rivers National Preserve	0.5821	0.3646	0.0010	0.0006	0.0004	0.0002
Yukon Delta National Wildlife Refuge	0.6360	0.2737	0.0061	0.0037	0.0050	0.0031
Yukon Flats National Wildlife Refuge	0.4900	0.2775	0.0042	0.0018	0.0031	0.0013

Table 7-7. Annual total sulfur deposition (kg/ha/year) from 4 km model results.

Area	BY		FY - BY		Source Group D: New O&G	
	Max	Avg	Max	Avg	Max	Avg
Alaska Maritime National Wildlife Refuge	1.3901	0.7953	0.0107	0.0024	0.0110	0.0031
ANWR 1980 Additions	0.6371	0.3024	0.0272	0.0004	0.0030	0.0003
ANWR Area 1002	0.4174	0.2657	0.0097	0.0027	0.0105	0.0031
ANWR Wilderness	0.6758	0.3073	0.0026	0.0005	0.0027	0.0005
Cape Krusenstern National Monument	0.8894	0.5760	0.0010	0.0008	0.0008	0.0007
Gates of the Arctic National Park	0.6509	0.3532	0.0018	0.0005	0.0016	0.0005
Gates of the Arctic National Preserve	0.5693	0.3462	0.0011	0.0006	0.0009	0.0004
Kobuk Valley National Park	0.4442	0.4244	0.0010	0.0009	0.0008	0.0007
Noatak National Preserve	1.6426	0.5671	0.0027	0.0009	0.0025	0.0008

Table 7-8. Annual sulfur deposition (kg/ha/year) from 12 km model results.

Area	BY		FY – BY		Source Group D: New O&G	
	Max	Avg	Max	Avg	Max	Avg
Denali National Park	5.2264	1.3317	0.0002	0.0001	0.0002	$<5x10^{-5}$
Denali National Preserve	2.9022	0.7403	0.0002	0.0001	0.0002	0.0001
Alaska Maritime National Wildlife Refuge	1.2280	0.6151	0.0040	0.0016	0.0048	0.0016
ANWR Area 1002	0.3740	0.2655	0.0067	0.0028	0.0069	0.0031
ANWR 1980 Additions	1.4280	0.3900	0.0037	0.0004	0.0026	0.0003
ANWR Wilderness	0.8921	0.3201	0.0026	0.0006	0.0026	0.0005
Bering Land Bridge National Preserve	1.2527	0.3194	0.0010	0.0006	0.0010	0.0005
Cape Krusenstern National Monument	0.8309	0.6178	0.0008	0.0006	0.0008	0.0006
Gates of the Arctic National Park	2.0757	0.5934	0.0015	0.0003	0.0013	0.0004
Gates of the Arctic National Preserve	1.3703	0.5792	0.0009	0.0003	0.0008	0.0002
Innoko National Wildlife Refuge	1.0570	0.5045	0.0004	0.0002	0.0002	0.0001
Kanuti National Wildlife Refuge	0.7707	0.3340	0.0001	0.0001	0.0001	0.0001
Kobuk Valley National Park	1.8360	0.9901	0.0010	0.0006	0.0008	0.0005
Koyukuk National Wildlife Refuge	1.6282	0.4042	0.0004	0.0002	0.0003	0.0001
Noatak National Preserve	1.5042	0.6445	0.0023	0.0009	0.0019	0.0007
Nowitna National Wildlife Refuge	1.2023	0.3841	0.0002	0.0001	0.0001	0.0001
Selawik National Wildlife Refuge	0.7517	0.4114	0.0007	0.0004	0.0006	0.0003
Tetlin National Wildlife Refuge	1.2188	0.8454	$<5x10^{-5}$	$<5x10^{-5}$	$<5x10^{-5}$	$<5x10^{-5}$
Wrangell-St. Elias National Park	1.6987	0.7748	$<5x10^{-5}$	$<5x10^{-5}$	$<5x10^{-5}$	$<5x10^{-5}$
Wrangell-St. Elias National Preserve	2.0423	0.7703	$<5x10^{-5}$	$<5x10^{-5}$	$<5x10^{-5}$	$<5x10^{-5}$

Area	BY		FY – BY		Source Group D: New O&G	
	Max	Avg	Max	Avg	Max	Avg
Yukon-Charley Rivers National Preserve	2.2625	0.8619	0.0001	$<5x10^{-5}$	$<5x10^{-5}$	$<5x10^{-5}$
Yukon Delta National Wildlife Refuge	1.8961	0.5908	0.0004	0.0003	0.0003	0.0002
Yukon Flats National Wildlife Refuge	0.9819	0.3617	0.0002	0.0001	0.0002	0.0001

8.0 SEA SALT SENSITIVITY ANALYSIS

Results presented in Section 7 indicate that sea salt aerosol (SSA) emissions exert a strong influence on predicted PM concentrations in coastal areas. Furthermore, there is good reason to believe that SSA emissions are over estimated by a substantial amount as illustrated by the comparison of predicted sodium (Na) with historical monthly average Na^+ ion concentrations filter samples collected at the Barrow NOAA observatory between 1997 and 2009 (Figure 8-1).

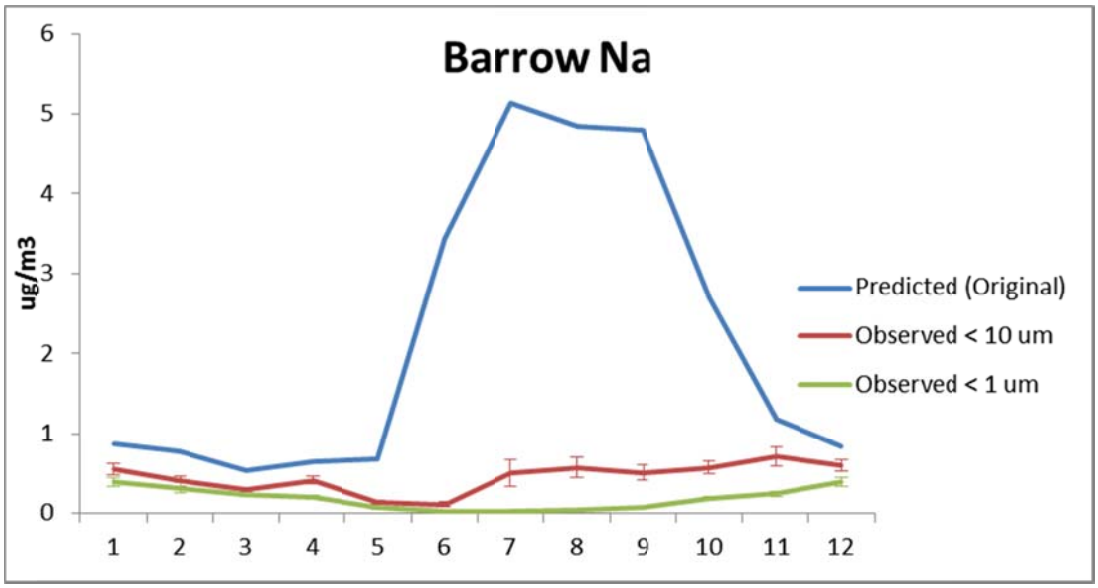

Figure 8-1. Observed and predicted monthly mean sodium concentrations at Barrow: predicted concentrations (<2.5 µm) for 2012 (blue line), observed submicron (< 1 µm; green line) and total < 10 µm (red line) Na ion concentration for 1997 – 2009; error bars are ± 1 standard error (data courtesy of NOAA and the DOE ARM Program - https://saga.pmel.noaa.gov/data/stations/; see Quinn et al., 2000 for measurement details).

While the influence of SSA on model predictions can be approximately bounded by examining results with and without SSA (estimated as the sum of sodium [Na] and particulate chloride [PCL]) included as was done, for example, in Figure 7-4. However, this does not account for excess sodium nitrate formation via substitution of SSA chloride ions by nitrate ions from other sources (including nitrate generated from anthropogenic sources) or the likely over estimation of SSA sulfates. Thus, biases resulting from nitrate and sulfate over estimation will remain even after subtracting Na and PCL from the model predictions.

Due to the absence of any contemporaneous speciated PM data with which to constrain uncertainties in SSA emission estimates, it was not possible to fully evaluate alternative SSA emissions algorithms for the arctic environment within this study. We therefore conducted a sensitivity test analysis in which CAMx was rerun with substantially reduced SSA emissions for selected time periods during 2012, thus providing an indication of the degree of sensitivity of predicted ozone, $PM_{2.5}$ and visibility impairment to SSA emissions.

SSA emissions for the sensitivity runs were generated using a new experimental SSA emissions preprocessor (Koo, 2017) recently developed for an air quality modeling study being conducted

in the Gulf of Mexico region (GOMR). Preliminary comparisons of CAMx results in the GOMR generated using the new SSA preprocessor with available contemporaneous particulate Na measurements suggested that SSA emissions generated by the new preprocessor, which were substantially lower than those generated by the current preprocessor, resulted in a substantial reduction in the Na over prediction bias. Application of the new preprocessor to the Arctic AQ Study modeling domain resulted in substantially lower estimates of SSA emissions during both winter and summer periods as shown in Figure 8-2: large reductions are evident over the open ocean with smaller but still substantial reductions in coastal areas. While no contemporaneous Na observations are available with which to evaluate the new preprocessor for this study, the much lower SSA emission estimates generated by the new preprocessor provided a convenient tool for our SSA sensitivity analysis.

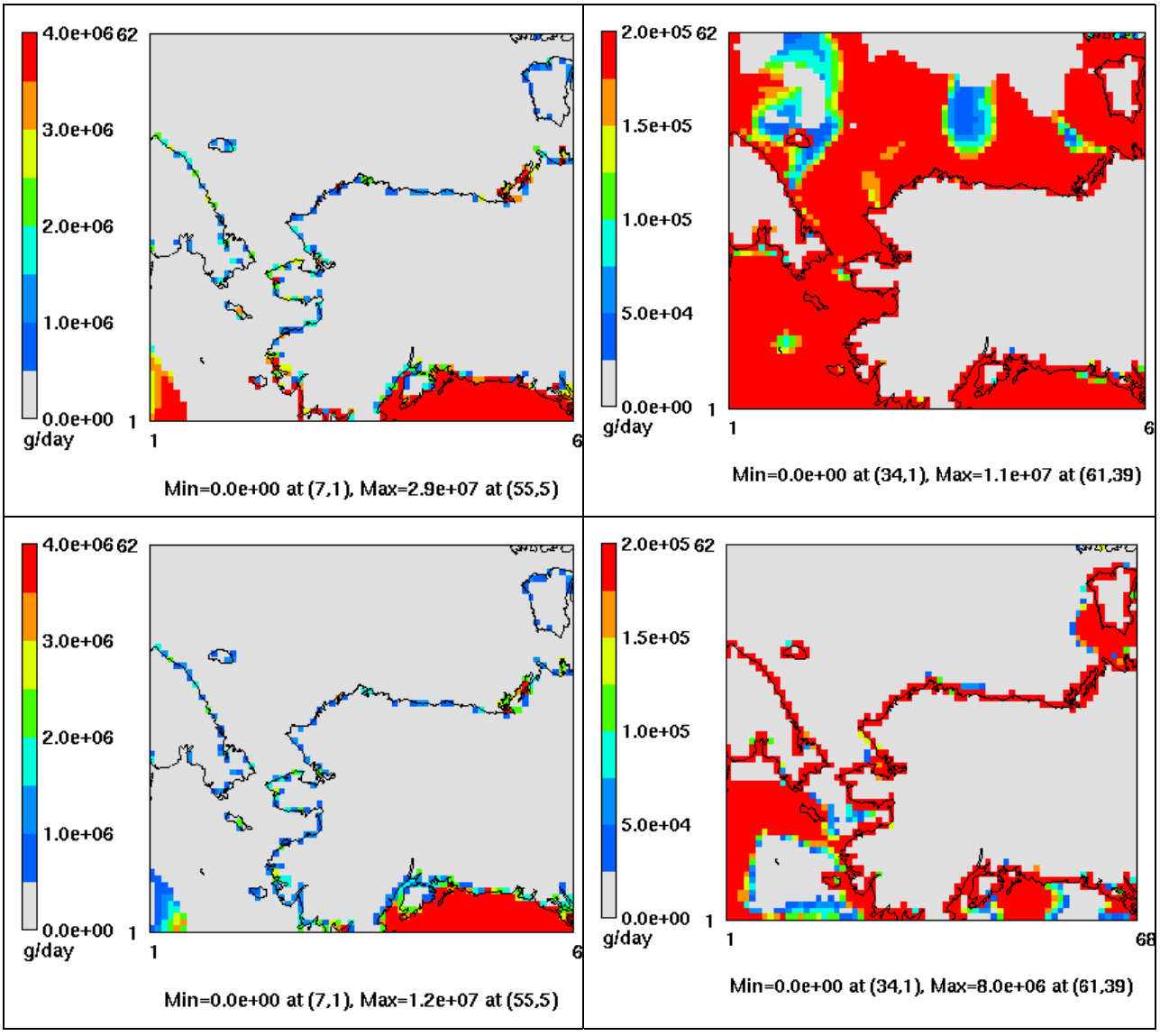

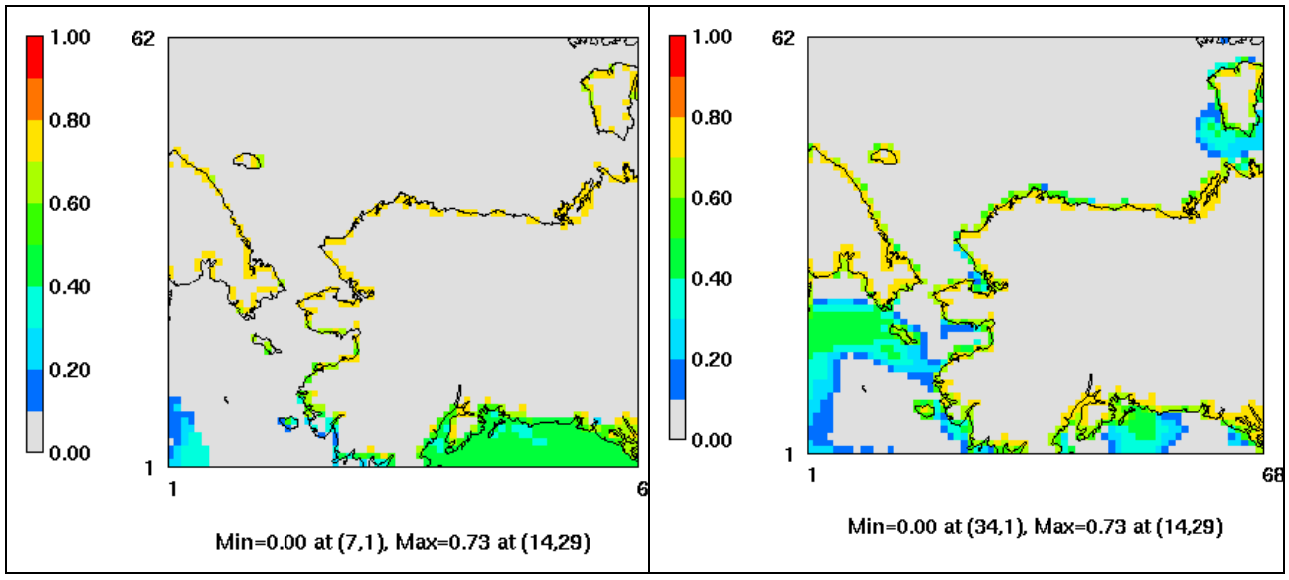

Figure 8-2. Comparison of SSA emissions from old preprocessor (top row), new preprocessor (middle row), and ratio of new to old (bottom row) for 1 February (left column) and 1 August (right column).

For the sensitivity analysis, Ramboll Environ generated new SSA emissions using the new preprocessor in a new 36 km CAMx simulation. In addition to lower SSA emissions from the revised preprocessor, modifications were made to the way in which SSA-related species were extracted from GEOS-Chem for use as global boundary conditions for the 36 km CAMx simulation.[12] These modifications resulted in substantial reductions in particulate sodium and chloride global boundary conditions, thus further reducing SSA concentrations within the modeling domain. No other modifications were made to the 36 km simulation inputs. Boundary conditions for the 12/4 km domain were then extracted from the new 36 km simulation.

For purposes of the sensitivity analysis, 12/4 km two-way nested simulations using the future year emissions scenario, SSA emissions from the new preprocessor, and revised BCs from the new 36 km simulation were conducted for two 10-day periods consisting of three spin-up days and seven analysis days each: 12 to21 April and 27 July to 5 August. These "April" and "August" periods were selected based on the occurrence of high predicted SSA and NO_3 concentrations at key specified Class II areas in the original simulation results. Results from these two sensitivity runs were then compared to results for the same time periods from the old model run to evaluate the impacts of reduced SSA emissions on predicted ozone, $PM_{2.5}$, and visibility impairment. Comparisons were also made between the original and reduced SSA model runs of gas and particle species – such as CO and elemental carbon – that are not expected

[12] Previously, 20% of the GEOS-Chem coarse mode SSA had been included in the CAMx fine mode SSA boundary condition; this was revised to 0%. Other changes to the SSA retrieval from GEOS-Chem for CAMx boundary conditions included correcting a double counting of fine mode SSA species, adjusting assumed SSA composition to match assumptions made when preparing boundary conditions for CMAQ, and explicitly accounting for the Na/Cl molecular weight ratio.

to be affected by SSA reductions. Results of these comparisons confirmed that differences between the two model runs are solely attributable to the SSA reduction and not due to any unforeseen factors.

Reductions in daily average Sodium (Na) concentrations between the original model run and the SSA sensitivity run are shown for three representative coastal locations in Figure 8-3 (see Figure 1-3 for map of locations).[13] Na is used here as a conserved tracer of SSA. Reductions in coastal SSA concentrations average 3.6 µg/m^3 (96%) over both periods at these sites.

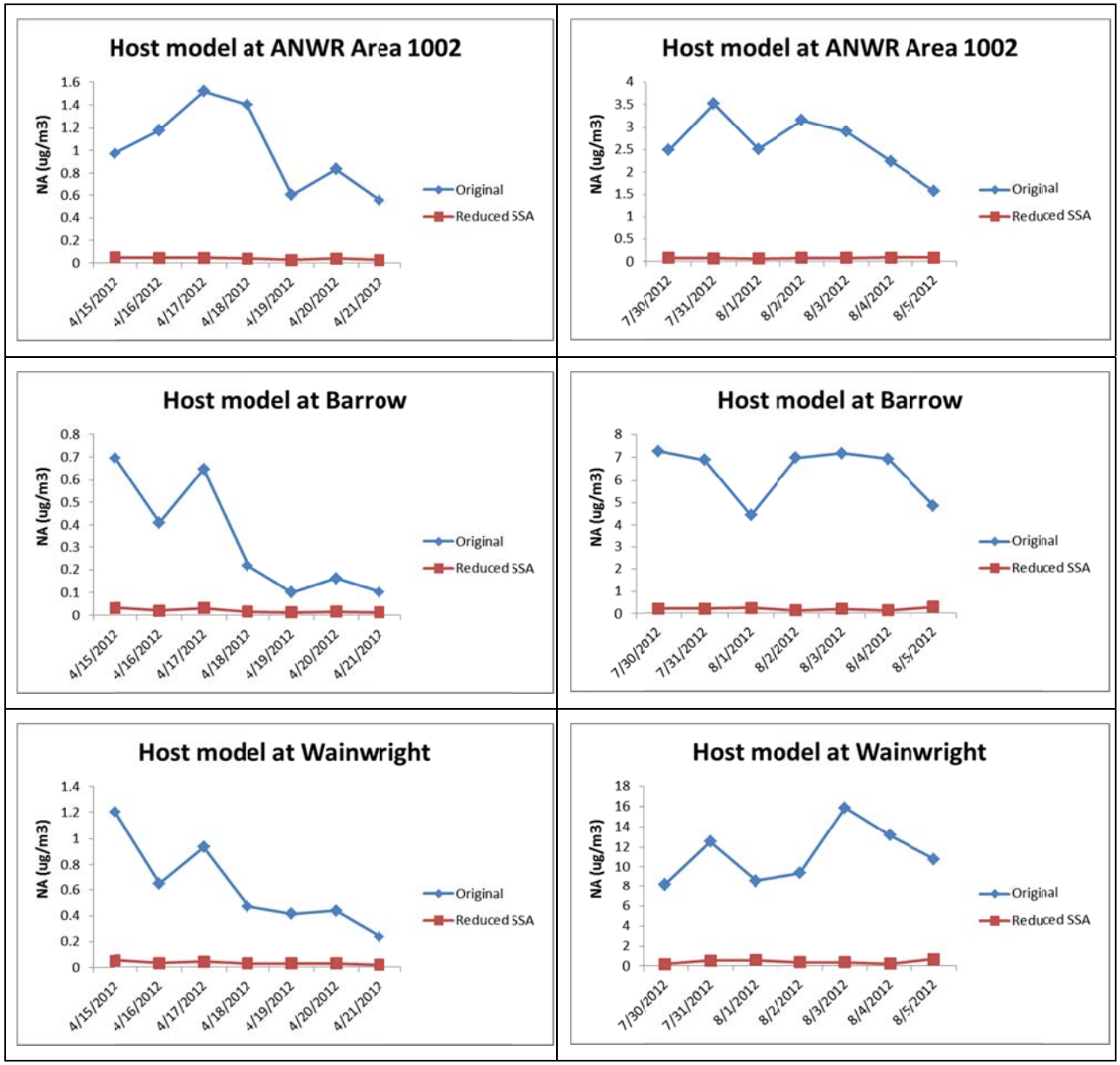

[13] Note that in this and subsequent figures, "Host Model" in the plot title refers to model output representing the combined impact of all sources rather than any individual source group contribution determined via the source apportionment methodology.

Figure 8-3. Comparison of predicted daily average sodium (Na) concentrations from the original model run with the concentrations from the reduced SSA sensitivity run for days during April (left) and August (right) at Deadhorse (top), Barrow (middle) and Wainwright (bottom); note different vertical scales used due to wide variations Na concentrations.

Mean predicted Na concentrations from the original and SSA sensitivity runs for the April and August time periods are compared with mean monthly measured sodium ion concentrations at Barrow based on data collected between October 1997 and December 2009 in Figure 8-4. Predicted Na concentrations in the original model run were well above the observed range during summer (i.e., ice free) conditions but were much closer to observed values during winter-spring (when extensive sea ice is present). Note that the predicted Na values nominally represent Na present in fine ($PM_{2.5}$) particles. Application of the revised SSA emissions preprocessor in the reduced SSA run results in much lower and more realistic predicted Na in summer, although some under prediction appears to occur in winter-spring when predicted SSA emissions are suppressed by sea ice. SSA emissions from blowing snow and ice flowers that are not included in the revised SSA emissions preprocessor but have been found to be potentially substantial contributors to winter-spring SSA in the Arctic (Huang and Jaeglé, 2016) may account for this under prediction. Winter-spring SSA under the original SSA emissions preprocessor represents emissions from patches of ice-free ocean as diagnosed by WRF (see Sec. 3.5). Thus the original SSA emissions preprocessor may have generated semi-realistic SSA emissions during winter-spring for the wrong reasons.

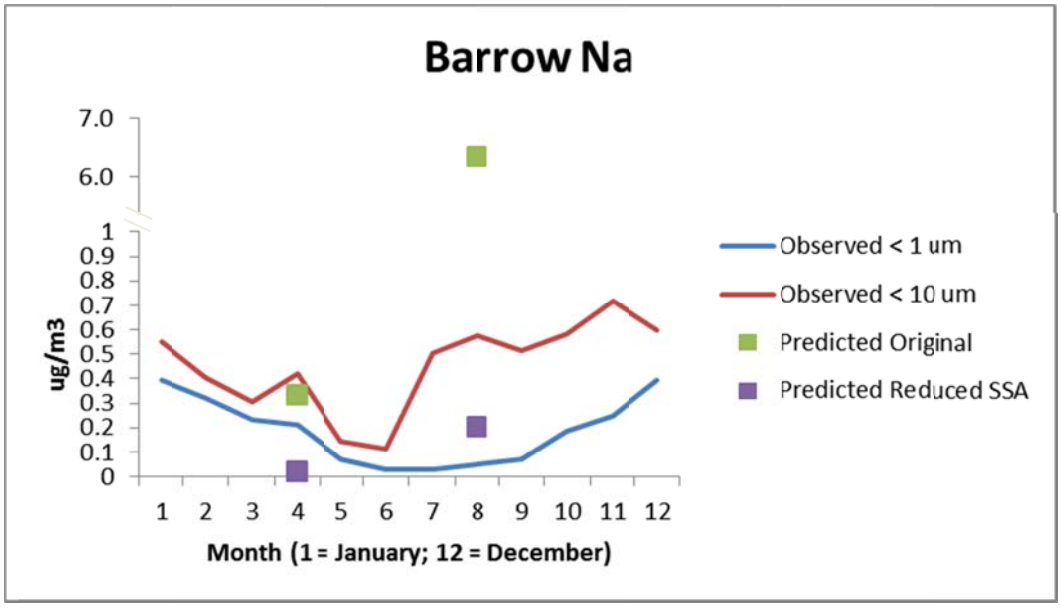

Figure 8-4. Observed and predicted mean Na concentrations at Barrow: monthly mean observed submicron (< 1 µm; blue line) and total < 10 µm (red line) Na^+ ion concentration for 1997 – 2009 (data courtesy of NOAA and the DOE ARM Program - https://saga.pmel.noaa.gov/data/stations/; see Quinn et al., 2000 for measurement details); predicted mean Na concentrations (< 2.5 µm) for the seven-day April and August modeling periods from the original model run (green squares) and reduced SSA model run (purple squares).

As expected, reduced SSA emissions were found to result in large reductions in particulate nitrate due to reduced sodium nitrate formation as shown, for example, at ANWR Area 1002 in the top row of Figure 8-5. The PSAT nitrate source contribution estimate for Source Group D (NSB New Oil and Gas sources) is similarly reduced as shown in the bottom row of Figure 8-5.

Nitric acid concentrations were found to be higher in the Reduced SSA run as expected due to reduced neutralization by sodium ions (not shown).

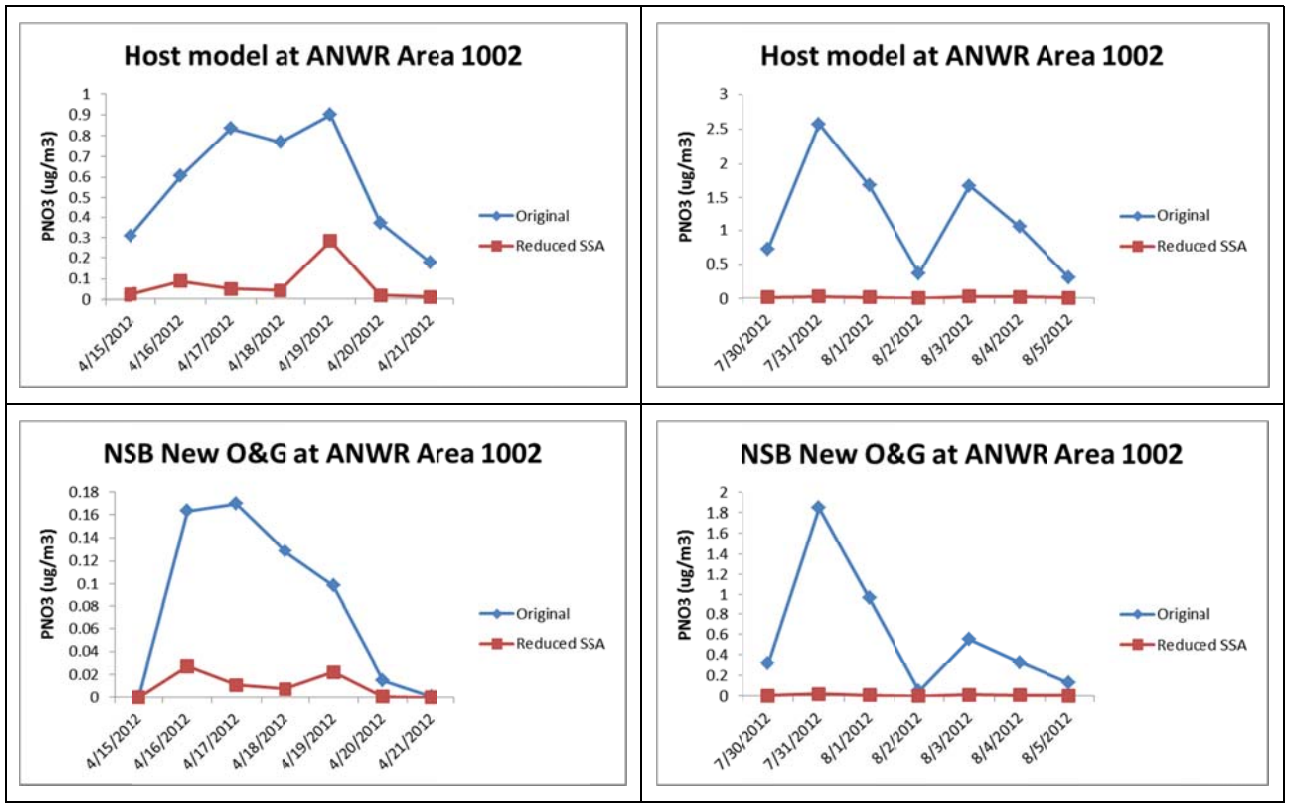

Figure 8-5. Comparison of predicted daily average particulate nitrate (PNO3) concentrations from the original model run with the concentrations from the reduced SSA sensitivity run for days during April (left) and August (right) at ANWR Area 1002: contributions from all sources (top), contributions from new oil and gas sources (Source Group D; bottom); note differences in scale due to wide variations PNO3 concentrations.

Comparison of daily maximum 1-hour ozone between the two model runs revealed only small changes in ozone with most values increasing slightly in the reduced SSA run relative to the original model run. The positive changes averaged 0.74 ppb during the August period (when increases were the largest on average) with a maximum increase on a single day at a single location of 1.4 ppb (which happened to occur on April 15th). Some ozone reductions occurred but they were generally well below 0.5 ppb. The ozone increases are likely due to increased NO_x regeneration from nitric acid as the reduced particulate nitrate results in higher levels of nitric acid. It is possible that some of the ozone increases may have been counteracted by decreased UV scattering – and hence decreased UV actinic flux – in in the reduced SSA run.

The impact of revised SSA emissions preprocessor on total $PM_{2.5}$ concentrations at ANWR, Barrow, and Wainwright is illustrated in Figure 8-6. Reductions in total $PM_{2.5}$ result primarily from reduced SSA mass but reductions in certain other species (notably particulate nitrate) also contribute to the lower $PM_{2.5}$.

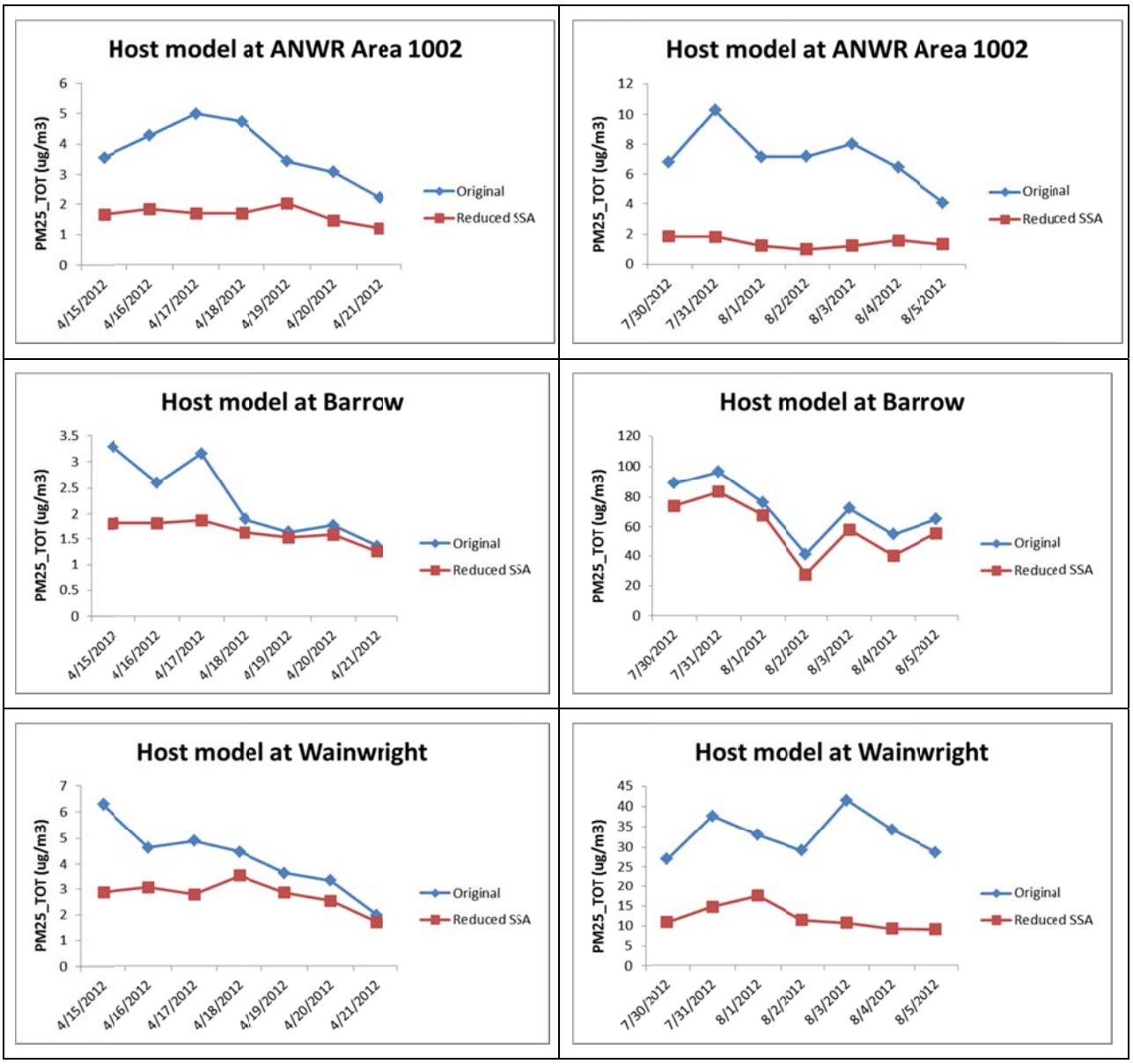

Figure 8-6. Comparison of predicted daily average $PM_{2.5}$ concentrations from the original model run with the concentrations from the reduced SSA sensitivity run for days during April (left) and August (right) at Deadhorse (top), Barrow (middle) and Wainwright (bottom); note differences in scale due to wide variations $PM_{2.5}$ concentrations.

Average differences and percent reductions in Na, particulate nitrate (PNO3) and total $PM_{2.5}$ between the original and reduced SSA runs for the April and August periods at ANWR Area 1002 are summarized in Table 8-1. Based on the NO_3/Na molecular weight ratio (62/23), these results indicate that on average as much as approximately 18% of the Na was in the form of $NaNO_3$ in the original model run while all or nearly all of the PNO3 was neutralized by Na at this coastal location. As a result, reducing SSA emissions to more realistic levels (at least in the summer ice-free season) produces a similarly sized relative reduction in PNO3 as there apparently is extremely limited availability of free ammonium for nitrate neutralization. Results

for total $PM_{2.5}$ in Table 8-1 show that a large fraction of the total $PM_{2.5}$ mass is associated with neutralized Na.

Table 8-1. Summary of average differences and average percentage change in sodium (Na), particulate nitrate (PNO3) and total fine particulate matter ($PM_{2.5}$) from all sources between the original and reduced SSA model runs for the 7-day periods in April and August at ANWR Area 1002.

Period	Original ($\mu g/m^3$)	Reduced SSA ($\mu g/m^3$)	Avg. Difference Original - Reduced SSA ($\mu g/m^3$)	Avg. % Change Original - Reduced SSA
Na				
April	1.007	0.040	0.968	96%
August	2.637	0.080	2.556	97%
PNO3				
April	0.566	0.072	0.494	89%
August	1.192	0.015	1.177	99%
$PM_{2.5}$				
April	3.751	1.665	2.087	54%
August	7.147	1.444	5.702	79%

As expected, the influence of SSA emission reductions is smaller in areas farther away from the coast as illustrated for Gates of the Arctic National Park in Figure 8-7. Gates of the Arctic is located in the farthest inland portion of the 4 km modeling domain (see Figure 1-3). While the reduced SSA results show large percent reductions in Na as at other locations, overall Na levels are low and the resulting impact on PNO3 and total $PM_{2.5}$ are small relative to other locations. Note that while reductions in PNO3 for three days during the August period are large in relative terms, concentrations of PNO3 on these days are quite low.

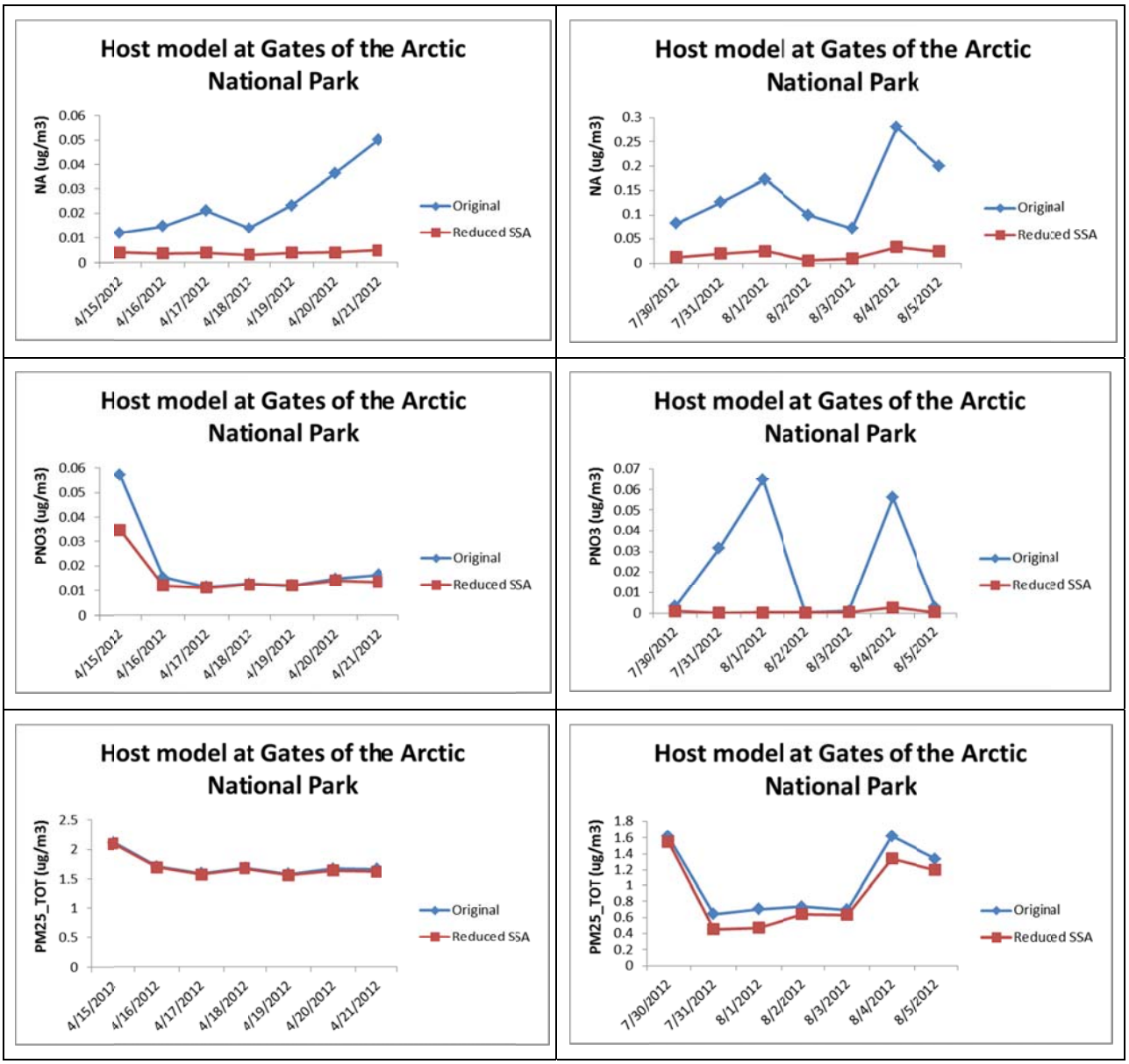

Figure 8-7. Comparisons of predicted daily average Na (top), PNO3 (middle), and $PM_{2.5}$ at Gates of the Arctic National Park for the original and reduced SSA runs during the April (left) and August (right) 7-day time periods.

Sensitivity of modeled visibility impacts from new oil and gas sources (Source Group D) to over prediction of SSA emissions are summarized in Figure 8-8 for ANWR Area 1002 (the Class I/II area most impacted by NSB sources), Gates of the Arctic National Park, and Denali National Park. Since a portion of Gate of the Arctic and Denali are outside of the 4 km domain (see Figure 1-3), these comparisons were based on 12 km resolution model output. These results show that reducing SSA emissions to more realistic levels results in lower estimates of visibility impacts where large impacts are predicted on the basis of the original model run. These reductions are almost entirely due to the above noted reductions in PNO3. The maximum change in haze index

is reduced from an increase of nearly 9 dv to an increase of 1.2 dv at ANWR Area 1002 during the August period whereas impacts are well below 1 dv at the other two areas even in the original model run. These results suggest that, even with more realistic SSA emission estimates, the new oil and gas sources (Source Group D) are predicted to result in peak day visibility impacts exceeding the 1 dv threshold at coastal locations in ANWR on at least a few days during the year. The implications for reductions in significant visibility impacts at other Class I/II areas are less clear as only spatial averages over each area (rather than the maximum grid cell) are shown here and the maximum visibility impacts during the modeled days during the April and August periods in the original model run are below the annual 8th highest values shown in Tables 7-3 and 7-4. A complete analysis of a full annual run with reduced SSA would be needed to determine if a more realistic SSA estimate would result in visibility impacts at these other areas dropping below the 0.5 or 1.0 dv thresholds. Nevertheless it is conceivable that the annual maximum daily Δdv at Denali National Park, which was just above the 0.5 threshold in the original model run (see Table 7-4), could fall to just below the 0.5 threshold with reduced SSA.

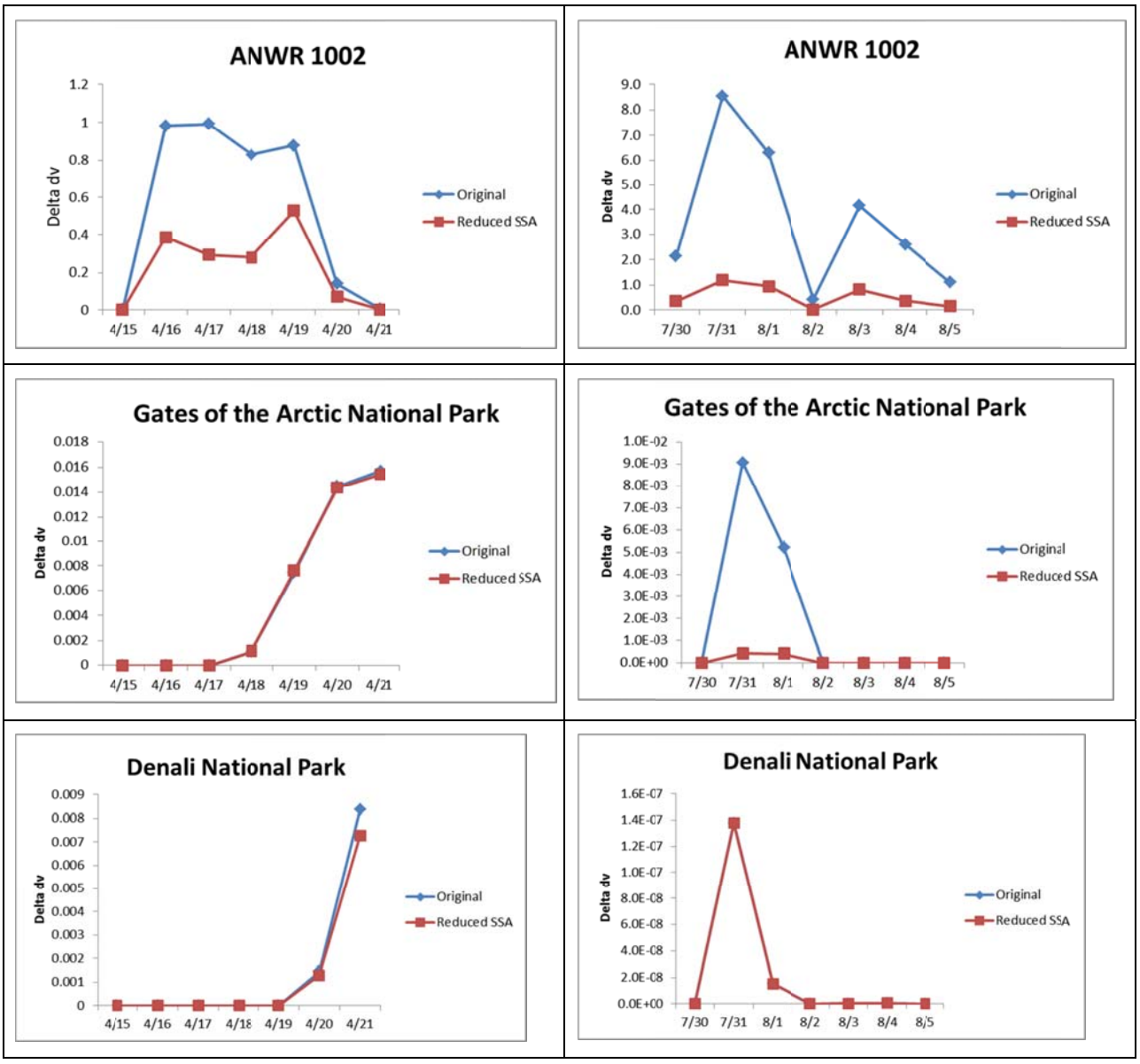

Figure 8-8. Comparison of predicted change in daily average haze index due to emissions from Source Group D (new oil & gas sources) between the original and reduced SSA model runs for ANWR Area 1002 (top), Gates of the Arctic National Park (middle), and Denali National Park (bottom) during modeled days in April (left) and August (right); all results based on spatial average 12km resolution output.

9.0 REFERENCES

Abt, 2014. Modeled Attainment Software, User's Manual. Abt Associates Inc., Bethesda, MD. April. (https://www3.epa.gov/ttn/scram/guidance/guide/MATS_2-6-1_manual.pdf).

Adelman, Z., U. Shanker, D. Yang and R. Morris, 2014. Three-States Air Quality Modeling Study – CAMx Photochemical Grid Model Final Model Performance Evaluation Simulation Year 2008. University of North Carolina at Chapel Hill, Institute for the Environment and ENVIRON International Corporation. September. (http://vibe.cira.colostate.edu/wiki/Attachments/Modeling/3SAQS_Base08b_MPE_Final_30Sep2014.pdf).

Alaska Department of Environmental Conservation (ADEC), 2011a. Emissions, Meteorological Data, and Air Pollutant Monitoring for Alaska's North Slope. December 21, 2011. Prepared by MACTEC Engineering and Consulting. http://dec.alaska.gov/air/ap/docs/North_Slope_Energy_Assessment_FINAL.pdf.

ADEC, 2011b. A preliminary assessment of fugitive dust from roads in eight Alaska villages in the Northwest Arctic Borough. Alaska Department of Environmental Conservation, July. https://dec.alaska.gov/air/am/projects&Reports/dust_NWAB_03-05.pdf

Allen, D. J., K. E. Pickering, R. W. Pinder, B. H. Henderson, K. W. Appel, and A. Prados, 2012. Impact of lightning-NO on eastern United States photochemistry during the summer of 2006 as determined using the CMAQ model. Atmos. Chem. Phys., 10, 107–119.

BOEM, 2014. AQScenarioSummary-rev.docx. Provided by H. Crowley, U.S. Department of the Interior, Bureau of Ocean Energy Management (May 12).

Brashers et al., 2015. Arctic Air Quality Modeling Study WRF Model Performance Evaluation, BOEM Arctic Air Quality Impact Assessment Modeling Study. By Ramboll Environ, Lynnwood, WA.

Colella, P., P.R. Woodward, 1984. The Piecewise Parabolic Method (PPM) for Gas-dynamical Simulations. J. Comp. Phys., 54, 174-201.

ENVIRON, 2012. Dallas-Fort Worth Modeling Support: Improving Vertical Mixing, Plume-in-Grid, and Photolysis Rates in CAMx, Prepared for: Texas Commission on Environmental Quality. August. http://www.tceq.state.tx.us/assets/public/implementation/air/am/contracts/reports/pm/5821110365FY1206-20120820-environ_dfw_modeling_support.pdf

ENVIRON, 2014. CAMx User's Guide: Comprehensive Air Quality Model with Extensions, Version 6.1. ENVIRON International Corporation, Novato, CA. April.

Ramboll Environ, 2016. Draft Technical Support Document: Cumulative and Visibility Impacts Analyses. Ramboll Environ, Novato, CA.

Emery, C., Koo, B., Karamchandani, P., Hsieh, W.C., Wentland, A., Wilson, G., Yarwood, G., Updates to CAMx, 2016. Secondary Organic Aerosol Chemistry, Heterogeneous Aerosol Chemistry, and Wet Deposition, Final Report prepared for U.S. Environmental Protection Agency, September.

Emmons, L. K., S. Walters, P. G. Hess, J.-F. Lamarque, G. G. Pfister, D. Fillmore, C. Granier, A. Guenther, D. Kinnison, T. Laepple, J. Orlando, X. Tie, G. Tyndall, C. Wiedinmyer, S. L. Baughcum, and S. Kloster, 2010. Description and evaluation of the Model for Ozone and Related Tracers, version 4 (MOZART-4), Geosci. Model Dev., 3, 43–67.

Fields Simms, P., R. Billings, M. Pring, R. Oommen, D. Wilson, and M. Wolf. 2014. Arctic Air Quality Modeling Study: Emissions Inventory – Final Task Report. Prepared by Eastern Research Group, Inc., Sacramento, CA for U.S. Dept. of the Interior, Bureau of Ocean Energy Management, Alaska OCS Region, Anchorage, AK. OCS Study BOEM 2014-1001. 169 pp.

FLAG, 2010. Federal Land Managers' Air Quality Related Values Work Group (FLAG) – Phase I Report – Revised (2010). Natural Resource Report NPS/NRPC/NRR – 2012/232. (http://nature.nps.gov/air/pubs/pdf/flag/FLAG_2010.pdf).

FLAG, 2000. Federal Land Managers' Air Quality Related Values Work Group (FLAG) – Phase I Report (December 2000). http://www.nature.nps.gov/air/Pubs/pdf/flag/FlagFinal.pdf.

Gantt, B., Kelley, J.T., and J.O. Bash, 2015. Updating sea spray aerosol emissions in the Community Multiscale Air Quality (CMAQ) model version 5.0.2. Geosci. Model Dev., 8, 3733–3746, 2015; doi:10.5194/gmd-8-3733-2015.

Guenther, A. B., T.Karl, P.Hartley, C.Weidinmyer, P.Palmer, and C.Geron, 2006. Estimates of global terrestrial isoprene emissions using MEGAN (Model of Emissions of Gases and Aerosols in Nature). Atmos. Chem. Phys. 6, 3181-3210.

Hong, S-Y and Y. Noh, 2006. A New Vertical Diffusion Package with an Explicit Treatment of Entrainment Processes. Monthly Weather Review, 134, 2318-2341, http://dx.doi.org/10.1175/MWR3199.1

Huang, J. and L. Jaeglé, 2016. Wintertime enhancements of sea salt aerosol in polar regions consistent with a sea-ice source from blowing snow. Atmos. Chem. Phys. Discuss., doi:10.5194/acp-2016-972, November.

Karl, T. G., T.J. Christian, R.J. Yokelson, P. Artaxo, W.M. Hao, and A. Guenther, 2007. The Tropical Forest and Fire Emissions Experiment: method evaluation of volatile organic compound emissions measured by PTR-MS, FTIR, and GC from tropical biomass burning, Atmos. Chem. Phys., 7, 5883–5897.

Kemball-Cook, S., G.Yarwood, J.Johnson, B.Dornblaser, and M.Estes, 2015. Evaluating NO_x Emission Inventories for Regulatory Air Quality Modeling Using Satellite and Air Quality Model Data. Atmos. Env. (submitted).

Koo, B., C.-J. Chien, G. Tonnesen, R. Morris, J. Johnson, T. Sakulyanontvittaya, P.

Piyachaturawat, and G. Yarwood, 2010. Natural emissions for regional modeling of background ozone and particulate matter and impacts on emissions control strategies. Atmos. Environ., 44, 2372-2382.

Koo, B., 2017. Personal communication, Bonyoung Koo, Ramboll Environ, Novato, CA.

Mavko, M. and R. Morris, 2013. DEASCO3 Project Updates to the Fire Plume Rise Methodology to Model Smoke Dispersion. Technical Memo prepared as part of Join Science Fire Program (JSP) project Deterministic and Empirical Assessment of Smoke's Contribution to Ozone. December 3. (https://wraptools.org/pdf/DEASCO3_Plume_Rise_Memo_20131210.pdf).

Morris, R., C. Emery, J. Johnson, and Z. Adelman, 2012. Technical Memorandum No. 12: Sea Salt and Lightning. WRAP West-wide Jump-start Air Qualoty Modeling Study (WestJumpAQMS). June 25. (http://www.wrapair2.org/pdf/Memo_12_SeaSalt_Lightning_June25_2012_final.pdf).

Nopmongcol, U., B. Koo, E. Tai, J. Jung, P. Piyachaturawat, C. Emery, G. Yarwood, G. Pirovano, C. Mitsakou, and G. Kallos, 2011. Modeling Europe with CAMx for Phase II of the Air Quality Model Evaluation International Initiative (AQMEII). ENVIRON International Corp., Novato, CA.; Coordinating Research Council, Inc., Alpharetta, GA.

Oltmans, S.J., B.J. Johnson, and J.M. Harris, 2012. Springtime boundary layer ozone depletion at Barrow, Alaska: meteorological influence, year-to-year variation, and long-term change. J. of Geophys. Res., 117, D00R18, doi: 10.1029/2011JD016889.

Quinn, P.K., T.S. Bates, T.L. Miller, D.J. Coffman, J.E. Johnson, J.M. Harris, J.A. Ogren, G. Forbes, T.L. Anderson, D.S. Covert, and M.J. Rood, 2000. Surface submicron aerosol chemical composition: What fraction is not sulfate? J. of Geophys. Res., 105, D5, 6785-6805, March 16.

Ruiz, L.H. and G. Yarwood, 2013. Interactions between organic aerosol and NOy: Influence on oxidant production. Prepared for the Texas AQRP (Project 12-012), by the University of Texas at Austin, and ENVIRON International Corporation, Novato, CA (http://aqrp.ceer.utexas.edu/projectinfoFY12_13/12-012/12-012%20Final%20Report.pdf).

Sauvage, B., R. V. Martin, A. van Donkelaar, X. Liu, K. Chance, L. Jaeglé, P. I. Palmer, S. Wu, and T. M. Fu, 2007. Remote sensed and in situ constraints on processes affecting tropical tropospheric ozone, Atmos. Chem. Phys., 7, 815–838

Sakulyanontvittaya, T., T. Duhl, C. Wiedinmyer, D. Helmig, S. Matsunaga, M. Potosnak, J. Milford, and A. Guenther, 2008. Monoterpene and sesquiterpene emission estimates for the United States. Environ. Sci. Techno. 42, 1623–1629.

Quinn, P.K. et al., 2000. Surface submicron aerosol chemical composition: what fraction is not sulfate? J. Geophys. Res., 105(D5), 6785-6805.

Sarwar, G., Simon, H., Xing, J., and R. Mathur, 2011. Importance of tropospheric ClNO2 chemistry across the Northern Hemisphere. Geophys. Res. Lett., 41, 4050–4058, doi:10.1002/ 2014GL059962.

Tai, E., M. Jimenez, O. Nopmongcol, G. Wilson, G. Mansell, B. Koo, and G. Yarwood, 2008. Boundary Conditions and Fire Emissions Modeling. ENVIRON International Corp., Novato, CA, September.

Tost, H., P. J. Joeckel, and J. Lelieveld, 2007. Lightning and convection parameterisations - uncertainties in global modeling, Atmos. Chem Phys., 7(17), 4553–4568.

U.S. EPA, 2007. Guidance on the Use of Models and Other Analyses for Demonstrating Attainment of Air Quality Goals for Ozone, $PM_{2.5}$, and Regional Haze. EPA-454/B-07-002, U.S. Environmental Protection Agency, Research Triangle Park, NC, April. U.S. EPA, 2014. Draft Modeling Guidance for Demonstrating Attainment of the Air Quality Goals for Ozone, $PM_{2.5}$, and Regional Haze. U.S. Environmental Protection Agency, December.

U.S. EPA, 2014. Draft Modeling Guidance for Demonstrating Attainment of Air Quality Goals for Ozone, $PM_{2.5}$ and Regional Haze. U.S. Environmental Protection Agency, Research Triangle Park, NC. December. (http://www.epa.gov/ttn/scram/guidance/guide/Draft_O3-PM-RH_Modeling_Guidance-2014.pdf).

U.S. EPA, 2015. Technical Support Document, Preparation of Emissions Inventories for the Version 6.2, 2011 Emissions Modeling Platform. U.S. Environmental Protection Agency, Research Triangle Park, NC. (https://www.epa.gov/sites/production/files/2015-10/documents/2011v6_2_2017_2025_emismod_tsd_aug2015.pdf)

USDA, USDOI, EPA, 2011. Memorandum of Understanding among the U.S. Department of Agriculture, U.S. Department of The Interior, and U.S. Environmental Protection Agency, Regarding Air Quality Analyses and Mitigation for Federal Oil And Gas Decisions Through the National Environmental Policy Act Process, June 2011.

Wiedinmyer, C. and H. Friedli, 2007. Mercury Emission Estimates from Fires: An Initial Inventory for the United States. Environmental Science & Technology 2007 41 (23), 8092-8098 doi: 10.1021/es071289o.

Wiedinmyer, C., B. Quayle, C. Geron, A. Belote, D. McKenzie, X. Zhang, S. O'Neill, and K. Klos Wynne, 2006. "Estimating Emissions from Fires in North America for Air Quality Modeling." Atmos. Environ., 40, (19), 3419-32.

Wiedinmyer, C., S. K. Akagi, R. J. Yokelson, L. K. Emmons, J. A. Al-Saadi, J. J. Orlando, and A. J. Soja. "The Fire Inventory from Ncar (Finn): A High Resolution Global Model to Estimate the Emissions from Open Burning." Geoscientific Model Development 4, no. 3 (2011): 625-41. (http://www.geosci-model-dev.net/4/625/2011/gmd-4-625-2011.html)

Zhang, L., S. Gong, J. Padro, L. Barrie, 2001. A size-segregated particle dry deposition scheme for an atmospheric aerosol module. Atmos. Environ., 35, 549-560.

Zhang, L., J. R. Brook, and R. Vet. 2003. A revised parameterization for gaseous dry deposition in air-quality models. Atmos. Chem. Phys., 3, 2067–2082.